Copyright Warning & Restrictions

The copyright law of the United States (Title 17, United States Code) governs the making of photocopies or other reproductions of copyrighted material.

Under certain conditions specified in the law, libraries and archives are authorized to furnish a photocopy or other reproduction. One of these specified conditions is that the photocopy or reproduction is not to be "used for any purpose other than private study, scholarship, or research." If a, user makes a request for, or later uses, a photocopy or reproduction for purposes in excess of "fair use" that user may be liable for copyright infringement,

This institution reserves the right to refuse to accept a copying order if, in its judgment, fulfillment of the order would involve violation of copyright law.

Please Note: The author retains the copyright while the New Jersey Institute of Technology reserves the right to distribute this thesis or dissertation

Printing note: If you do not wish to print this page, then select "Pages from: first page # to: last page #" on the print dialog screen

ABSTRACT

DEVELOPMENT OF ENVIRONMENTALLY BENIGN MICROENCAPSULATION WITH POLYMER MICROSPHERES AND LIPOSOMES

by

Baohua Yue

Microencapsulation means applying a shell-like coating to encapsulate the contents of interest in a particle form with a size range of few micrometers or below. In this work, aqueous liposome systems and polymer based encapsulation of fine particles in supercritical CO_2 were studied. Compared to many other microencapsulation methods, these two methodologies feature reduction/prevention of using organic solvents, making them particularly attractive as green technology.

For polymer microencapsulation, a novel in situ polymerization based process to encapsulate various types of fine particles, include drugs, fire retardant, inorganic nanoparticles, and carbon nanotubes, was developed. In the process, host particles, monomers and other components are first mixed together followed by polymerization and encapsulation. Thin-film coating was achieved for particle size above 1μm. For nanoparticles, surface functionalization was employed for increasing interfacial interactions and dispersion. Under appropriate conditions, nano-silica particles were found undergoing sol-gel transition to form porous monoliths. Dispersion, debundling, and polymer encapsulation of single-walled carbon nanotubes (SWNTs) were also reported.

Despite the great potential posed by bio-mimetic phospholipids in drug delivery, commercial products are quite limited. To address the structure stability of liposome-

based microencapsulationm in a more fundamental level, we studied the mechanism of spontaneous formation of monodispersed unilamellar vesicles with scattering technique using neutron and light sources. Vesicle phase was studied systematically as a function of lipid concentration, salinity, temperature and time duration, etc. The results contribute to the understanding and selection of appropriate lipid system and process for microencapsulation of drugs.

DEVELOPMENT OF ENVIRONMENTALLY BENIGN MICROENCAPSULATION WITH POLYMER MICROSPHERES AND LIPOSOMES

by
Baohua Yue

A Dissertation
Submitted to the Faculty of
New Jersey Institute of Technology
In Partial Fulfillment of the Requirements for the Degree of
Doctor of Philosophy in Environmental Science

Department of Chemistry and Environmental Science

January 2006

APPROVAL PAGE

DEVELOPMENT OF ENVIRONMENTALLY BENIGN MICROENCAPSULATION WITH POLYMER MICROSPHERES AND LIPOSOMES

Baohua Yue

Dr. Michael C.-Y. Huang, Dissertation Advisor — Date
Assistant Professor of Chemical Engineering
New Jersey Institute of Technology

Dr. Robert Pfeffer, Dissertation Advisor — Date
Distinguished Professor of Chemical Engineering
New Jersey Institute of Technology

Dr. Rajesh Dave, Committee Member — Date
Professor of Mechanical Engineering
New Jersey Institute of Technology

Dr. Somenath Mitra, Committee Member — Date
Professor of Chemistry and Environmental Science
New Jersey Institute of Technology

Dr. Zafar Iqbal, Committee Member — Date
Research Professor of Chemistry and Environmental Science
New Jersey Institute of Technology

BIOGRAPHICAL SKETCH

Author: Baohua Yue

Degree: Doctor of Philosophy

Date: January 2006

Undergraduate and Graduate Education:

- Doctor of Philosophy in Environmental Science,
  New Jersey Institute of Technology, Newark, NJ, 2006
- Master of Science in Chemical Engineering,
  New Jersey Institute of Technology, Newark, NJ, 2005
- Bachelor of Science in Environmental Science,
  Jilin University, P. R. China, 2000

Major: Environmental Science

Publications

B. Yue, C. Y. Huang, M. P. Nieh, J. Katsaras, C. Glinka "Highly stable phospholipid unilamellar vesicles from spontaneous vesiculation: a DLS and SANS study". *Journal of Physical Chemistry B.* 2005, 109, 609.

B. Yue, J. Yang, Y. Wang, C. Y. Huang, R. Dave, R. Pfeffer "Particle encapsulation with polymers via in situ polymerization in superitical CO_2". *Powder Technology* 2004, 146, 32.

B. Yue, C. Y. Huang, M. P. Nieh, J. Katsaras, C. Glinka "Spontaneously forming unilamellar phospholipids vesicles". *Macromolecular Symposia* 2005, 219, 123.

B. Yue, C. Y. Huang "Polymer coating of pharmaceutical ingredients in supercritical CO_2". *Polymer Preprints* 2004, 45, 221.

B. Yue, J. Yang, C. Y. Huang, R. Dave, R. Pfeffer "Preparation of porous PMMA monolith containing silica nanoparticles in supercritical CO_2". *Polymer Preprints* 2005, 46(1), 750.

B. Yue, J. Yang, C. Y. Huang, R. Dave, R. Pfeffer "Synthesis of Macroporous PMMA/Silica Nanocomposite Monoliths in Supercritical CO_2". *Macromolecular Rapid Communications* 2005, 26, 1406.

B. Yue, J. Yang, C. Y. Huang, R. Dave, R. Pfeffer "Preparation of PMMA/silica hybrid nanocomposite particles in supercritical CO_2". submitted to *Industrial and Engineering Chemistry*, 2005.

B. Yue, Y. Wang, C. Y. Huang, Z. Iqbal, R. Pfeffer "Synthesis of PMMA/carbon nanotube composites in supercritical CO_2". submitted to *Macromolecules*, 2005.

B. Yue, J. Yang, Jose A Quevedo, C. Y. Huang, R. Dave, R. Pfeffer "Development and evaluation of environmentally benign techniques for polymer film coating of fine particles". *Proceedings, AICHE Annual Meeting*, 2004.

Y. Wang, B. Yue, D. Wei, C. Y. Huang, R. Dave, R. Pfeffer "Nanoparticle coating/ encapsulation with polymers by supercritical fluid processing". *Proceedings, World Congress on Particle Technology 4*, 2002.

To my beloved wife, Xianjin Jiang; children, Rachel and Edward; my parents, Jiaying Sun and Guangxing Yue; and parents-in-law, Fengrong Wang and Zhongmin Jiang.

ACKNOWLEDGEMENT

My sincere gratitude goes to Dr. Huang and Dr. Pfeffer, who not only gave me the utmost freedom in the laboratory and opened up new areas of interest, but also provided constant support, guidance, and encouragement. They have been more than advisors, mentors whom I learned so much from. I am also extremely grateful to my group director Dr. Dave for his continuous support of my research, and for exposing me to many opportunities.

My great appreciation also goes to Dr. Mu-Ping Nieh, NRC Canada, who brought me to the field of liposome and neutron scattering technologies. I would like to thank Dr. Iqbal for introducing me to carbon nanotubes research and constantly providing advice on my research. I am also grateful to my academic advisor, Dr. Mitra, for his active participation in my dissertation and constant help during my five-year study at NJIT. I want to thank Dr. Jun Yang for collaboration in many aspects of my research.

During my graduate research, I was fortunate to receive help from these people: Dr. Yulu Wang, Mr. Yogesh Ghandi, Dr. Xueyang Zhang, and Dr. Dongguang Wei.

Finally, I also want to thank Dr. Bozzelli and Dr. Kane for offering me a teaching assistantship.

TABLE OF CONTENTS

TABLE OF CONTENTS
(Continued)

Chapter **Page**

TABLE OF CONTENTS
(Continued)

Chapter **Page**

TABLE OF CONTENTS
(Continued)

Chapter **Page**

TABLE OF CONTENTS
(Continued)

Chapter **Page**

LIST OF TABLES

Table **Page**

LIST OF FIGURES

Figure **Page**

LIST OF FIGURES
(Continued)

Figure **Page**

LIST OF FIGURES
(Continued)

Figure **Page**

LIST OF FIGURES
(Continued)

Figure **Page**

LIST OF FIGURES
(Continued)

Figure Page

LIST OF SCHEMES

SCHEME **Page**

NOMENCLATURE

m	Mass, gram
t	Thickness of coating, μm
ρ	Density, gram/ml
R	Radius of particles, μm
T	Temperature, °C
P	Pressure, bar
S	Solubility, mole/ml
Z	Compress factor
I	Scattering intensity
Q	Scattering vector
Di	Diffusion coefficient
G	Autocorrelation function
k	Boltzmann constant
η_w	Viscosity

CHAPTER 1

INTRODUCTION

1.1 Microencapsulation

Particle handling is a critical process in many industries, especially chemicals and pharmaceuticals. Along with particle size and density, particle surface property is one of the most important characteristics for particle processing. Many technologies are used to control particle surface property, such as recrystallization, milling etc, but surface coating remains one of the most effective methods. Particle coating is often employed to enhance particle compatibility, flowability, wettability and dispersibility, or to serve as a protection barrier for controlled release or taste masking.

While coating of particles larger than hundreds of microns in diameter has been successfully carried, it remains a challenge to coat particles in the micron size range. The techniques used to encapsulate micron and submicron sized particles are usually referred to as "microencapsulation". By definition, microencapsulation means applying a coating or shell to encapsulate the contents in the form of a particle in the micrometer size range. The term has been broadly expanded to include emulsion, liposome, microparticles, and protein encapsulation. Most of these technologies fall into one of these two categories: colloid system or polymeric microspheres.

1.2 Colloid Systems

Colloid systems have the advantages of relatively high stability, repeatability and easy preparation. Colloid-based microencapsulation are usually prepared from the dispersed colloidal particles. Major methods include: single and multiple emulsions, andliposome

systems. Although liposome can also be classified into emulsion system, they are usually treated separately due to their biological nature.

1.2.1 Emulsions

Emulsion systems are formed due to the unique thermodynamic behavior of surfactants. Surfactants have hydrophilic and hydrophobic groups that allow them to interact with both solvents with like properties. Under different conditions, surfactant molecules self assembly into different structures, such as micelles, cubic phase, bilayers etc. Shown in Figure 1.1 is a schematic diagram of micelle composed of surfactant molecules, with hydrophilic head in water, and hydrophobic groups extending against water. The hydrophobic core may also contain some hydrophobic material, e.g. oil, to form oil-in-water emulsion. On the contrary, if the surfactant hydrophobic chains are extending out to the oil main phase, while hydrophilic head facing inside, then they form water-in-oil emulsion.

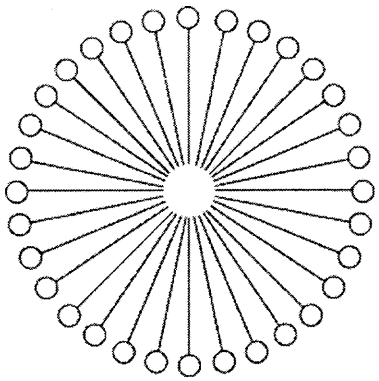

Figure 1.1 Schematic diagram of a micelle.

Oil-in-water emulsion process has been applied to encapsulate low molecular weight, hydrophobic molecules. In this method, the active agent and coating materials are dissolved in an organic solvent, and then dispersed in an aqueous solution containing a

surfactant. After evaporation of the organic solvent, microspheres loaded with actives are separated and dried. Using this process, Yen, et al., 2001 reported the synthesis of microspheres loaded with nalbuphine propionate for controlled release. Similarly, Ko, et al., 2002, microencapsulated drug components for controlled delivery. For water-soluble material, a non-aqueous emulsion is used for the encapsulation process. The aqueous phase is replaced by another solvent, which is a non-solvent for the active ingredient. With this method, Ogawa, et al., 1988, encapsulated leuprolide acetate with microcapsules of PLA and PLGA. Water-in-oil emulsion, in which aqueous droplets are dispersed in oil phase, is not often used.

Although single emulsion has been successfully used for encapsulation of small organic molecules. Single emulsion is usually not suitable for the microencapsulation of high molecular weight, hydrophilic biopharmaceuticals. In these cases, multiple emulsions may be used to encapsulate actives within the hollow center of the microsphere. Multiple emulsion means emulsion within emulsion, in reality; it typically refers to oil-in-water-in-oil (o/w/o) or water-in-oil-in-water (w/o/w) systems. In w/o/w emulsion, the active is dissolved in an aqueous solution and then dispersed in an organic polymer solution to form a primary emulsion. This emulsion is then added to the aqueous solution containing surfactant and mixed under stirring. The formed microspheres are collected by filtration after evaporation of the organic solvent. Wang, et al., 1999 and Capan, et al., 1999 encapsulated of DNA into microspheres for gene delivery system using multiple emulsion. Similarly, Blanco-Prieto, et al., 1997 and Yamaguchi, et al., 2002 used this approach to prepare protein and peptide loaded microspheres.

When using emulsion technology, there are always concerns regarding the stability of bioactive agents. Use of organic solvent and harsh conditions, such as strong shearing forces and extreme pH may affect the structure of the bioactive agents. Moreover, trace residual organic solvent in the final product may cause safety concerns.

1.2.2 Liposome

Liposomes are vesicles composed of natural lipid surfactants. Lipid molecules typically have one hydrophilic head and two hydrophobic chains that can be sponificated to fatty acids. Shown in Figure 1.2 is a schematic diagram of lipid vesicle. Liposomes were initially used as research tools to study the function of biological membranes, and later developed as a carrier system for delivery of molecules at the cellular and organismal level. The combined perspectives of membrane biophysics, cell biology and medicine has propelled liposomes to emerge as a major drug delivery system, with several drugs already marketed.

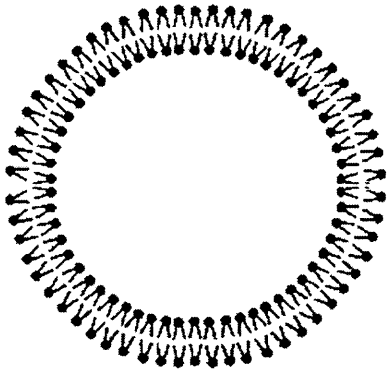

Figure 1. 2 Schematic diagram of a lipid vesicle.

Liposomes are man-made analogues of enclosed natural membranes. The special physicochemical characteristics of lipids, self-assembly properties, as well as their phase

behavior governed by their thermodynamic and kinetics, define the properties of liposomes. Their biomedical applications derive from their biocompatibility, colloidal characteristics and encapsulating properties. As a model biomembrane system, liposomes have helped to unravel many cell membrane functions. As a drug delivery system, they hold great promise for targeted delivery of a variety of biopharmaceuticals, including anticancer drugs(Jaracz, 2005), gene delivery (Lasic, 1997). Currently, the major areas of progress are in the delivery of anti-fungal agents by conventional liposome carriers, and anticancer chemotherapy using long-circulating liposomes.

Compared to other colloidal drug delivery systems, the advantages of liposomes range from manufacturing and physico-chemical to biological aspects. These include biocompatibility, as well as relatively low toxicity and immunogenicity. With respect to liposome formulation issues, they are relatively easy to prepare, as well as accessible raw materials. From physico-chemical point of view, the advantage of liposomes is the fact that they are usually not at thermodynamic equilibrium but represent a kinetically trapped system. Therefore, liposomes preserve their size, shape as well as encapsulated contents much better than microemulsions. Lipid bilayers also provides opportunities for attachment of various other molecules and ligands with specific function. Liposomes can be formulated as a solution, dry powder, aerosol, cream or lotion, and therefore practically all conventional administration routes can be employed.

Although liposome has been successfully used in several commercial drug delivery systems, its wide application is limited by the relatively poor stability(Lasic, 1993). Liposome produced by many size reduction techniques, such as extrusion and sonication, tend to equilibrate back to their original states, which are large in diameter

and polydisperse. Thus a method for the preparation of highly stable liposomes is desirable for drug delivery.

1.3 Polymer Microspheres

Polymer coating is one of the most widely used methods for taste-masking and controlled release in pharmaceutical development. Polymer coating technologies fall into one of two categories: polymerization or deposition based approaches.

1.3.1 Surface Polymerization

Surface polymerization has been used to directly encapsulate solid particles. In this technology, a surfactant first adsorb onto a solid surface. The surfactants usually contain functional groups that interact with solid surface and functional groups that directly or indirectly polymerize with monomers in the solution phase to form a polymer coating layer. Guo, et al. 2004 investigated encapsulation of silica particles with polystyrene using surface polymerization. In their process, silica particles are first modified with vinyl groups and then copolymerize with styrene. Similarly, Luna-Xavier, 2002 studied surface coating of silica particles with PMMA using surface polymerization. In their study, silica particles were coated using a cationic initiator, 2,2'-azobis (isobutyramidine) dihydrochloride (AIBA), and a nonionic polyoxyethylenic surfactant and then polymerized with MMA to form a core-shell structure. Shim, 2002 reported similar work of the surface modification of zinc oxide particles with polymethylmethacrylate (PMMA) using suspension interfacial polymerization. The encapsulation of active component in polymer nanoparticles for anticancer treatment was illustrated by Chiannikulchi, 1989.

1.3.2 Interfacial Polymerization

Interfacial Polymerization was pioneered by Dupont to manufacture nylon. In interfacial polymerization-based microencapsulation, an organic or aqueous solution of the active component containing monomer A is dispersed and emulsified in a continuous phase containing monomer B. The polymerization between A and B at the liquid droplet surface results in the formation of a film coating. Aboubakar et al. 1999 employed interfacial polymerization to synthesize poly(isobutylcyanoacrylate) for encapsulation of insulin.

1.3.3 Fluidization

Compared to the polymerization based methods mentioned above, deposition based technologies are more developed in industry. Among them, Fluid bed is one of the most widely used for fine particle coating, Wurster coating, in pharmaceutical industry. In this coating process, core materials are fluidized, while coating materials are sprayed onto the fluidized particles. This method can work with particles of a large range of sizes. Coating material solutions of aqueous or organic solvents can be used. Recently, Ivanova et al. 2005 used fluid bed to encapsulate water sensitive products.

1.3.4 Spray Drying

Similar to fluid bed coating in principle, spray drying has been used for encapsulation and coprecipitation of drug particles and excipients. During spray drying, core material and coating material are dissolved or suspended in an organic or aqueous solution. The suspension or solution is sprayed into drying chamber, where the solvent is evaporated and composite particles composed of the core and coating materials are produced. Lin et

al. 2005 used spray drying as a method for preparation of anticancer drug doxorubicin in PLGA-based microparticles.

These above technologies have found wide applications in chemical and pharmaceutical industries; however, each has drawbacks. First of all, they all involve the use of organic solvents or aqueous media to mediate the coating. As a result, energy-consuming particle separation and drying processes are usually necessary. Second, the use of organic solvents causes environmental and health concerns. Third, coating obtained in spray drying and fluid bed is often not uniform and is very sensitive to operating conditions, such as temperature, air flow rate, etc.

1.3.5 Dry Coating

In search for environmentally friendly coating method, Pfeffer et al. 2001 at New Jersey Center for Engineered Particulates developed a dry coating procedure. In dry coating, host and guest particles are blended in a mixing device. Through continuous interparticle compaction, small guest particles attach to the surface of large core particles through van der Waals forces. Strong mechanical forces are required to deagglomerate the fine guest particles during this dry coating process. Due to the nature of this mechanism, coating uniformity has been a primary concern for this process.

1.3.6 Supercritical Processing

Another environmentally friendly coating method involves the use of supercritical fluid. Supercritical fluid has unique advantages in that it has liquid-like dissolution power and gas-like transport property. Among all the supercritical fluids, supercritical CO_2 ($scCO_2$)

is the most widely studied. Coating with supercritical fluid has been carried out with several processes: RESS, AESS, SAS, PGSS, with SAS being the most successful.

In SAS (supercritical antisolvent process), polymer is dissolved in an organic solvent that is miscible with CO_2, while the core material is dispersed or dissolved in the same solvent. After the solution is sprayed into $scCO_2$, the solvent is extracted and the dissolved materials quickly precipitate out to form coating or composite particles. Using RESS and SAS, Wang et al. (2002 2004) successfully coated various particles with polymers in $scCO_2$.

Although this technique has been successfully applied to coat various particles and drugs, like fluid bed coating, the process is very sensitive to changes in pressure, solution concentration, etc. The use of organic solvents also compromises its environmental benefit.

After reviewing the available coating technologies, it is realized that development of efficient and clean polymer coating technologies may help to overcome the negatives associated with the above technologies.

1.4 Dissertation Objectives and Outline

1.4.1 Objectives

1.4.1.1 Preparation of Highly Stable Liposome for Microencapsulation. As described above, the preparation of highly stable lipid vesicles is critical to the success of liposome as microencapsulation device for drug delivery. Therefore, the first objective is to investigate the preparation of highly stable lipid vesicles and characterize them. With the

availability of Dynamic Light Scattering (DLS) and Small Angle Neutron Scattering (SANS), the phase behavior of lipid aqueous solution are studied in detail.

1.4.1.2 Development of Novel Polymer Microencapsulation in $scCO_2$. The second objective of this thesis is to develop an efficient and clean polymer coating technology to encapsulate fine particles. Since supercritical CO_2 has been proven to be an effective green solvent, it is used as a media for polymerization-induced microencapsulation. Polymers are form in situ and precipitate or attach through reaction onto particle surface to form coating layer. Various physical and chemical characterization methods will be used, including DSC, TGA, SEM, TEM, BET and FTIR.

1.4.2 Outline

Following this Introduction, Chapter 2 presents a summary of the previous work done in supercritical coating and liposome technology. First, a survey is presented on two widely studied supercritical processing methods for particle coating: Rapid Expansion of Supercritical Solution (RESS) and Supercritical Antisolvent Process (SAS). Next, fundamentals of liposomes are described. Theoretical background as well as conventional preparation methods are introduced.

Chapter 3 describes a new polymerization based study on microencapsulation of micron-sized particles. First, PMMA coating of Dechlorane is studied as model system. PMMA was synthesized in $scCO_2$ from dispersion polymerization and forms a coating layer on the surface of Dechlorane particles. The coating morphology control is investigated with the help of SEM results. Coating mechanism is proposed based on TGA and SEM results. Second, this mechanism is confirmed by results from PVP coating of Dechlorane particles. This novel coating technology was expanded to pharmaceutical

coating, where PVP was synthesized to encapsulate Hydrocortisone and Lysozyme particles.

Chapter 4 presents a new method using supercritical CO_2 as a media to encapsulate silica nanoparticles with PMMA. Commercially available and home-made are used as core material. Surface functionalization was applied to home-made particles to change particle surface property. Modified particles were found to interact favorably with PMMA and form a homogenous nanocomposite.

Chapter 5 describes the microencapsulation of single wall carbon nanotubes with PMMA via in situ polymerization. Taking advantage of the high diffusivity of CO_2, the reactants easily penetrate the CNT matrix, leading to high coating uniformity. The CNTs used were pretreated to attached double-bond containing molecules, which serves as bridges to chemically attach PMMA molecules to CNT surface.

Chapter 6 is an extension of the work in Chapter 4. In this work, we studied the formation of PMMA monolith containing silica nanoparticles. Single-body macroporous monolith with the silica homogenously embedded can be synthesized easily in this process. The monolith surface morphology can be controlled by varying silica loading ratio, silica particle size, etc.

Chapter 7 presents preparation and characterization of highly stable lipid vesicles. Lipid vesicles are prepared from mixtures of lipids with different chain length and charge behavior. Without using of high energy input, unilamellar lipid vesicles form spontaneously in aqueous solution after simple dilution and vortexing. The vesicle size and structure were studied with DLS and SANS.

Chapter 8 presents recommendations based on this research and suggestions for future work.

CHAPTER 2

SUMMARY OF PREVIOUS WORK

In this chapter, brief reviews of polymeric microencapsulation with supercritical process and liposome microencapsulation are provided.

2.1 Polymeric Particle Coating Using Supercritical Processes

Billions of gallons of organic solvents are used every year for chemical synthesis and processing. Use of water as solvent is limited by it's inherent properties. In the search for environmentally friendly solvent, people turned to supercritical fluid.

2.1.1 Supercritical Fluid

A supercritical fluid is a fluid that is beyond its critical temperature (Tc) and pressure(Pc), as shown in Figure 2.1, each fluid has its own critical point.

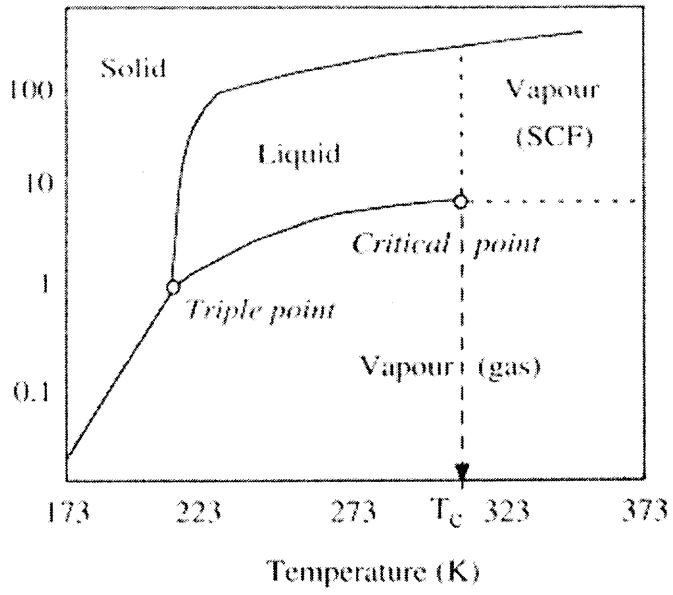

Figure 2.1 Schematic P-T phase diagram of supercritical fluid.

The density and viscosity of a supercritical fluid are between their values in the gas and liquid state. The density can be controlled by adjusting pressure and temperature. The solvent strength is related to the density of a fluid; hence, the solvent properties of a supercritical fluid can be relatively easily adjusted. As shown in Figure 2.2, supercritical fluid is highly compressible near critical point.

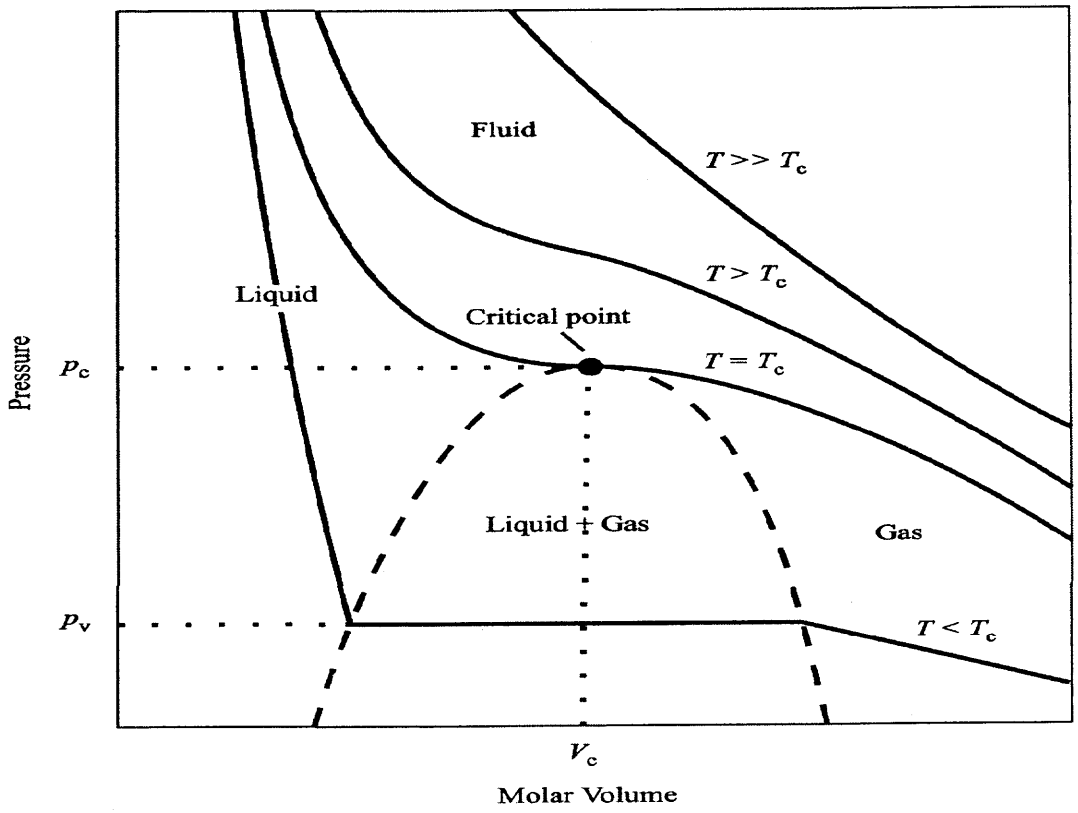

Figure 2.2 Schematic P-V phase diagram of supercritical fluid.

Supercritical fluid also has other unique physicochemical properties, such as high diffusivity and low viscosity. McHugh and Krukonis, 1986 compared typical diffusivities of small organic solutes in supercritical CO_2 over a range of pressure and temperature. It was found that the diffusivity in CO_2 at 40 °C in the range between 70-200 bars range from 10^{-3} to 10^{-4} cm^2/sec, which is significantly higher than liquid value around 10^{-5}

cm^2/sec. The viscosity of the supercritical fluid falls in between that of a gas and a liquid. Below the critical point, its viscosity is close to gaseous state. Above the critical point, the viscosity of supercritical CO_2 increases as the pressure goes up, but it is still lower than that of liquid even at high pressure. For example, at 300 bars and 47 °C the viscosity of supercritical CO_2 is 0.09 cp, one order of magnitude lower than that of water (McHugh and Krukonis 1986).

Among all supercritical fluids, supercritical CO_2 is of particular interest, because it is inexpensive, nontoxic, nonflammable, and easily recyclable. In addition, the relatively mild critical conditions, T_c = 32 °C and P_c = 74 bars, are easily accessible. In addition, supercritical CO_2 has a relatively high solvent strength (dissolving power).

Table 2.1 Critical Points of Common Fluids

Fluid	**Pc**	**ρc**	**Tc**
Carbon Dioxide	73.77	467.6	304.13
Methane	45.92	162.7	190.56
Ethane	48.72	206.6	305.33
Water	220.6	322.0	647.10

Because of its remarkable solvent strength, supercritical CO_2 was widely used for extraction and separation in the food and pharmaceutical industries. Recently, scientists have used $scCO_2$ as a reaction media for various reactions, such as catalysis and polymerization.

2.1.2 Rapid Expansion of Supercritical Solutions (RESS)

In a typical RESS process, materials are dissolved in $scCO_2$ and the solution is atomized through a nozzle. The quick supersaturation due to volume expansion results in precipitation of coating material in the form of particles of small size and narrow distribution. The coating material may precipitate onto host particle surfaces or onto reactor walls. The drawback of the RESS technique is that only few groups of polymers dissolve in $scCO_2$, which greatly restricts its application. To overcome the low solubility of many materials, cosolvent is often added to facilitate solid dissolution in $scCO_2$. RESS is normally used for formation of single or multicomponent particles. The particle size varies with pressure difference, nozzle size, solubility etc.

Several researchers have explored drug/polymer coprecipitation with RESS process. Tom, et al., 1994 coprecipitated pyrene with PLA to form composite particles in a RESS process. Pyrene solution and PLA dissolved in $scCO_2$ with cosolvent $CHClF_2$ were sprayed into the expansion chamber and precipitate out. Kim, et al., 1996 investigated the coprecipitation of naproxen with PLA. First, the authors extracted PLA and naproxen into $scCO_2$ and then sprayed the solution through a nozzle for precipitation.

The RESS process was also used to coat/encapsulate particles by Mishima, et al., 2000. In the RESS coating process the material to be coated and the coating material (polymer) are both dissolved in SC CO_2 with or without a cosolvent. The solution is then released from a nozzle (de-pressurized), generating microparticles with a polymer coating on the surface. In RESS the rapid de-pressurization of the supercritical solution causes a substantial lowering of the solvent power of CO_2 leading to very high super-saturation of solute, precipitation, nucleation and particle growth. However, the application of the

RESS process is severely limited by the fact that polymers, in general, have very limited solubility in SC CO_2 at temperatures below 80 °C (O'Neill, et al., 1998). Also, the operating pressure in RESS is usually above 200 bars so that it is less attractive economically.

Tsutsumi, et al., 1995; used a combination of the RESS process and a fluidized bed for coating particles. In their research, a solution of coating material in SC CO_2 rather than in an organic solvent is sprayed into the fluidized bed of particles to be coated. However, particles less than 30-50 μm fall into Geldart's group C particle classification and are very difficult to fluidize. Hence this method cannot be used to coat ultrafine particles

Pessey, et al., 2000; 2001 also demonstrated particle coating using a supercritical fluid process. Their research involved the thermal decomposition of an organic precursor and the deposition of copper onto the surface of core particles in SC CO_2 under conditions of temperature up to 200 °C and pressure up to 190 bars. However, their methods are less attractive from the point of view of safety and cost and probably cannot be applied to the pharmaceutical industry since high temperature could adversely effect or even destroy most drug powders.

Recently, Wang et al. developed a modified RESS for particle coating by using a solution of polymer in supercritical CO_2. The results show that the coating of glass beads with PVCVA and HPC was successfully achieved using this technique. The use of a co-solvent improved the solubility of polymers and also affected the degree of crystallinity of the polymer coating on the surface of glass beads. The extraction and precipitation technique took advantage of the properties of a supercritical solution in that the polymer

would nucleate, grow and deposit on the host particle surface due to changes in its solubility caused by adjusting the temperature and pressure.

2.1.3 Supercritical Antisolvent Processes (SAS)

For materials that do not dissolve in $scCO_2$, a supercritical antisolvent process (SAS) is usually applied, in which supercritical CO_2 acts as an antisolvent to induce the nucleation and precipitation of a solute. In this process, materials are dissolved or suspended in an organic solvent that is miscible with $scCO_2$. The solution or suspension is then sprayed into $scCO_2$ through an atomizer. An instantaneous supersaturation facilitated by fast mutural mass transfer leads to precipitation of dissolved material in the form of nanoparticles. In the SAS process, the particle size, size distribution, morphology and crystallization are strongly dependent on the mass transfer, which is affected by temperature, pressure, solution concentration, CO_2 flow rate, solution flow rate and nozzle design.

Wang et. al. successfully developed SAS coating for nanoparticles with Eudragit (2003). A suspension of silica nanoparticles in a polymer solution was sprayed into SC CO_2 through a capillary tube. The subsequent mutual diffusion between SC CO_2 and polymer solution droplets resulted in high degree of supersaturation, causing a heterogeneous polymer nucleation induced by the phase transition, with the silica nanoparticles acting as nuclei. Thus the nanoparticles were individually encapsulated in polymer with very little agglomeration. For larger 600nm particles the thickness of the polymer coating were controlled by adjusting the ratio of polymer to host particles. In a separate research, hydrocortisone particles were shown to be successfully coated with PLGA in the SAS coating process. At a low 1:4 polymer to drug weight ratio the drug

surface was only partially coated and no encapsulation (encapsulation efficiency of zero) occurred. At polymer to drug ratios of 1:2 and 1:1, the coated drug particles exhibited a sustained release behavior.

SAS is also used for coprecipitation of a drug substance and a polymer. In 1997, Falk, et al. successfully studied the formation of drug/polymer composite particles with the SAS process. In their research, a solution of drugs and PLA were sprayed into SC CO_2 as an antisolvent to induce co-precipitation of drug and PLA. However, coprecipitation of drug and polymer requires that both be dissolved in a suitable solvent which is a challenge for two solutes that have different thermodynamic properties and undergo different precipitation pathways. An important feature of the SAS process is that the organic solvent can be almost completely removed by simply flushing with pure CO_2. Thus, dry particles are produced after a CO_2 extraction step following organic solution injection.

Due to the nature of these two spray based technologies, they are very sensitive to operation parameters, such as pressure drop, spraying rate, nozzle size, etc.

2.2 Liposome for Microencapsulation

Liposomes are dispersed colloidal particles of enclosed lipid bilayer membranes, which encapsulate an aqueous core inside. Their properties are determined by their lipid molecular composition, number of layers, particle size distribution etc, all are critical for their stability and interaction characterstics. Liposome morphology is normally determined by their preparation procedure, which is an indication that liposome systems are kinetically stable.

Various types of liposomes are used for drug delivery, but unilamellar vesicles in the size range of ~100 nm are the most often used (Lasic, 1993). Unilamellar vesicles usually have monodisperse size distribution, which enhances their stability. The small size increases their circulation time in human body, increases the volume of biodistribution and allows extravasation through blood vessels, but it also reduces the amount of encapsulated contents per mass of lipid.

The physico-chemical properties of liposomes as well as the fundamental physical and chemical concepts which underly their structure, stability and interaction characteristics have also been established. Liposome properties have been studied through some measurable characters, such as order parameter of the bilayer, phase transitions and mechanical properties of the bilayer which are related to the bending and stretching elastic modulus, and surface properties, which can be explained by the Poisson-Boltzmann treatment in the case of electrostatic stabilization and with Scaling concepts in the case of steric stabilization. This approach has enabled theoretical understanding of the observed phenomena as well as rational construction of liposomes with improved stability or specifically designed interaction properties. Primarily, liposome properties are determined by their composition, which defines their membrane mechanics (elasticity, which is inversely proportional to membrane permeability) and surface properties, which in turn define interaction characteristics.

Despite the successes of several liposome drugs, major pharmaceutical companies have yet to embrace this promising technology (Lasic, 1998). Main reasons include: lack of reproducible production procedures which can be scaled up and applied under good manufacturing practice (GMP) conditions; minimal efforts devoted to sterility and

pyrogenicity; lack of means to obtain stable and therapeutic levels of drug loading in liposomes and especially in small liposomes; lack of suitable quality control assays.

Several companies are manufacturing and supplying apparatuses for liposome production and characterization. The most important of them include extrusion, homogenization, detergent dialysis, particle size analysis, and zeta potential.

Liposomes of different sizes and characteristics usually require different methods of preparation. The most common method for multilamellar vesicle preparation is hydration, in which solid lipids are dissolved in water at temperatures higher than their phase transition temperature. Thus formed multilamellar vesicles are usually in the range of several microns, have broad size distribution and poor stability. High energy input, such as sonicaion and extrusion, is required to reduce vesicle size down to hundreds of nanometers from these multilamellar vesicles. But with time small vesicles produced with this method tend to equilibrate back to their original state, e.g. large multilamellar vesicles (Barenholz 1994).

Recently, spontaneously formed unilamellar vesicles (ULVs) have attracted great interests for application as vehicles for drug delivery (Lee, 2002) and gene therapy (Gregoriadis et al., 1995; Maurer et al., 1999). Over the last decade or so, spontaneously forming ULVs have been observed in many cationic-anionic surfactant mixtures (Kaler et al., 1989, 1992; Murthy et al., 1991; Yatcilla et al., 1996; Villeneuve et al., 1999; Bergstrom et al., 1999; Bergstrom and Pedersen, 2000) and cationic surfactant systems (Viseu et al., 2000). Although some of them are believed to be thermodynamically stable, with low polydispersities, issues concerning biocompatibility and biodegradability must be considered for biologically relevant applications.

Phospholipids share many of the characteristics exhibited by surfactants. However, unlike surfactant systems, phospholipids are the main constituents of cell membranes, making them a promising group of materials suitable for engineering biocompatible systems. In the past, spontaneously formed ULVs were found in phospholipid mixtures composed of long- and short-chain lipids (Gabriel and Roberts, 1984; Ollivon et al., 2000). However, their stability, as a function of total lipid concentration, (Clp), and polydispersity were seldom studied. Other approaches used in obtaining monodispersed ULVs were either through micelle-to-vesicle transitions induced by a temperature jump (Andelman et al., 1994; Lesieur et al., 2000; Nieh et al., 2001, 2002) or through a simple dilution of the system (Schurtenberger et al., 1984, 1985; Egelhaaf and Schurtenberger, 1999). Regardless of the method, the average vesicle radius, $\langle Ro \rangle$, has always been found to vary as a function of Clp, an indication that ULVs were sensitive to their external environment. Two exceptions that we are aware of are an indirect measurement of a surfactant mixture composed of sodium dodecyl sulfate and didodecyldimethyl ammonium bromide reported by Marques et al. (1998) and a surfactant aqueous mixture of sodium oleate/octanol (Gradzielski et al., 1999).

Several theories of spontaneous ULV formation have been developed over the past few decades. Since the formation of ULVs from a symmetric bilayer (same chemical composition in both the outer and inner bilayer leaflets) costs energy (Israelachvili, 1992), entropy gain has usually been thought of as the main reason for the formation of stable vesicular structures. Safran et al. (1990, 1991) have shown that vesicles can be more stable than lamellar structures in the limit of large bending rigidity, kb, if the attractive interactions between the two surfactants in a mixture are sufficiently strong. On

the other hand, Bergstrom (1996, 2001) and Bergstrom and Eriksson (1996, 1998) have studied the stability of ULV in surfactant mixtures taking into account a variety of contributions to the system's total energy including geometrical packing, electrostatics, headgroup interactions, chain conformation, and mixing. Yuet and Blankschtein (1996a,b) have determined the size distribution of ULVs in surfactant mixtures based on a detailed molecular-thermodynamic model. Another study that has attempted to simultaneously tackle the theoretical and experimental issues was carried out by Oberdisse et al. (1996), Oberdisse and Porte (1997), and Oberdisse (1998) using the so-called "vesicle cell model" (VCM) to investigate the effect of charge density (ρ), dilution, salinity, and kb on the size of the ULVs.

Despite all of the above-mentioned studies, there is still no clear understanding of the factors affecting the vesicle size distribution in a given experimental situation. In addition, it has been shown that, at least in some cases, ULVs are not equilibrium structures, but are kinetically trapped (Marques, 2000; Leng et al., 2003).

Although microencapsulation with supercritical fluid processes and liposome systems have been briefly reviewed in this chapter, some of this material will be repeated in Chapters 3, 4, 5, 6 and 7 so that the research described in each of these chapters can stand on its own as a publishable research paper.

CHAPTER 3

MICROENCAPSULATION OF PARTICLES WITHOUT FUNCTIONAL MODIFICATIONS IN SUPERCRITICAL CO_2

In order for the research described in this chapter to stand on its own (as a publishable research paper), some of the pertinent prior work that has already been described in Chapter 2 may be repeated here.

3.1 Introduction

Polymeric particle coating finds wide applications in various important industries :pharmaceutical, food, fertilizer, cosmetics, electronic and biomedical, just to name a few. It is often a crucial industrial process in particle handling to enhance compatibility, flowability, wettability and dispersibility, or to serve as a barrier for controlled release or masking (Pfeffer, et al. 2001). Conventional polymeric particle coating usually involves solution chemistry and the use of a large amount of organic solvents may raise serious air and water pollution concerns. Therefore, effective and clean coating methods are of strong interest.

There has been a continuing growth of interest in replacing conventional organic solvents with environmentally friendly supercritical fluids in chemical processes. Among them, supercritical carbon dioxide ($scCO_2$) emerged as an excellent candidate due to its superb characteristics and properties: it is inexpensive, nontoxic, nonflammable, readily available, easily recycled, and as a solvent, it possesses both gas-like diffusivities and liquid-like densities and solvencies. Successes in applying $scCO_2$ as a solvent or

processing medium have been found in various areas from the well-established supercritical extraction and separation to the relatively new engineered particle formation (Yeo, et al. 1993). One area that has seen very much progress is polymer synthesis and processing (Cooper, et al. 2000).

From the aspect of processing, polymers can be fractionated, purified, impregnated or foamed by using $scCO_2$ as a processing solvent. One of the recent interesting applications is coating of particles with polymers via rapid expansion of supercritical solution (RESS) or via a supercritical antisolvent (SAS) process (Wang, 2002, 2004). In the RESS process, dissolved polymers precipitate out after CO_2 depressurization, while in the SAS process, the solvents that initially dissolve the polymers are extracted by $scCO_2$, and the polymers precipitate on the surface of the host particles. Because many polymers exhibit low solubility in $scCO_2$, organic solvents are often used as either solvents (in SAS) or co-solvents (in RESS), which may cloud the environmental benefit of using $scCO_2$. In addition, homogeneous and complete encapsulation is often difficult to achieve.

In the area of polymer synthesis, following the seminal work of fluoropolymer synthesis in $scCO_2$ by DeSimone et al. in 1992, many common polymers were produced using $scCO_2$ as the reaction medium. Dispersion polymerization, an important industrial process, is one of the most studied methods for polymer synthesis in $scCO_2$. It features an initially homogeneous solution reaction, where monomer, initiator and surfactant are all dissolved in a solvent. The system becomes heterogeneous once the molecular weight of the polymer exceeds the solubility limit and polymer precipitates. The polymers produced by this method usually form spherical particles with a size range between 100nm to

10μm. Exploiting the favorable transport properties and controllability of the reaction in $scCO_2$, researchers have synthesized many important vinyl polymers using dispersion polymerization.

In this paper, we present a new coating method based on the principles of dispersion polymerization in $scCO_2$. Common filler material, Dechlorane Plus® 515 (DCR) particles, with an average size of 12μm were chosen as model host particles and were introduced into the high pressure coating vessel. Poly(methyl methacrylate) (PMMA) and water-soluble poly(1-vinyl-2-pyrrolidone) (PVP) were synthesized in-situ via dispersion polymerization in $scCO_2$ during the coating process.

It is found that the new coating method is efficient for selected systems. Uniform encapsulation was obtained even at low polymer to particle weight ratio and the coated particles exhibited good flowability. In the presence of excessive monomer, polymer particles either coagulated and attached to the polymer-coating layer or precipitated out as loose agglomerates. On the other hand, when a small amount of monomer was used, thin film coating was achieved. The coating thickness and morphology can be controlled by changing process parameters including the monomer to particle weight ratio, reactor pressure, and the concentrations of the surfactant stabilizer and initiator. The effects of the process parameters will be discussed individually in the Results and Discussions section.

3.2 Experimental Section

3.2.1 Materials and Equipment

Dechlorane Plus® 515 particles from Occidental Petroleum Corporation, an aliphatic chlorine-containing crystalline organic compound (Figure 3.1), in the form of free-flowing powders were used as the host particles without further processing. The melting temperature of Dechlorane is 350°C. Methyl methacrylate (MMA), 1-Vinyl-2-pyrrolidone (2-VP), poly (dimethyl siloxane) methacrylate (PDMS-MA) (Figure 3.1) and 2,2'-Azobisisobutyronitrile (AIBN) were obtained from Sigma-Aldrich and were used as received. Carbon dioxide gas was purchased from Matheson with 99>% purity.

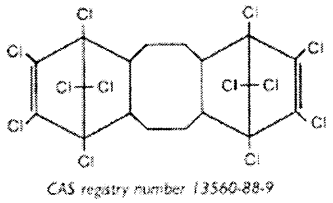

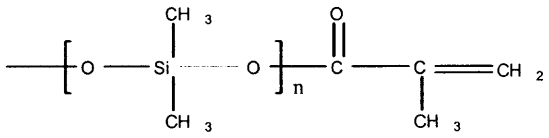

Figure 3.1 Molecular structures of Dechlorane Plus® 515 (upper) and PDMS-MA macromonomer (lower).

The experiment setup is shown in Figure 3.2 and consists of a 25-ml Parr Instruments high-pressure reactor vessel with two sapphire windows at both ends. There are four openings on the reactor side walls which are designed for the thermocouple, pressure transducer and safety disc, inlet for reactant and CO_2 injection, and outlet for CO_2. The thermocouple and pressure transducer were connected to Watlow panel meters

for digital readout. The reactor pressure was manually controlled by pumping or releasing CO_2 through the inlet/outlet. Electric silicon rubber heating tape was wrapped around the reactor and the temperature was controlled by changing the voltage applied to the heating tape.

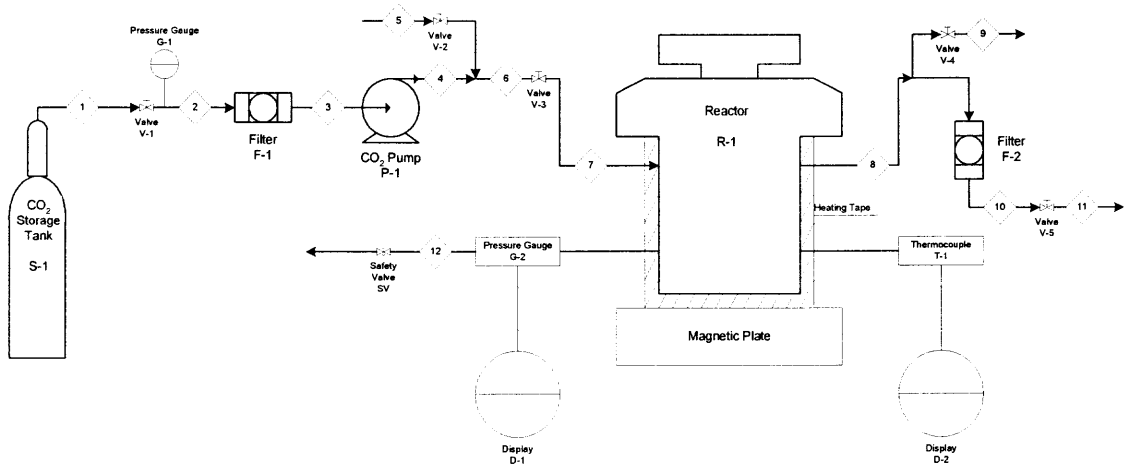

Figure 3.2 Schematic diagram of the high-pressure reaction system used in this study.

3.2.2 Procedure

Coating via polymerization-induced phase separation was conducted in the high-pressure reaction vessel. During polymerization, AIBN acts as free-radical initiator and PDMS-MA functions as a surfactant. The structure of PDMS-MA and the schemes of reactions are shown in Figure 3.1 and Scheme 1, respectively. All components were premixed and charged into the reactor followed by purging with low-pressure CO_2 gas. After purging, liquefied CO_2 was pumped into the reactor by a Haskel Air Driven pump at room temperature until an appropriate pressure was reached. An experimentally determined CO_2 T-P diagram was used to project the initial load pressure at room temperature to the desired final pressure at the reaction temperature (Figure 3.3). Before the reaction started, the monomer, surfactant and initiator were all dissolved in CO_2 and the heavy

DCR particles stayed at the bottom of the vessel during the reaction. No stirring was applied to suspend the DCR particles in $scCO_2$ since the DCR particles are loosely packed and the high diffusivity of the reactant in supercritical CO_2 reduces spatial inhomogeneity in the void spaces among the DCR particles. Repeated experiments were conducted to show that there was no significant difference in the results with and without stirring.

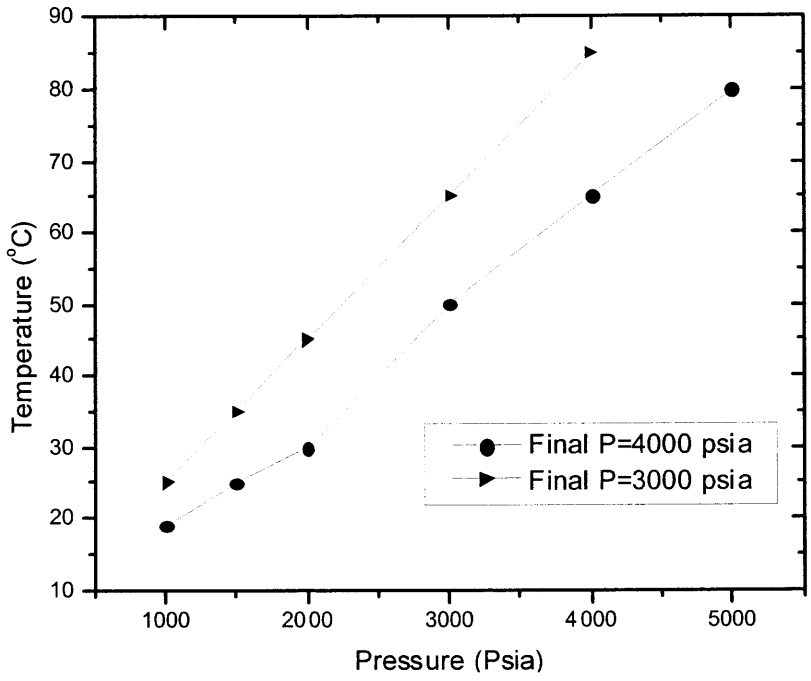

Figure 3.3 Experimentally determined T-P diagram at two different final pressures. The initial load pressure at room temperature is determined from this diagram.

The vessel was then heated to 65°C to initiate the free-radical polymerization and the pressure reached its desired final value. The reactor remained closed during the experiment and a decrease in pressure of 100~200 psia due to volume shrinkage from the polymerization was observed after the reaction completed. Most of the experiments were run for 48 hours (reaction time) after which CO_2 was released and the reactor was cooled down to room temperature followed by sample collection.

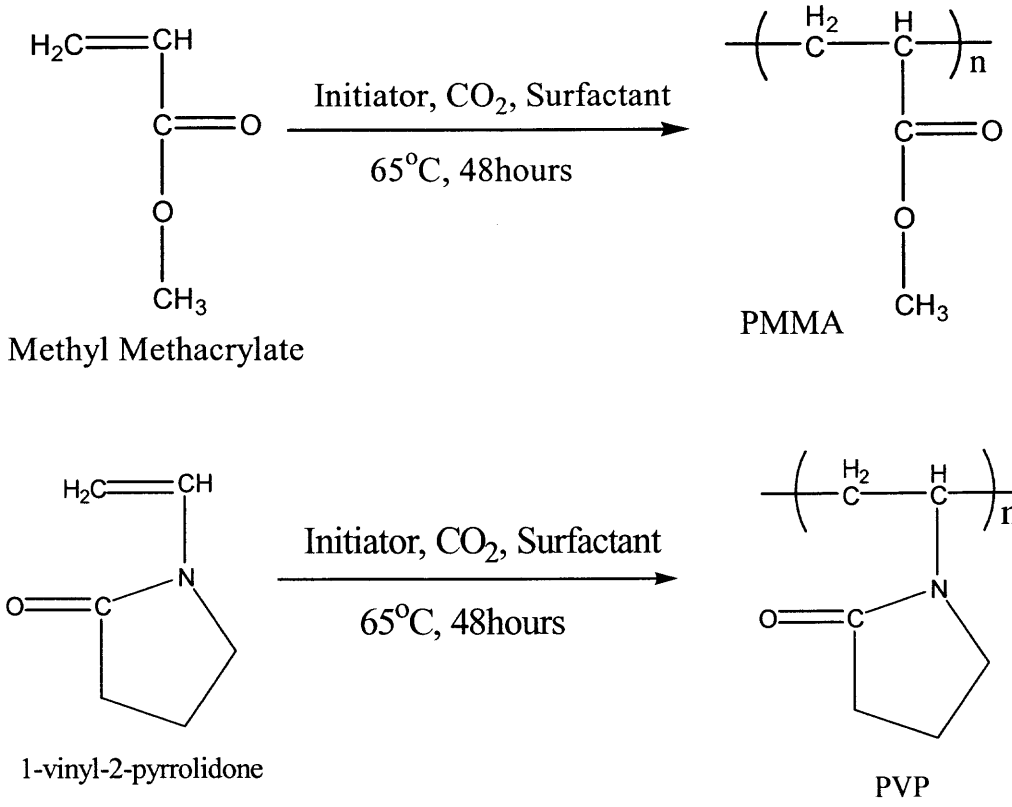

Scheme 3.1 Polymerization of methyl methacrylate (MMA) and 1-Vinyl-2-pyrrolidone (2-VP) in supercritical CO_2.

3.2.3 Characterization

The homogeneity of coating and the morphology of the polymer were examined with a LEO32® field emission scanning electron microscope (FESEM). Specimens were coated with a thin carbon film before FESEM characterization. The mass of coated polymer on the DCR particles' surface was determined by thermogravimetric analysis (TGA) using a NETZSCH STA409PC LUXX® thermal analyzer. O_2 was supplied during the TGA experiment and a heating rate of 5°C/min was applied until the maximum temperature of 500°C was reached. A Beckman Coulter LS-230® particle size analyzer was used to measure the particle size distribution before and after coating. Samples were first

dispersed in ethanol and were sonicated in a water bath for half an hour to break the loose agglomerates before each measurement.

3.3 Results and Discussions

3.3.1 Dispersion Polymerization in $scCO_2$

We first examine our synthesis results of PMMA and PVP via dispersion polymerization in $scCO_2$. Synthesis of PMMA has been reported by many groups under different conditions (Desimone 1992, Shiho 2000); however, synthesis of PVP has been reported only by DeSimone et al. in 2000. The progress of the reaction was monitored visually through two sapphire windows on the reactor with the help of an illuminating light source. Initially, the reaction medium was transparent with observable traces of strong convective motions. Approximately two hours after the reaction condition was reached, the turbidity of the medium started to increase slowly. After four hours, there was no light penetrating through the reaction medium and a milky-white appearance similar to conventional aqueous latex was observed in the areas close to the windows. However, no particle precipitation was observed until a few hours later - depending on the initial monomer concentration. After the reaction completed, polymer in the form of free-flowing white powders were collected. The sizes of the polymer particles in this study were found to be in the range of a few hundred nanometers. Figures 4 (a) and (b) are SEM micrographs of typical PMMA and PVP particles obtained in our experiments. The reaction conditions are listed in Table 3.1.

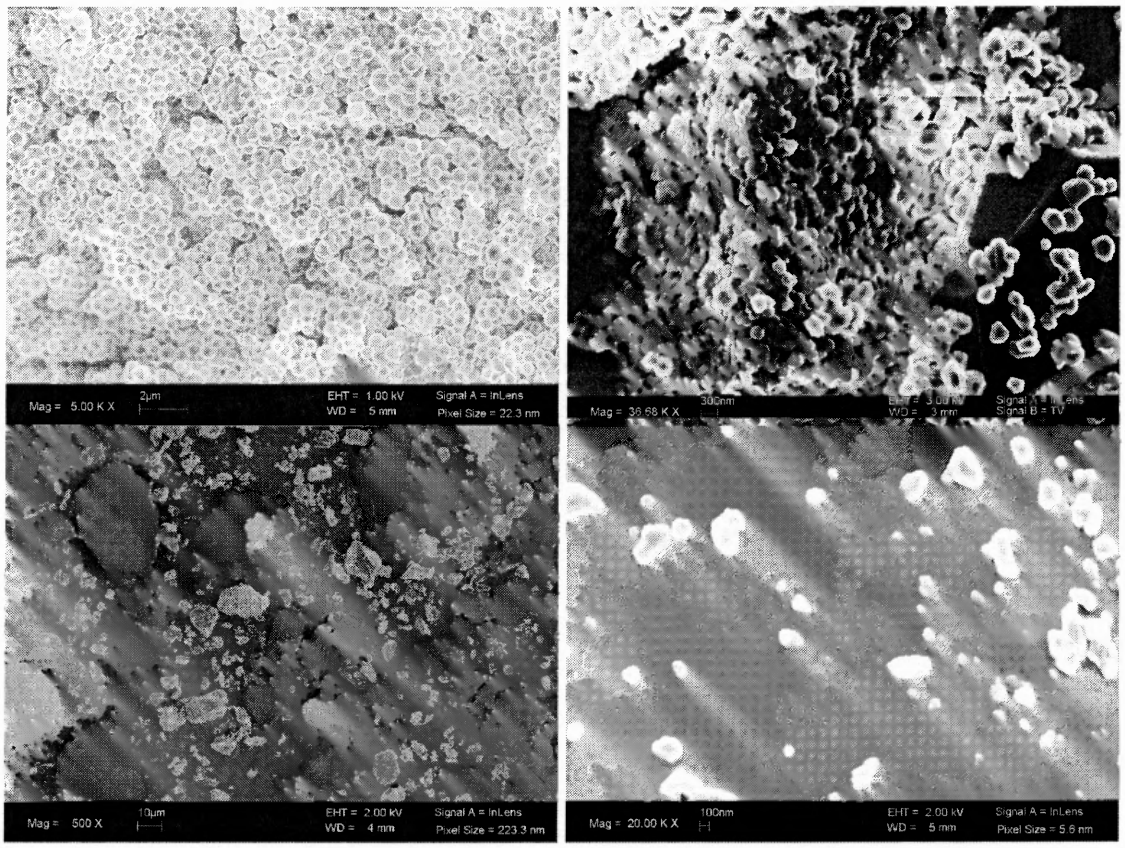

Figure 3.4 SEM micrographs of (a) aggregated PMMA particles synthesized in $scCO_2$ under reaction condition 1, (b) aggregated PVP particles synthesized in $scCO_2$ under condition 13, (c) uncoated DCR 515 particles showing crystalline morphology, and (d) bare surface of DCR before coating.

It has been well accepted that in dispersion polymerization, phase separation of polymer in the medium occurs almost immediately after the reaction starts with a very low conversion (Li, et al. 2000). The main production of polymer will then shift to sites in the dispersed polymer domains, which are stabilized by stabilizers such as block copolymers or macromonomers. Given an initial monomer concentration, the number density of polymer particles depends on the initiator concentration and the extent of stabilization. Flocculation before depressurization or coagulation after depressurization may occur as a consequence of insufficient stabilization. Lowering the pressure of $scCO_2$ or decreasing the monomer concentration may decrease solvency to the "tails" of the

stabilizers and therefore reduce steric repulsion. In general, higher surfactant concentration and higher initiator concentration or lower monomer concentration leads to smaller polymer particles.

Table 3.1 Reaction Conditions for Particle Encapsulations. Entries 1-11 are Conditions for PMMASsynthesis and Coating, while 12 and 13 are for Poly(1vinyl-2-pyrrolidone) Synthesis and Coating

Entry	DCR (g)	Monomer (ml)	AIBN (g), % in MMA	Surfactant (ml), % in MMA	Pressure (psia)
1	0	2	0.04, 2%	0.40 20%	4000
2	1	2	0.04, 2%	0.40 20%	4000
3	1	2	0.04, 2%	0.04, 2%	4000
4	1	2	0.04, 2%	0.00, 0%	4000
5	1	1	0.02, 2%	0.20 20%	4000
6	1	1	0.02, 2%	0.20 20%	3000
7	1	1	0.02, 2%	0.20 20%	2000
8	1	0.5	0.01, 2%	0.10 20%	4000
9	1	0.33	0.01, 3%	0.05, 17%	4000
10	1	0.2	.004, 2%	0.04 20%	4000
11	1	0.2	0.04 20%	0.04 20%	4000
12	0	2	0.04, 2%	0.40 20%	4000
13	1	1.5	0.03, 2%	0.30 20%	4000

3.3.2 Coating with Dispersion Polymerization

In addition to homogeneous nucleation in dispersion polymerization, introducing inert fine DCR particles to the reactor may induce heterogeneous nucleation. It will be shown later that polymerization occurred simultaneously on the surface of DCR particles, where small nucleated polymer domains on the surface expanded through polymerization and developed into an encapsulating layer. This mechanism of polymer growth is more likely a precipitation polymerization compared to conventional dispersed polymerization according to the following three aspects: first, the reaction sites are constrained on the immobile solid substrates instead of the dispersed polymer particles wandering throughout the medium; second, the specific area is much smaller; and third, the role of

stabilizers is different. The final size, appearance, and degree of coagulation of polymer particles produced in dispersion polymerization depend strongly on the efficiency of stabilization; such dependence is much less sensitive in precipitation polymerization.

As will be demonstrated later, the final morphology on the host particles depends on the deposition and coagulation of the dispersed polymer particles, followed by possible plasticization and fusion of the deposited polymer particles. If an excessive amount of dispersed polymer particles are produced, the coating morphology exhibits a rough surface consisting of coagulated small polymer particles. On the other hand, a lean polymer production leads to smooth thin-film coating. Fusion of polymer particles due to plasticization under high $scCO_2$ pressure leads to a smoother morphology; however, strong stabilization may hinder fusion. A detailed discussion of the effects of several process parameters including monomer concentration, reaction pressure, stabilizer concentration, and initiator concentration is presented below.

1) Effect of monomer concentration. In this study, the reactions were conducted at five different MMA (ml) /DCR (g) ratios: 2/1, 1/1, 1/2, 1/3 and 1/5 to study the effect of monomer concentration. Reaction conditions were listed in Table 1. Figures 4 (c) and (d) are SEM micrographs of bare DCR particles before coating which featuring crystalline facets and smooth surfaces. SEM micrographs of the coated products were shown in Figures 5 (a)-(j) in which the coating thickness decreased dramatically with decreasing MMA/DCR ratio, accompanied by certain morphological changes. When the MMA/DCR ratio was 2/1 (Figures 5(a) and (b)), DCR particles were covered by thick layers of coagulated PMMA particles with excessive PMMA particles or agglomerates scattered around. Reducing the monomer concentration to 1/1 ratio (Figure 3.5 (c) and

(d)) caused separate PMMA particles to undergo coagulation and fusion into the PMMA layer on the DCR surface. These micrographs indicate that PMMA was synthesized simultaneously through dispersion and precipitation polymerizations. Polymer particles formed via dispersion polymerization had the tendency to aggregate on the polymer layer developed on the surface of DCR. $ScCO_2$-plasticization facilitated fusion of the coagulated polymer particles and increased the coating thickness.

When the ratio is decreased to 1/2 (Figure 3.5 (e) and (f)), film coating with smooth morphology and complete coverage was observed. There is, however, some trace amount of incomplete fusion of PMMA particles into the coated polymer layer. For the ratios of 1/3 and 1/5 (Figures 5 (g)-(j)), only smooth thin-film coating with a reduced thickness was observed; no separate particles were observed. The micrographs indicate that higher monomer concentration favors the formation of polymer particles since dispersion polymerization has a higher reaction rate as compared to precipitation polymerization. It is also evident that plasticization of PMMA in $scCO_2$ facilitates the formation of a smooth coating surface via fusion of the attached polymer particles. The smooth morphology observed at low monomer concentration may result from a decrease of solvency to the stabilizer and therefore a decrease in stabilization power, which enhances the rate of fusion.

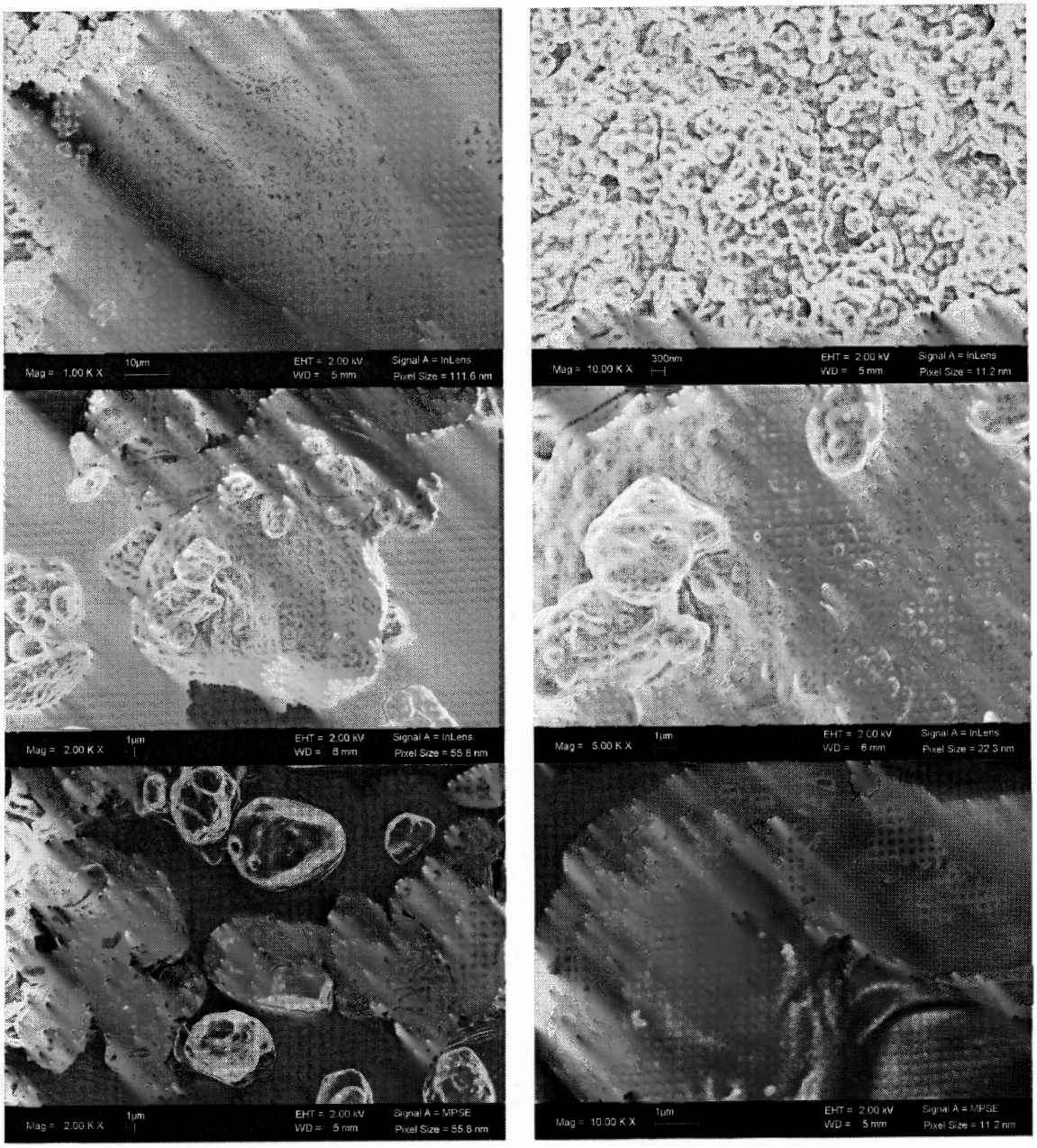

Figure 3.5 SEM micrographs of PMMA-coated DCR particles show the effect of MMA to DCR ratio on coating morphology. Images in the right column are the magnified surface features of the left. Significant morphology changes were observed at different MMA/DCR ratios. MMA/DCR =2/1 (a, b); 1/1 (c, d); 1/2 (e, f); 1/3 (g, h); 1/5 (i, j), respectively.

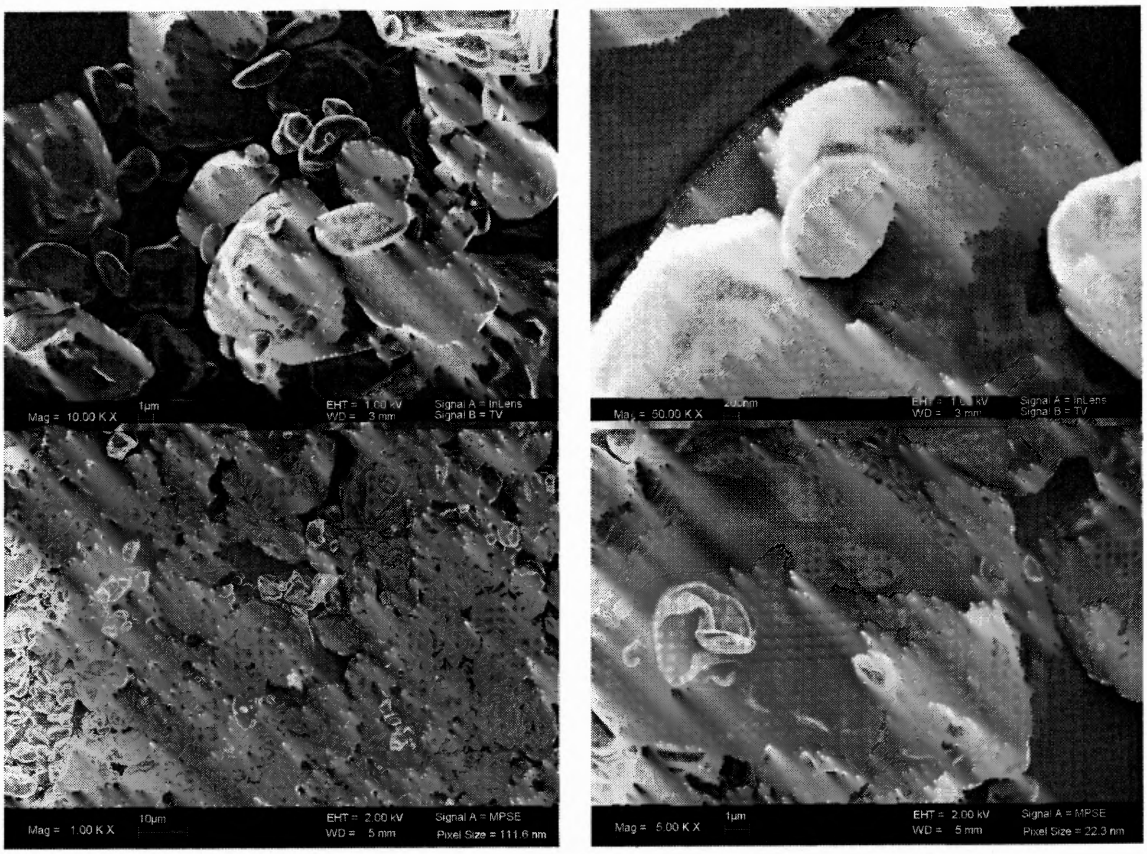

Figure 3.5 (continued) SEM micrographs of PMMA-coated DCR particles show the effect of MMA to DCR ratio on coating morphology. Images in the right column are the magnified surface features of the left. Significant morphology changes were observed at different MMA/DCR ratios. MMA/DCR =2/1 (a, b); 1/1 (c, d); 1/2 (e, f); 1/3 (g, h); 1/5 (i, j), respectively.

The approximate mass of PMMA in each sample was measured using Thermal Gravimetric Analysis (TGA). As seen in Figure 3.6, the decomposition temperature for DCR was found at 350°C, in agreement with the reported data. We used this temperature as the reference point to determine the polymer content in coated DCR particles. Samples from MMA/DCR ratios of 2/1, 1/1, 1/2 and 1/5 were tested; a sample at a ratio of 1/2 prepared without surfactant was also tested. Taking into account a 15% residue left at T=350°C for pure PMMA, the calculated mass percentages of PMMA in coated samples are 67%, 44%, 24% and 5% for MMA/DCR ratios of 2/1, 1/1, 1/2 and 1/5, respectively. Considering the density of MMA = 0.94g/ml and the amount of MMA

placed in the reactor, the corresponding polymerization yields at these four ratios are approximately 100%, 78%, 63% and 26%. The calculated polymerization yields at high MMA/DCR ratios (2/1, and 1/1) are within the typical range for pure PMMA synthesized in dispersion polymerization under similar reaction conditions. This implies that most of the polymer was formed in the $scCO_2$ and then attached to the DCR particles. The yield for the lowest MMA/DCR ratio 1/5 is smallest (26%). From Figures 5 (i) and (j), it suggests that the lower the MMA/DCR ratio, the more prevalent the precipitation polymerization is. On the other hand, dispersion polymerization is dominant when the monomer concentration is high.

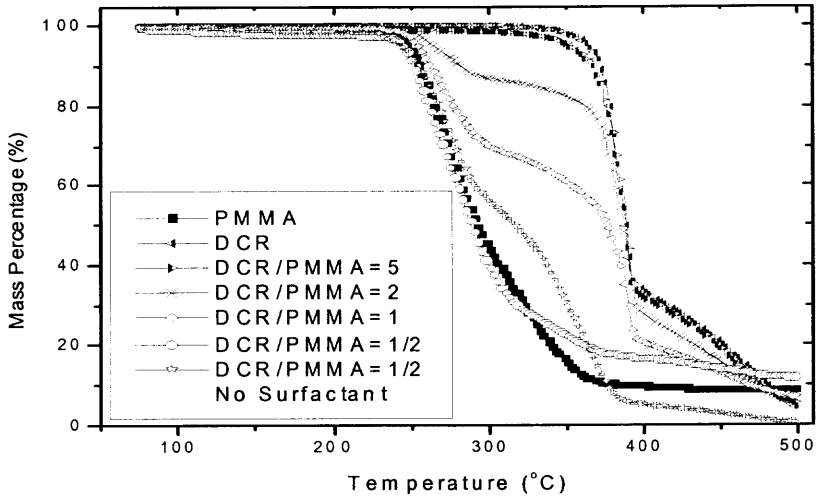

Figure 3.6 TGA analysis for samples from four different MMA/DCR ratios: 2/1, 1/1, 1/2 and 1/5.

Figure 3.7 shows the particle size distribution obtained from light scattering (Beckman Coulter LS-230®) as an indication of the agglomeration of DCR particles. The average particle diameter increased from 12 μm for the bare DCR to 19 μm, 23 μm, and 39 μm of the coated DCR at the MMA/DCR ratios of 1/5, 1/2, and 1/1, respectively. The increase in the average particle size is obviously due to coating and coating-induced agglomeration, as shown in the SEM micrographs.

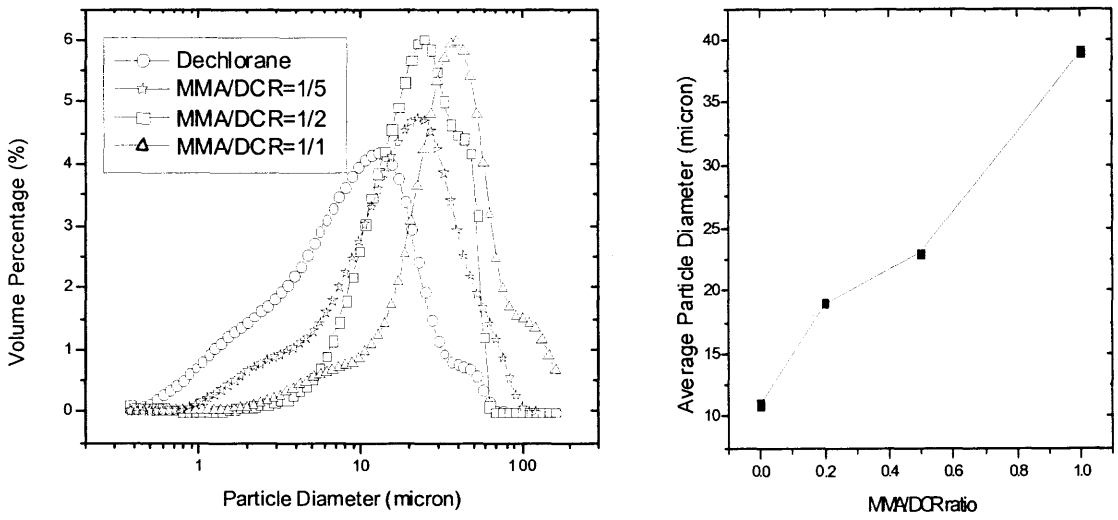

Figure 3.7 Particle size distributions and average sizes from four different MMA/DCR ratios: 0/1, 1/1, 1/2 and 1/5. As shown in (a) the peak position of particle diameter shifts to the right as polymer amount increases. Average sizes at three ratios are given in (b).

Based on the information obtained from TGA, and the average size of the agglomerates obtained from particle size analysis, we can make a rough estimate of the coating thickness. Assuming *all* the bare DCR particles are spherical with a "*uniform*" effective radius r_o =6 μm and a "*uniform*" effective radius r_1 after coating, the weight percentage x(%) of PMMA obtained from TGA can be expressed as:

$$\chi = \frac{\left(r_1^3 - r_o^3\right)\rho_P}{r_o^3\rho_D + \left(r_1^3 - r_o^3\right)\rho_P} \tag{3.1}$$

where the densities of PMMA and DCR are $\rho_P = 1.2g/cm^3$ and $\rho_D = 1.8g/cm^3$, respectively.

After rearrangement, the average radius of a coated DCR particle is given as:

$$r_1 = r_o\left[\frac{\chi\left(\frac{\rho_D - \rho_P}{\rho_P}\right) + 1}{1 - \chi}\right]^{\frac{1}{3}} \tag{3.2}$$

and the coating thickness t:

$$t = r_1 - r_o = r_o \left\langle \left[\frac{\chi\left(\frac{\rho_D - \rho_P}{\rho_P}\right) + 1}{1 - \chi} \right]^{\frac{1}{3}} - 1 \right\rangle \tag{3.3}$$

The average agglomeration number N of the DCR particles can then be estimated as:

$$N \approx \left(\frac{R}{r_1} \right)^3 \tag{3.4}$$

where R is the mean radius of the agglomerates obtained from particle size analysis.

The results calculated from Eqs. (2)-(4) are listed in Table 3.2, where the agglomeration number increased with the increasing amount of polymer. This estimation is by no means accurate; nevertheless, it indicates only mild agglomeration formed in our process, as also attested by the SEM images. It is important to note that complete and uniform encapsulation can be achieved through our process and the layer thickness and morphology can be adjusted by changing the monomer concentration. This is very difficult to achieve for other supercritical processes such as SAS or RESS.

Table 3.2 Estimate of Particle Size, Coating Thickness and Degree of Agglomeration at Three Different MMA/DCR Ratios

MMA/DCR Ratio (ml/g)	PMMA content (%)	Diameter of coated DCR agglomerates (μm)	Mean Radius of Individual Coated Particle (μm)	Coating Thickness (μm)	Degree of Agglomeration
1/1	44	39	7.7	1.7	16
1/2	24	23	6.7	0.7	5
1/5	5	19	6.3	0.3	3

2) Effect of CO_2 Pressure. One of the most appealing features of using $scCO_2$ as a reaction or processing medium is that the solvent strength and density can be tuned by changing the temperature or pressure. This unique feature allows one to control the solvent properties for polymerization coating. In addition, the plasticization in high-

pressure $scCO_2$ can significantly lower the glass transition temperature and facilitate the formation of a smooth morphology.

Figure 3.8 shows SEM micrographs of DCR coated with MMA/DCR=1/1 at three different pressures: 4000, 3000, and 2000 psia. At P=4000psia, the morphology (shown in Figures 8 (a) and (b)) exhibited residues of PMMA particles that underwent fusion into the encapsulating layer. When the pressure is reduced to 3000 psia, small PMMA particles aggregated on the surface of polymer layer as shown in Figures 8 (c) and (d). The effect of plasticizing was not as obvious compared to the case of P=4000 psia. Further lowering the pressure to 2000 psia, resulted in many scattered polymer aggregates with irregular shapes and widely distributed sizes collected along with the DCR particles (Figures 8(e) and (f)). This is due to poor stabilization under low pressure. The magnified micrograph in Figure 3.8 (f) shows uneven polymer coating with coagulated polymer particles manifesting limited plasticizing at low pressure.

Surfactant stabilizer plays a vital role in dispersion polymerization. It has been reported that increasing surfactant concentration results in a smaller average size of dispersed polymer particles and an increase of particle number density [17]. The yield of polymerization is also found to be lower in an un-stabilized system than in a stabilized system, as confirmed by our TGA analysis in Figure 3.6. Since there have been extensive studies on the effect of stabilizer concentration on polymer property, only the effect on coating morphology is addressed here.

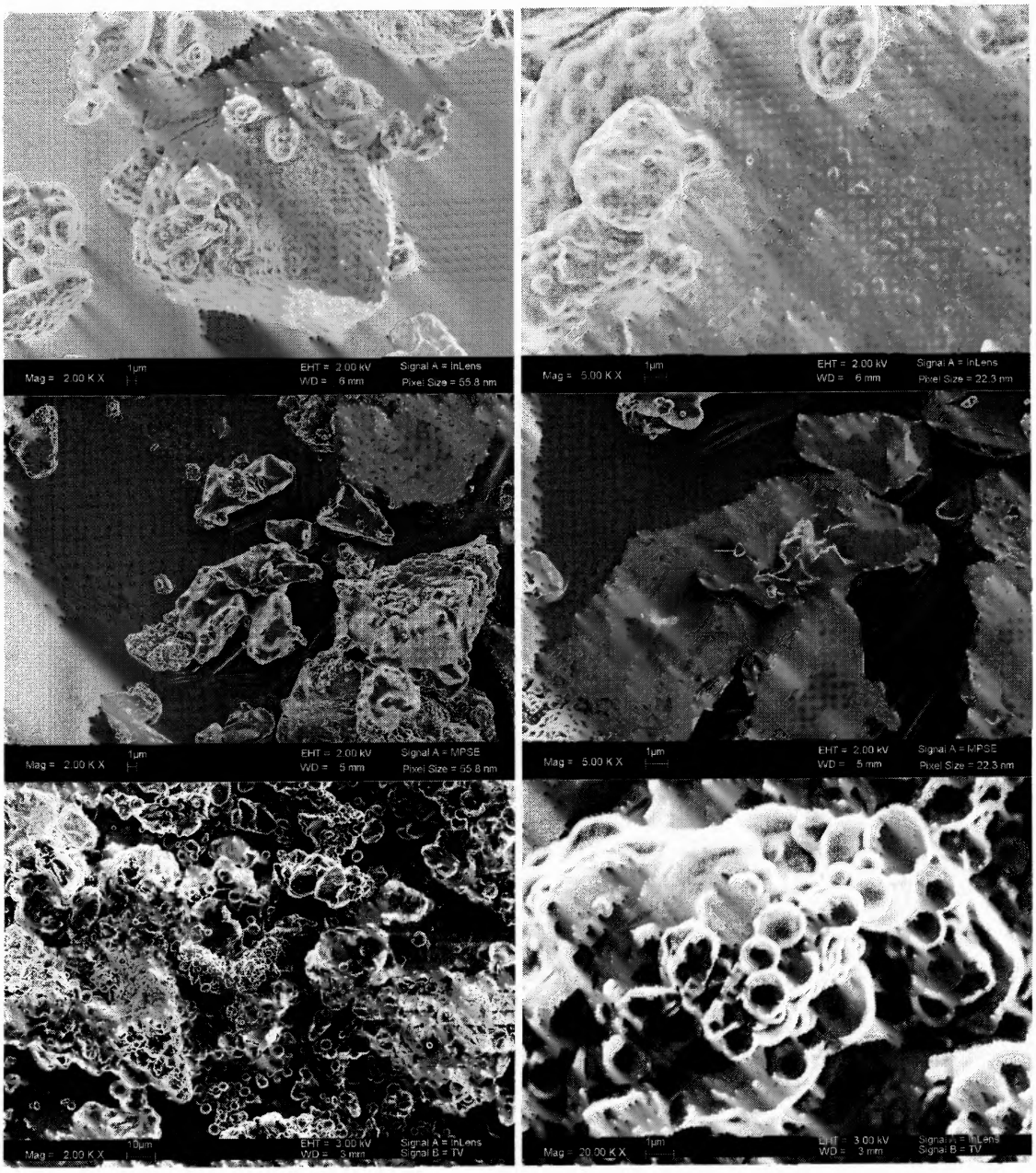

Figure 3.8 SEM micrographs of PMMA coating at three different pressures: 4000 (a, b); 3000 (c, d); and 2000 (e, f) psia. The MMA/DCR ratio=1. Images in the right column are the magnified surface features.

3) Effect of Stabilizer concentration. Figure 3.9 depicts the coating morphology at three PDMS-MA to MMA ratios: 20 vol%, 2 vol% and 0 vol% under conditions of P=4000 psia and MMA/DCR ratio=2/1. The SEM micrographs show that higher stabilizer concentration results in higher number density of polymer particles and less flocculation

and fusion of polymer particles on the surface of DCR. In Figure 3.9(a) and (b), excessive polymer particles aggregate together resulting in a rough morphology on the surface of DCR. As the PDMS-MA concentration is lowered to 2 vol%, the surface morphology is smoother. However, scattered polymer particles with a wide size distribution and irregular shapes are also observed which denotes insufficient stabilization in dispersion polymerization (Figure 3.9(c)). Figure 3.9(d) shows some incomplete fusion of attached particles on a much smoother surface compared to Figure 3.9(b). Strikingly, when no stabilizer is used, PMMA cannot be coated on DCR, as depicted in Figures 9 (e) and (f), where large PMMA particles are scattered around the bare DCR host particles. This observation suggests the necessity of stabilization during nucleation and growth of polymer domains on the surface of DCR; the role of the surfactant stabilizer may not be solely for providing steric repulsion but for facilitating surface precipitation polymerization.

4) Effect of the Initiator Concentration. Theory in Initiator molecules break into free radicals and initiate polymerization once the temperature is raised to a certain level. Increasing initiator concentration produces more free radicals and thus more nucleation sites are created. Figure 3.10 shows the SEM micrographs of the coating for two initiator (I) to MMA ratios at 2 wt% and 20 wt% under conditions of MMA/DCR=1/5 and P=4000 psia. It is found that uniform thin-film coating was achieved at both the low and high initiator concentrations. However, under higher initiator concentration (20%), small PMMA particle aggregates were observed on the coated surface (Figures 10 (c) and (d)). This is in agreement with the established dispersion polymerization that the number density of PMMA particles increases with the initiator concentration.

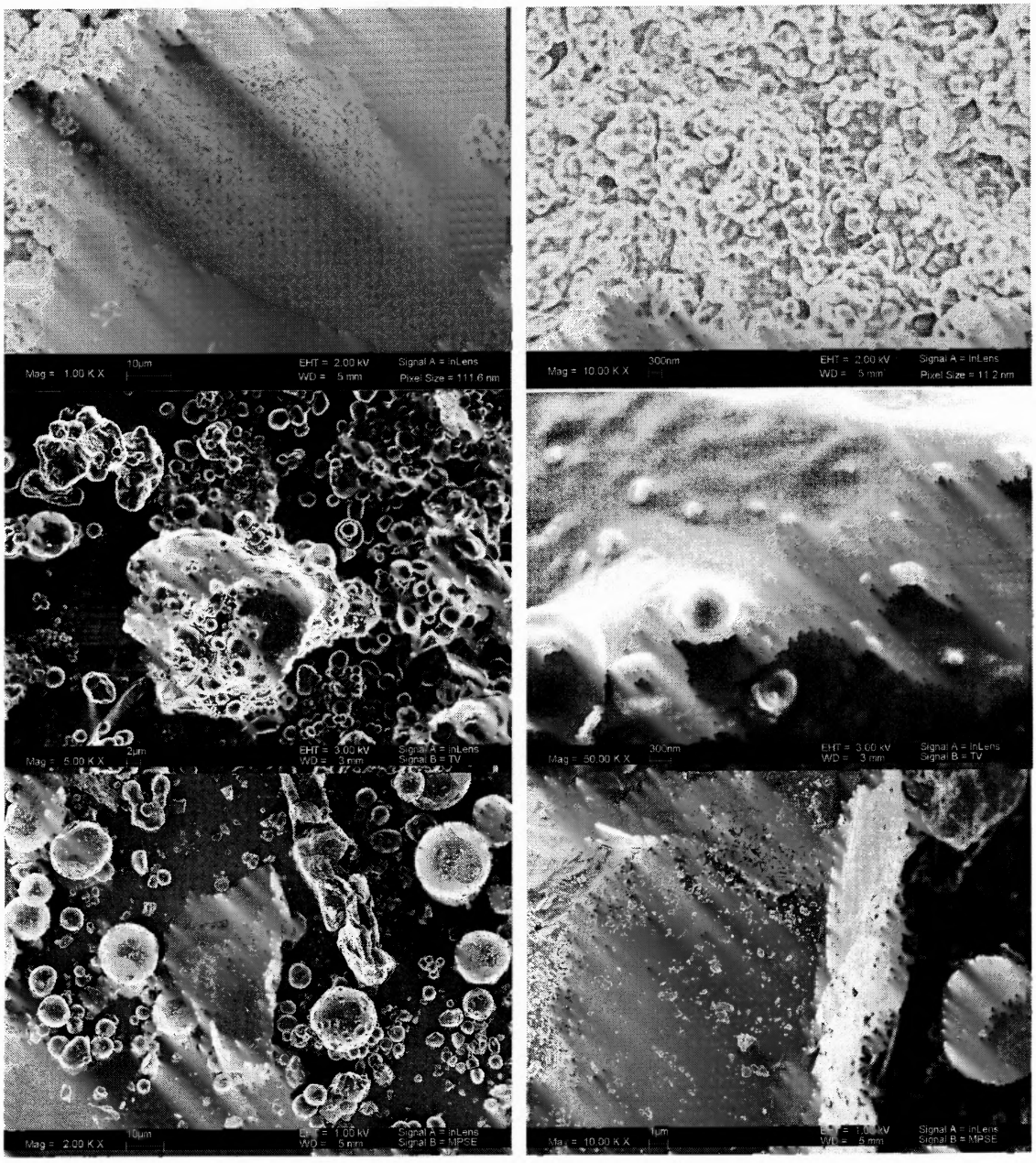

Figure 3.9 SEM micrographs of PMMA coating show the effect of surfactant concentration on coating morphology. PDMS-MA/MMA =20 (a, b); 2 (c, d); and 0 (e, f) vol% respectively. The MMA/DCR ratio=2. Images in the right column are the magnified surface features. Note that no coating was observed when no surfactant was applied.

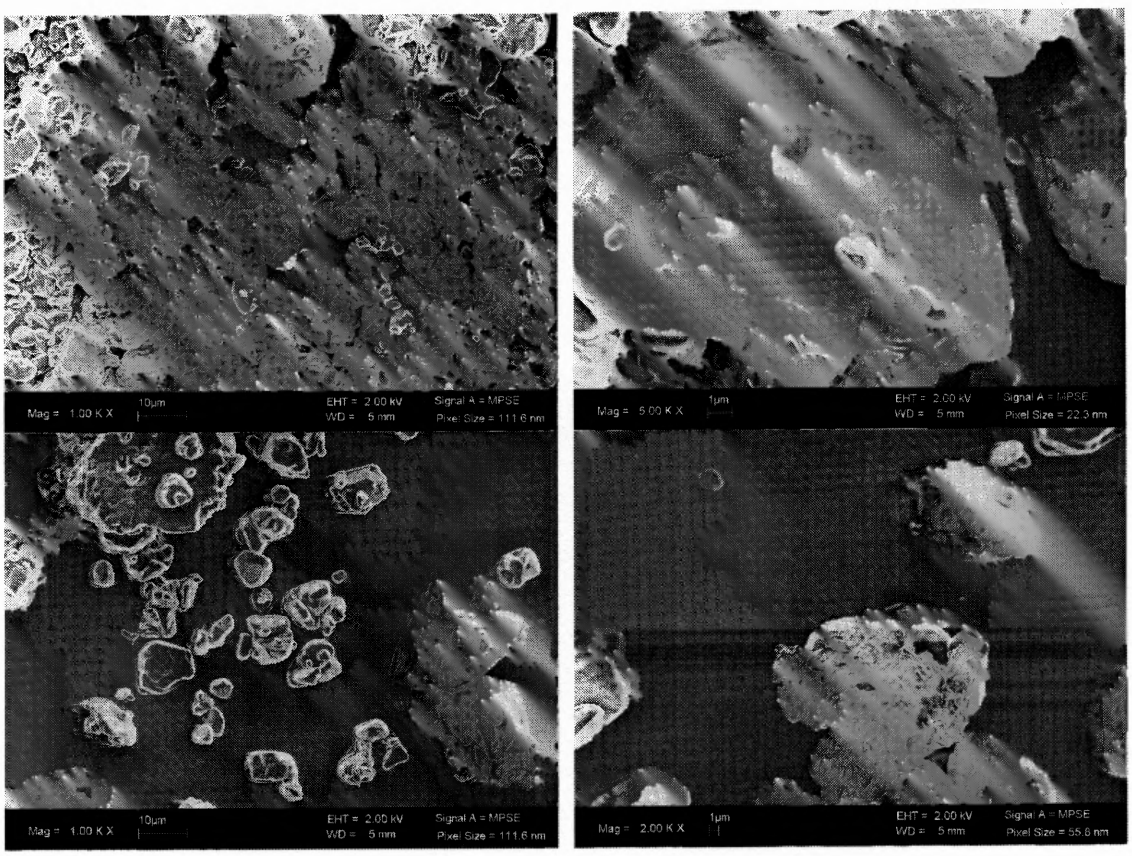

Figure 3.10 SEM micrographs of PMMA coating show the effect of initiator concentration on coating morphology. The MMA/Dec ratio=1/5. I/MMA= 2 (a, b), 20 (c, d) wt. % respectively. Though excessive initiator may produce very small PMMA particles attached to DCR surface (as shown in (c) and (d)), most coated areas are smooth and uniform.

3.3.3 Coating Mechanism from Molecular Weight Distribution

Under the same condition, polymers synthesized from dispersion and precipitation polymerization should have significant difference in molecular weight. To verify the hypothesis of coexistence of dispersion and precipitation polymerization during the coating process, PMMA was extracted with THF from the coated particles and analyzed with Gel Permeation Chromatography (GPC). The results were listed in Table 3.3. Bimodal distribution observed above serves as an indirect evidence of coexistence of dispersion and precipitation.

Table 3.3 GPC Results for PMMA Extracted From the Coated DCR Particles

Entry	MMA/DCR Ratio	Mn1	PDI1	Mn2	PDI2	Morphology from SEM
1	Pure PMMA	95,559	2.59	X	X	PMMA Particles
2	2/1	63,213	1.36	11,861	1.01	Particle & Film Coating
3	1/1 (4000 psi)	45,884	1.17	11,857	1.04	Particle & Film Coating
4	1/1 (3000 psi)	62,667	1.28	12,544	1.05	Particle & Film Coating
5	1/1 (2000 psi)	103,031	3.94	12,030	1.02	Particle & Film Coating
6	1/2	125,331	1.38	11,957	1.07	Particle & Film Coating
7	1/3	X	X	12,325	1.16	Film Coating
8	1/5	X	X	12,789	1.19	Film Coating

Note: Mn1 means number based molecular weight average from the first peak. PDI1 means polydispersity from the first peak. X means data negligible.

3.3.4 Coating with PVP

To test the effectiveness and expandability of our encapsulating method, a common water-soluble polymer and pharmaceutical excipient, poly(1-vinyl-2-pyrrolidone) (PVP) was synthesized for encapsulating DCR using the same surfactant. As shown in Figure 3.11, monodisperse submicron-sized PVP particles were synthesized under the condition of VP/DCR=1.5/1, AIBN=2% and P=4000psia. Similar to the coating of PMMA, PVP formed a complete and smooth coating layer on the DCR surface. Nevertheless, separate PVP particles were in loose physical contact with the coated PVP layer or with other PVP particles. Some of the PVP particles detached from the coated PVP layer and left clear dented markes (Figure 3.11(b)). The observed morphology suggests that the PVP particles were well protected by the stabilizers. Figures depict the evidence in support of our hypothesis that parallel polymerizations (dispersion vs. precipitation) occurred simultaneously in the beginning of the process, followed by possible deposition and coagulation of particles onto the surface of the host particles. The final morphology of the coating should be tuned with the process variables mentioned above.

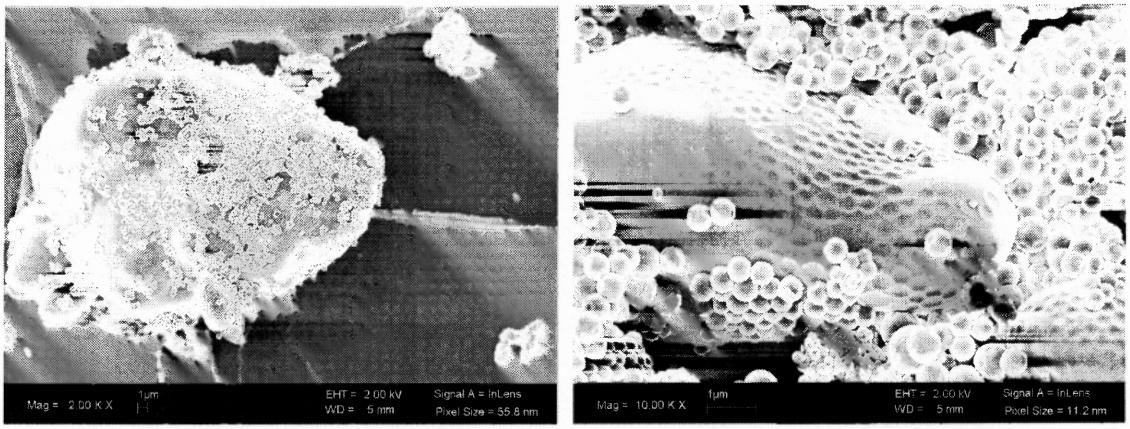

Figure 3.11 SEM micrographs of coating of DCR with PVP. A thick and smooth PVP layer covering DCR surface was loosely attached by PVP particles. 2-VP/DCR=3/2. Micrograph (b) shows clear marks left by the PVP particles falling off the PVP covered surface.

3.3.5 Coating of Pharmaceutical Actives

3.3.5.1 Introduction. Polymer coating, as a barrier for controlled release or taste masking, is an important step in certain pharmaceutical solid dosage formulations. There has been growing interest in using environmentally friendly coating method for pharmaceutical processing. In this work, a new green chemistry approach was developed to coat drug particles through in-situ polymerization in supercritical CO_2 ($scCO_2$). Surface coating follows a mechanism of polymerization-induced phase separation. Hydrocortisone (HC) and Lysozyme particles were used as core materials; water-soluble polymer poly (1-vinyl-2-pyrrolidone) was synthesized as the coating material. Results showed that this new coating method was highly efficient for selected systems. Compared to the well-studied SAS coating method[1], this procedure has been shown to offer many advantages, including easier processing and elimination of VOC. Due to the initial homogeneity of dispersed reactants, uniform coating layers with complete coverage and controllable thickness were obtained.

3.3.5.2 Experimental. Materials: Hydrocortisone and Lysozyme (Figure 3.1) were supplied by ICN Biomedical Inc. and used without any further processing. Monomer 1-Vinyl-2-pyrrolidone (2-VP), surfactant poly (dimethyl siloxane) methacrylate (PDMS-MA) and initiator 2,2'-Azobisisobutyronitrile (AIBN) were obtained from Sigma-Aldrich and were used as received. Carbon dioxide gas was purchased from Matheson with 99>% purity. Figure 3.1 shows the SEM images of the uncoated HC and Lysozyme surface morphologies. Sharp edges were observed due to the breakage of drug crystals. HC has wide size distribution, ranging from tens of nanometers to tens of microns. Lysozyme are in the form of large particles in the size range of tens to hundreds of microns.

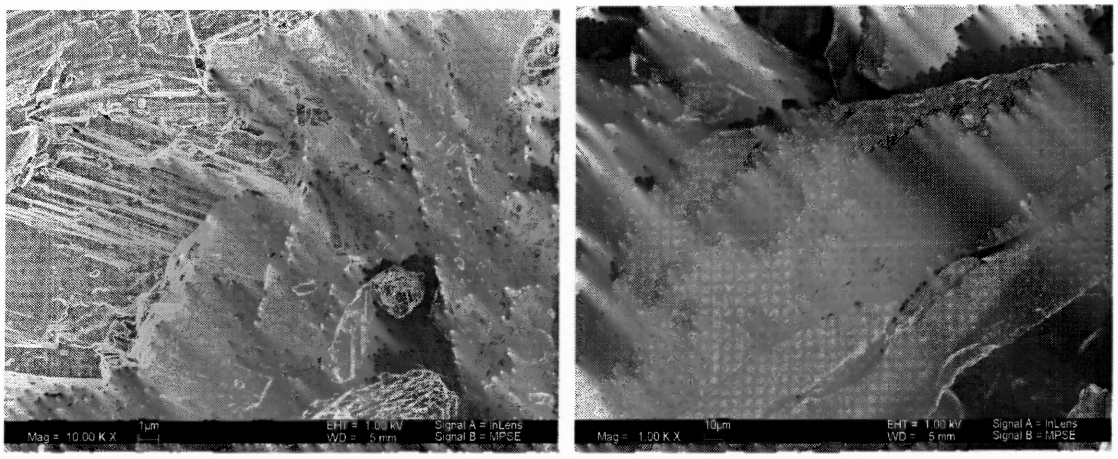

Figure 3.12 Left: original HC particles; Right: original Lysozyme particles. In situ polymerization was carried out with the same procedure as described above in coating of Dechlorane particles.

3.3.5.3 Results and Discussion. In addition to homogeneous nucleation in dispersion polymerization, introducing inert fine drug particles to the reactor may induce heterogeneous nucleation. Instead of growing in the $scCO_2$ as suspended colloidal particles, the growing particles have high tendency to attach onto the host particle surfaces. This mechanism of polymer growth is more likely a precipitation

polymerization compared to conventional dispersed polymerization because of the following two aspects: first, the reaction sites are constrained on the immobile solid substrates instead of the dispersed polymer particles moving throughout the medium; second, the specific area is much smaller. Figure 3.13. shows coated HC particles. As shown in the left image, when large amount of monomers are available, polymers are produced both in the $scCO_2$ media and on the surface, and those formed in CO_2 may then attach onto the polymer covered drug particle surface. However, with decreased amount of polymer, the precipitation-like polymerization dominates and thus produces a film coating, as shown in the right image. The degree of agglomeration also increases with increasing amount of polymer.

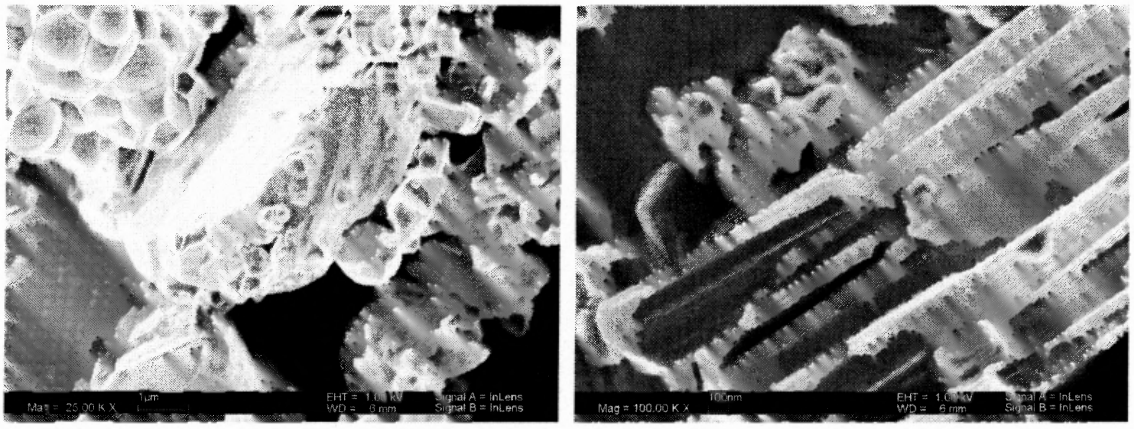

Figure 3.13 Left: VP/HC ratio=1/2, in which excessive agglomerated PVP particles were observed on the upper left corner of the micrograph. Right: VP/HC=1/4, in which uniform film coating was obtained.

Similarly, Lysozyme was also successfully coated with PVP, as clearly shown in Figure 3.14. The large drug particles with sharp edges were completed covered with polymer. The increasing amount of polymer leads to thicker coating and rougher surface morphology.

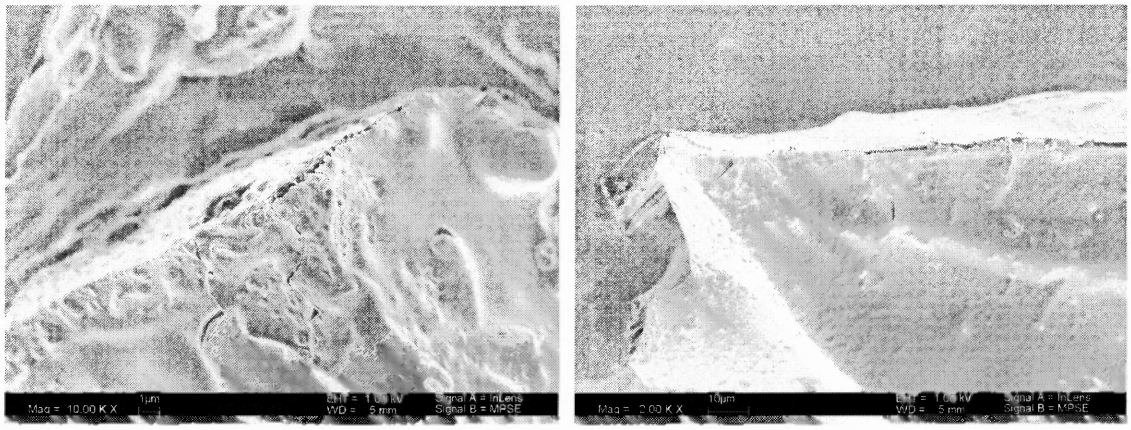

Figure 3.14 Left: 2-VP/Lysozyme=1/2; right: 2-VP/Lysozyme =1/4.

3.4 Conclusions

Fine particles were encapsulated successfully with PMMA and PVP polymers via in-situ polymerization in $scCO_2$. PDMS-MA macromonomer was used as a stabilizer. Changing process variables such as monomer concentration, reaction pressure, stabilizer concentration, and initiator concentration can control the coating thickness, surface morphology, and the degree of particle agglomeration. Particles of various shape and broad size distribution were all encapsulated. Experimental results indicated complete surface coverage. In particular, smooth film encapsulation has been achieved by our method which is difficult to obtain using other supercritical fluid processes such as SAS or RESS. Being essentially a one-pot synthesis process, it eliminates the need for organic solvents in the whole process and operations related to separation. All the raw materials become parts of the final coated product in the end, making it an efficient and environmentally friendly process.

SEM micrographs from our experiment showed that dispersed polymer particles can deposit and aggregate on a thin polymer layer coated on the host particles then undergo plasticization, coagulation, and fusion into a thicker layer. When the pressure was low or the concentration of stabilizer was high, smooth thin-film coating attached by uncoagulated polymer particles was found. These observations suggest that the polymerization occurs simultaneously through two parallel routes: reaction in dispersed polymer particles and reaction in the polymer domains nucleated on the surface of the host particles which later develop into a uniform polymer encapsulating layer. The latter resembles a precipitation polymerization, in contrast to a conventional dispersion polymerization. It is characterized by lower average molecular weight, lower yield, which were proved by GPC results. GPC data also indicated bimodal distribution in polymer molecular weight, which is a strong indication of the coexistence of dispersion and precipitation polymerization.

It was also found that the stabilizer plays an important role in polymer growth and particle coarsening on the surface of host particles. Without the stabilizer, PMMA can not be coated on the host particles; with too much stabilizer, coagulation and fusion of polymer particles will be hindered. Changes of various process variables affect dispersion polymerization and the coating mechanism. High pressure favors plasticization and increases the mobility of the polymers which lead to a smoother morphology.

The new coating method has shown excellent results in encapsulation of fine particles; it's success in using common pharmaceutical polymer to coat two pharmaceutical particles make it a promising alternative in pharmaceutical particle

coating. This coating method can also be expanded to various other particles in other important industries: petrochemical, fertilizer, food, etc.

CHAPTER 4

MICROENCAPSULATON OF SILICA NANOPARTICLES IN SC CO_2

In order for the research described in this chapter to stand on its own (as a publishable research paper), some of the pertinent prior work that has already been described in Chapter 3 may be repeated here.

4.1 Introduction

Every year, billions of pounds of organic solvents are used worldwide as reaction media, dispersants, processing and cleaning agents. Alternatives that can reduce or eliminate the emissions of hazardous volatile organic compounds (VOC) have been vigorously pursued. To this account, $scCO_2$ has gained extensive interest as an environmentally friendly solvent for chemical synthesis and processing to reduce emission.

Supercritical fluid is a physical state under conditions above the critical temperature (T_c)and critical pressure (P_c) of the solvent. Fluid in such a state exhibits physicochemical properties between those in liquid and gas: liquid-like density and solvent strength, making it soluble to many organic compounds while gas-like viscosity and diffusivity enhancing the transport properties and thus providing an easy route for otherwise difficult processes. In addition, thermodynamic and transport properties (e.g. density, viscosity, and diffusivity) can be tuned by process parameters such as pressure and temperature. Among many supercritical fluids been investigated, carbon dioxide, an inexpensive, non-toxic and non-flammable medium with an easily accessible critical point—T_c at 31.1°C and P_c at 73.8 bar, is the most salient in this category. These unique properties of $scCO_2$ make it suitable of applications in areas such as

organic synthesis, heterogeneous and homogeneous catalysis, and inorganic/metallorganic coordination chemistry. Environmental, chemical and economic advantages can be synergized by using $scCO_2$ as a solvent.

One of the application highlights is the synthesis and processing of polymeric materials. DeSimone first demonstrated the success of synthesizing fluorinopolymer in $scCO_2$ to replace conventional solvent in 1992. This breakthrough initiated a series of related research. One interesting research area is to use $scCO_2$ as a processing medium for the preparation of polymer nanocomposites. Polymer nanocomposite, finding applications in various important industries, such as biomedical industry, consists of a polymer matrix and one or more dispersed phases with nanoscale features. The incorporation of nanomaterials into polymer matrix is often intended to improve the mechanical, thermal or electrical properties of the composite material (Sumita, 1994). The confinement of polymer chains in nanoscale brings up various interesting phenomenon and properties that are not observed in regular macroscopic composites. The role of embedded nanoparticle in polymeric composites to external stimuli is still open and is under investigation (Ash, et al. 2001). In one possible scenario, only the mobility of the polymer chains around the nanoparticle surface is affected which results in solely near-field effect. On the other hand, the nanoparticles may affect long-range collective motions of the polymers or form cross-linking that enhances the mechanical property.

Conventional preparation methods for composites usually involve physical mixing of polymers and fillers through processes such as blending, extrusion, or solution casting. However, nanoparticles may have very high cohesive energy and form agglomerates; processes based on simple mixing are not effective to break up the agglomerates to form homogeneous nanocomposite. In the last decade, a few new approaches were investigated to make polymer

agglomerates; processes based on simple mixing are not effective to break up the agglomerates to form homogeneous nanocomposite. In the last decade, a few new approaches were investigated to make polymer inorganic composites via in-situ polymerization. von Werne et al. 2000, modified the surface of silica nanoparticles with initiators for atom transfer radical polymerization (ATRP) where polymer chains are tethered on particle surfaces and form a layer. Bourgeat-Lami et al. 1998, investigated silica styrene nanocomposites synthesized with dispersion polymerization in ethanol. Recently, supercritical processing has attracted growing interests for polymer nanocomposite fabrication due to its environmental friendliness and simple product collection and down-stream processing. In one approach, organic precursors were impregnated into the polymer matrix in supercritical CO_2 and then decomposed into inorganic particles after heating to form composites (Watkins 1991). The resultant nanoparticles or products are restrained from agglomeration in polymer matrices. Using this approach, platinum, copper, silver and iron nanoparticles have been embedded in a variety of polymer matrices with, unfortunately, higher polydispersity.

In this study, a new approach is reported to synthesize PMMA/silica nanocomposites in $scCO_2$ via in-situ dispersion polymerization. Both PMMA and silica are materials of wide applications and serve as a model system in this study. Monodisperse silica nanoparticles were synthesized with Stöber process (1968) and modified with 3-(trimethoxysilyl) propyl methacrylate (MPS) as filler particles. The modified silica nanoparticles were suspended in $scCO_2$ and the surface-grafted MPS molecules undergo copolymerization with MMA after initiation, allowing polymer chains to grow on the silica surface. With an adequate amount of stabilizer, dispersion

polymerization usually results in uniform product and high yield. Our results showed that silica particles were relatively well dispersed and embedded into the large polymeric particle matrix, forming nanocomposite material. One of the advantages of $scCO_2$ over conventional solvent is that high diffusivity makes reactants able to enter the vacancies between nanoparticles even when they form loose agglomerates. Nanoparticles and PMMA were chemically bonded through MPS, which makes their interactions much stronger than physically mixed composites. It was also found that surface modification of silica particles played a key role to improving the compatibility between silica and PMMA. Unmodified hydrophilic particles were excluded completely from the polymer, while a commercial hydrophobic particles(Aerosil® R972) failed to evenly distribute in the polymer matrix. The properties of the final composite particles are controlled by varying silica/polymer ratio, surfactant concentration, and silica particle size. Characterization results from SEM, TEM, TGA, and DSC are presented. This composite preparation procedure can be expanded to many other polymers and inorganic particles, such as titania or alumnia. It may have potential for industrial production of polymer inorganic nanocomposites.

4.2 Experimental Section

4.2.1 Materials

Chemicals used for polymerization, including monomer methyl methacrylate (MMA), surfactant poly-(dimethyl siloxane) methacrylate (PDMS-MA) (Figure 4.1) and initiator 2,2'-Azobisisobutyronitrile (AIBN), were obtained from Sigma-Aldrich (Milwaukee) and used as received. Tetraethyl orthosilicate (TEOS), ammonium hydroxide (NH_4OH) and

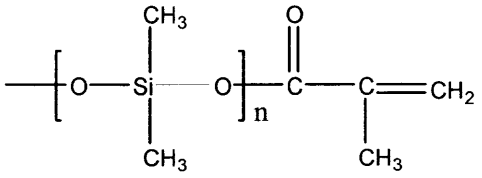

Figure 4.1 Surfactant PDMS-MA molecular structure.

4.2.2 Silica Nanoparticle Synthesis and Modification

Silica nanoparticles were synthesized according to a method reported by Stöber et al.[12]. In our process, TEOS was hydrolyzed to form silica particles in ethanol, with NH_4OH functioning as catalyst. Monodisperse spherical particles of controlled sizes ranged from tens to thousands of nanometers were synthesized in our lab by changing the concentrations of reactant and catalyst. In each synthesis, TEOS, ethanol, NH_4OH, and deionized water are mixed according to certain molar ratios and stirred for 2 days at room temperature. To synthesize silica particles of roughly 50nm in diameter, TEOS and NH_4^+ concentrations of 0.2M are used. While for 100nm silica particle synthesis, TEOS and NH_4^+ concentrations of 0.54M and 0.45M respectively are used. Silica particles synthesized by the above method are hydrophilic, with –OH groups on the silica particle surface.

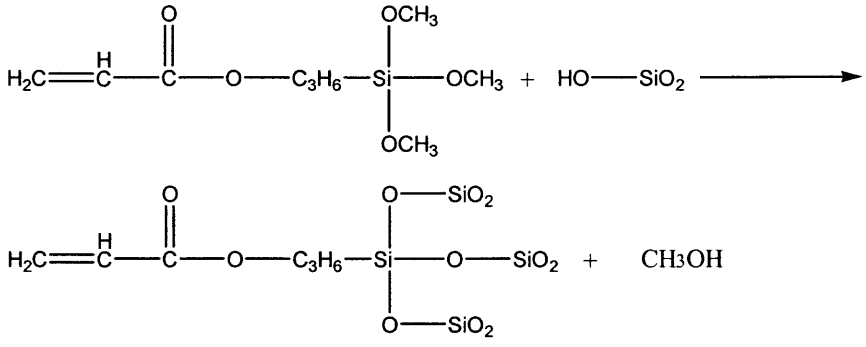

Scheme 4.1 Surface modification of hydrophilic silica particles with MPS.

To make the particle surface hydrophobic, we followed a well-established surface treatment[13] by adding coupling agent MPS into the silica particle dispersion and stirring the

solution for several more days. MPS does not only attach to the silica surface to render hydrophobicity, but also provide a methacrylate functional end group which allows tethered polymer chain to grow on the particle surface. The solution containing modified silica particles were then dialyzed with cellulose membrane against ethanol to eliminate the ammonia and free MPS molecules.

4.2.3 Composite Synthesis via Polymerization in $scCO_2$

The polymerization system setup is shown in Figure 4.2 which consists of a 25-ml Parr Instruments high-pressure reactor vessel with two sapphire windows at both ends. There are four openings on the reactor sidewalls which are separately designed for the thermocouple, pressure transducer and safety disc, inlet for reactant and CO_2 injection, and outlet for CO_2. The thermocouple and pressure transducer were connected to Watlow panel meters for digital readout. The reactor pressure was manually controlled by pumping or releasing CO_2 through the inlet/outlet. Heating was supplied with electric silicon rubber wrapped around the reactor and the temperature was controlled by changing the voltage applied to the heating tape.

Composite synthesis with in-situ dispersion polymerization was conducted in the high-pressure reaction vessel. During polymerization, AIBN acts as free-radical initiator and PDMS-MA functions as a surfactant stabilizer. All components were premixed and charged into the reactor followed by purging with low-pressure CO_2 gas. After purging, liquefied CO_2 was pumped into the reactor by a Haskel Air Driven pump at room temperature until an appropriate pressure was reached. An experimentally determined CO_2 T-P curve has been used to approximately project the initial load pressure at room temperature to the desired final pressure at the reaction temperature. Before the reaction started, the monomer, surfactant and initiator were all dissolved in CO_2, while the silica particles are suspended in the reactor vessel with

magnetic stirring. However, due to the low viscosity of the supercritical fluid inside the reactor, stirring is not very effective.

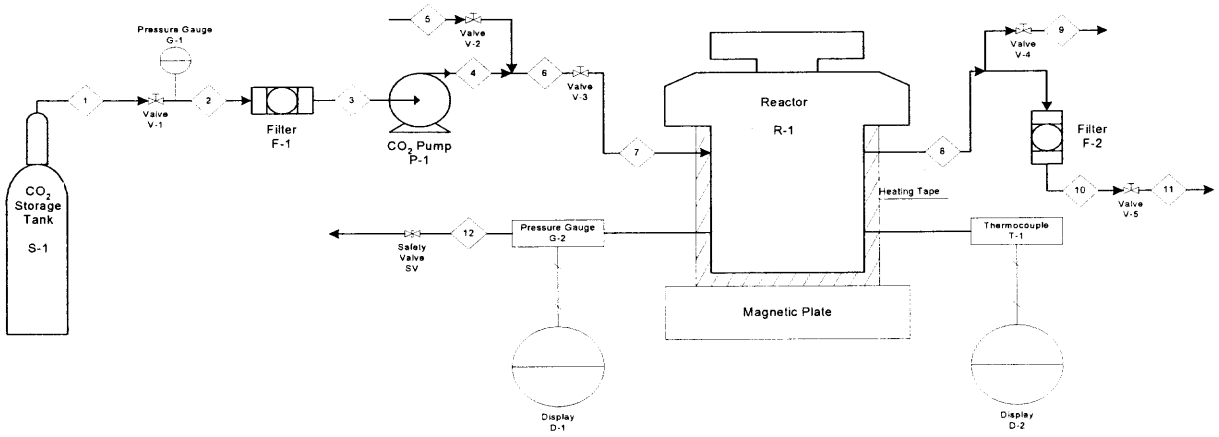

Figure 4.2 Schematic diagram of the experimental apparatus.

As the pressure reached its desired final value (4000 psia), the vessel was then heated to 65°C to initiate the free-radical polymerization. The batch reactor remained closed during the experiment and a pressure drop of 100~200 psia due to polymerization-induced volume shrinkage was commonly observed after the reaction completed. Each experiment was run for 24 hours, after when CO_2 was released and the reactor was cooled down to the room temperature for sample collection. Unless otherwise stated, in each batch 2 ml of monomer MMA, 0.02g of initiator AIBN, and 0.4ml of surfactant PDMS-MA was premixed first, followed by the addition of silica particles into the mixture. The reaction temperature is 65°C and the vessel pressure is 4000 psia. The silica to polymer weight ratio was 5 % for both Aerosil® particles and unmodified Stöber particles while different ratios were selected for MPS modified particles. After mixing, the suspension was further mixed in bath sonication for 5 minutes before it was finally transferred into the reactor.

4.2.4 Sample Characterization

The morphologies of the composites were examined with a LEO32® field emission scanning electron microscope (FESEM). Powder samples were prepared following the standard procedures fixed to the carbon film on the aluminum stub without any special treatment. Specimens were then coated with a carbon thin film to make the sample surfaces conductive for SEM characterization.

For the TEM sample preparation, the PMMA-SiO_2 composite particles were first embedded with Spurr resin and then cut with microtome. Due to microvoids and interfaces in the Spurr resin left between the composite particles, relatively thicker sections had to be cut to make an acceptable sample, which compromised image resolution. Micrographs were collected on a JEOL-2010F® TEM in the High-Angle Annular Dark Field mode. Brighter regions in the image are corresponding to the SiO_2 particles. The mass of polymer in the composite was determined by thermogravimetric analysis (TGA) using a NETZSCH STA409PC LUXX® thermal analyzer. Oxygen was supplied during the TGA experiment and a heating rate of 5°C/min was applied until the maximum temperature of 500°C was reached.

To determine the effect of encapsulated silica nanoparticles on polymer glass transition temperature (Tg) change, differential scanning calorimetry (DSC) tests were carried out on a TA-Q100® DSC. In each test, a heating-cooling-heating cycle between 50°C and 160°C was applied with a heating/cooling rate of 15°C/minute; the data from the second heating ramp was used to determine Tg.

4.3 Results and Discussion

4.3.1 Dispersion Polymerization in $scCO_2$

Synthesis of PMMA in $ScCO_2$ has been reported by many groups under different conditions[14-17] since the first work by DeSimone et al[18]. The progress of the reaction was monitored visually through two sapphire windows with the help of an illuminating light source. Initially, the reaction medium was transparent with observable traces of currents. Approximately two hours after the set condition was reached, the turbidity of the medium started to increase slowly. After four hours, there was no light penetrating through the reaction medium and a milky-white appearance similar to conventional aqueous latex was observed in the areas close to the windows. However, no particle precipitation was visually observed until a few hours later - depending on the initial monomer concentration. After the reaction completed, polymer in the form of free-flowing white powders were collected. The sizes of the polymer particles are usually in the range of a few hundred nanometers. Shown in Figure 4.3 is a SEM micrograph of typical PMMA particles obtained in our experiments.

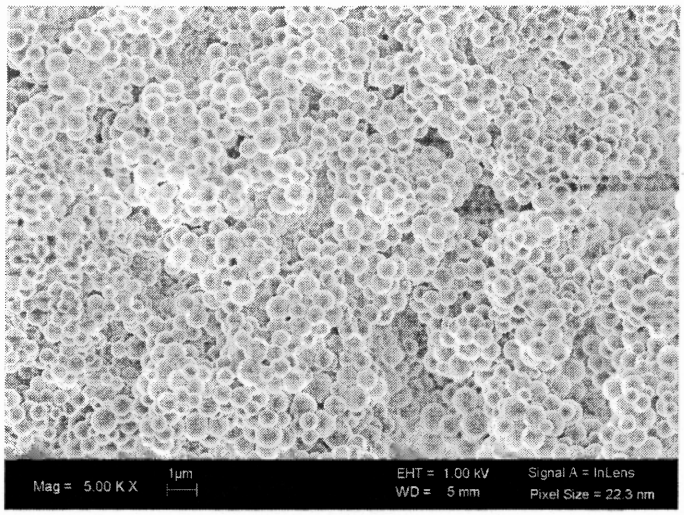

Figure 4.3 Typical PMMA particles synthesized.

It is known that in dispersion polymerization, phase separation of polymer in the medium occurs quickly after the reaction starts with a very low conversion. The growth of polymer will then mainly occur in the dispersed polymer domains, which are protected by stabilizers such as block copolymers or oligomers. Given an initial monomer concentration, the number density of polymer particles depends on the initiator concentration and the extent of stabilization. It was found that flocculation may occur as a consequence of insufficient stabilization. Lowering the pressure of $scCO_2$ or decreasing the monomer concentration may decrease solvency to the "tails" of the stabilizers and therefore reduce the steric repulsion.

4.3.2 Nanocomposite with Fumed Silica Particles

Two type of commercially available fumed silica, hydrophilic Aerosil® 200 (A200) and hydrophobic Aerosil ® 972 (A972) from Degussa were used as host particles. The Aerosil® particles are widely used as filler materials in various applications such as in polymer to enhance the mechanical properties. Due to the fuming manufacturing process, the Aerosil particles have branch-like agglomerated structures consisting of nano-size primary particles. Figure 4.4 depicts the SEM micrographs of these particles. The particle surfaces of A200 are not modified and the primary particle size is 12nm with an apparent specific surface area of $200m^2/g$. A972 are modified with DDS (Dimethyldichlorosilane) to render hydrophobicity and the primary particle size is 16 nm with an apparent specific surface area of $130m^2/g$. These particles have low bulk density and are highly fluffy in the air. The low viscosity and high diffusivity of $scCO_2$ make it able to penetrate into the inter-particle space. After CO_2 is pumped into the reactor, these fumed silica particles stayed at the bottom of the reactor. When the reaction is over, free-flowing particles were obtained.

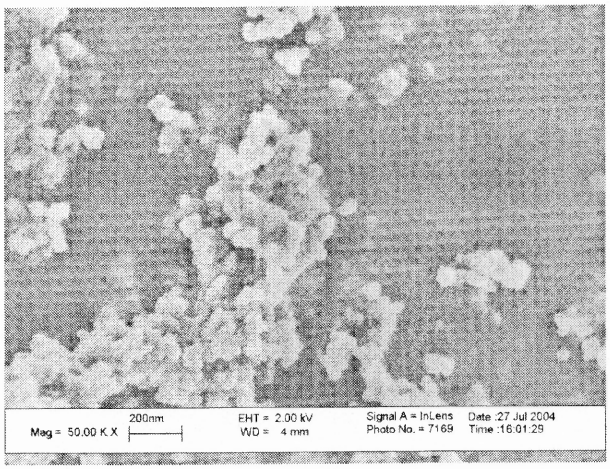

Figure 4.4 SEM micrographs of Aersoil® 200 particles.

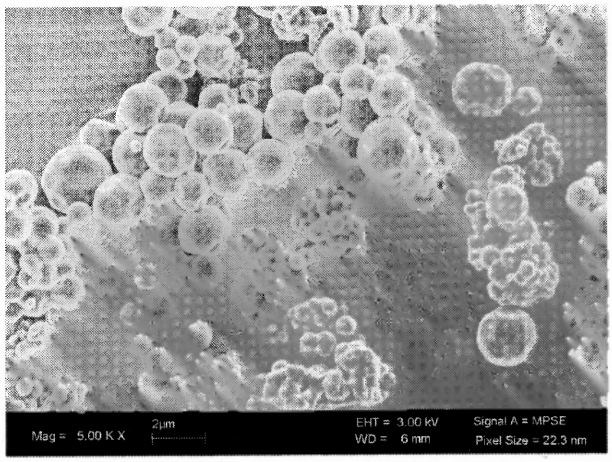

Figure 4.5 PMMA synthesized with the presence of hydrophilic Aerosil 200 particles.

Figure 4.5 shows the SEM micrographs of the product prepared from hydrophilic Aerosil 200 silica nanoparticles. Due to the disfavoring interactions between the hydrophilic surface and $scCO_2$, the fluffy silica agglomerates did not disperse well in $scCO_2$. The synthesized PMMA particles appear polydispersed (Figure 4.5) and partially agglomerated compared to those synthesized without nanoparticles (Figure 4.3). Such morphology suggests insufficient stabilization in the presence of the nanoparticles, possibly due to adsorption of surfactants on the nanoparticles. Partial encapsulations and poor dispersion of the nanoparticles were observed as in Figure 4.5.

Changing from hydrophilic surface to modified hydrophobic surface, it was found that A972 particles still did not disperse well in $scCO_2$ prior to polymerization. After the reaction, only partially free-flowing powders were obtained; and many polymer beads are tightly agglomerated with each other. In Figure 4.6, the SEM micrograph shows that some silica particles are embedded in the PMMA matrix, however, silica nanoparticles do not distribute evenly in the matrix. It is noted that large separate PMMA beads coexist with highly agglomerated polymer suggesting that the formed PMMA beads were not stabilized efficiently by surfactant.

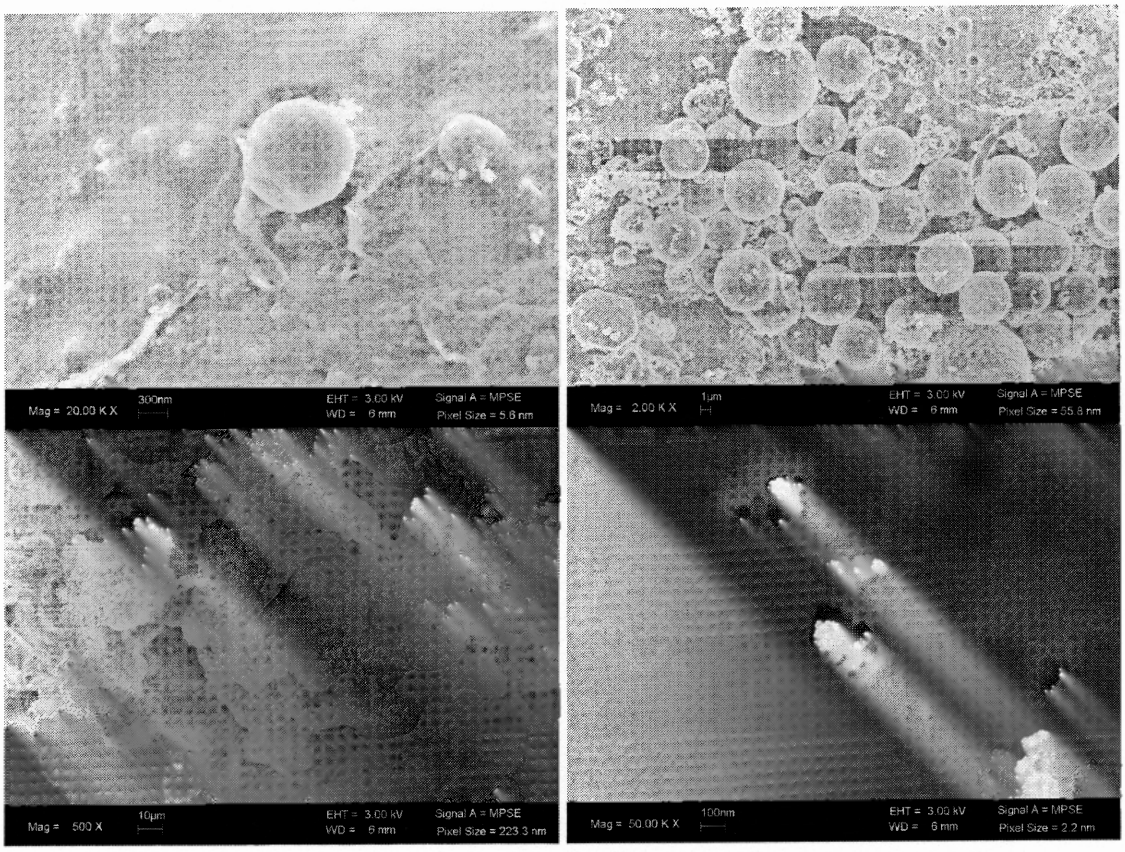

Figure 4.6 PMMA composite with Aersoil® 972 particles. Clockwise: a) coexistence of PMMA particles and composites.b) A972 particles scattered on PMMA particles. c) surface feature on one large PMMA particle. d) PMMA composite particles heavily agglomerated.

When silica nanoparticles are present in the polymerizing system, they may induce heterogeneous nucleation for polymer precipitation as the molecular weight of polymer reaches the solubility in $scCO_2$. The growth of polymer chains then continues simultaneously inside dispersed polymer particles formed via homogeneous nucleation and in the heterogeneously nucleated polymer sites deposited on the hydrophobic silica surface, which eventually develop into the encapsulating layer. The latter growth mechanism of polymer is more likely a precipitation polymerization compared to conventional dispersed polymerization: the reaction sites are constrained on the slow-motion solid substrates, building up a larger concentration gradient compared to the wandering dispersed polymer particles, which have much faster translational motion. The difference also appears in term of the susceptibility to the stabilizer concentration: the size and final appearance of polymer from dispersion polymerization depend strongly on the efficiency of stabilization; such dependence is milder for precipitation polymerization on solid substrates due to its less active involvement in colloidal motion and evolution kinetics of colloid population.

4.3.3 Nanocomposite with Stober Silica Particles

Compared to the Aerosol nanoparticles, Stöber particles do not agglomerate and remain discrete form. The hydrophilic characteristic of the surface can be modified into hydrophobic by grafting coupling MPS molecules, which provide methacrylate functional groups allowing PMMA chains and PDMS-MA to tether to the surface. Figure 4.7 shows the SEM micrographs of typical Stöber silica particles synthesized in our lab. In this study, particles with mean diameter of 50 and 100 nm were used. It is found that unmodified (hydrophilic) Stöber particles do not disperse well in $scCO_2$ and stay in the bottom of the reactor. As a result, PMMA particles collected after polymerization appeared similar as in the case of pure PMMA synthesis, as shown in Figure 4.8.

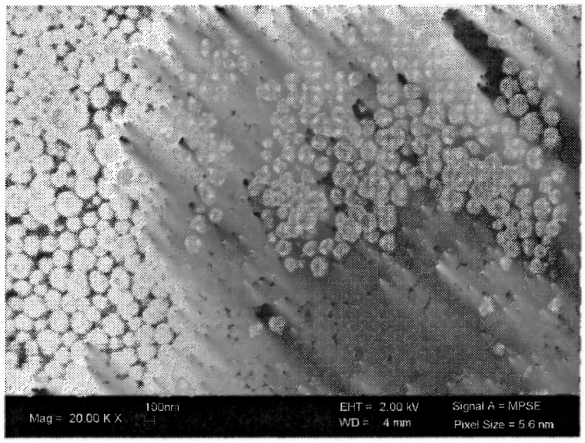

Figure 4.7 Typical Stöber silica particles synthesized.

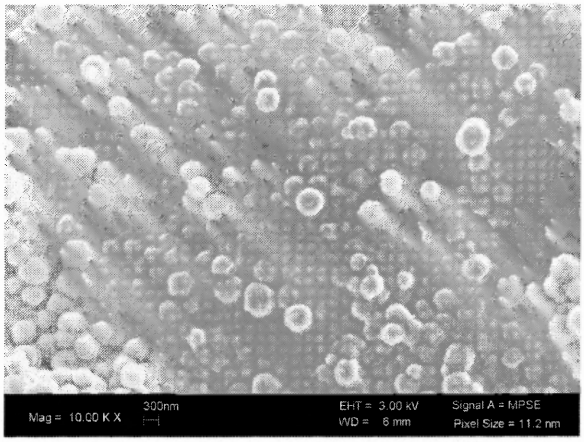

Figure 4.8 PMMA synthesized with the presence of unmodified hydrophilic Stöber particles.

On the other hand, MPS-modified silica particles formed an opaque suspension in $scCO_2$ that lasted for hours, indicating good colloidal stability. In a different study, Johnston et al. investigated in detail the stability of silica colloids in $scCO_2$. They found that silica particles can be well stabilized by PDMS or perfluoropolymer based surfactant for a significant amount of time under certain conditions. In our experiments, the favorite interaction of PDMS-MA and MPS may lead to PDMS attachment and thus improves the steric stabilization. Notice that silica particles used in our study is much smaller than in their case, which makes them easier to disperse. DeSimone et al. also experimentally proved that silica nanoparticles modified with

fluorinated chlorosilanes can be dispersed homogeneously in $scCO_2$. Increasing chemical affinity between the surface and $scCO_2$ facilitate the extent of dispersion for the nanoparticles. During polymerization, the end group of MPS will react with PMMA chain and PDMS-MA and thus enhance dispersion of the nano-particles in the solution and also prevent them from forming large agglomerates. However, the nano-particles also play a role as crosslinkers where tethered polymer chains form "bridges" chemically connecting these nanoparticles. The kinetic rate of bridging reaction determines the correlations among the particles and thus the homogeneity of the particle dispersion in the matrix. Changing the concentration of the crosslinkers also affects the morphology of the polymer: It also affects the size. A schematic diagram of the reaction mechanism is shown in Figure 4.9.

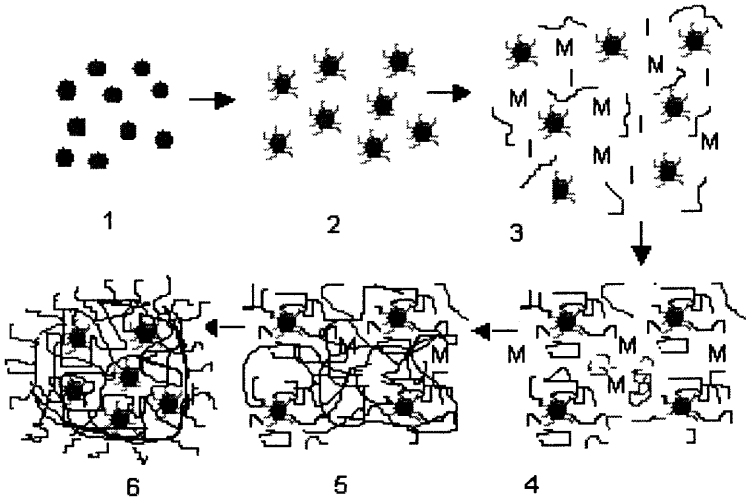

Figure 4.9 Schematic diagram of the composite synthesis from modified Stöber particles. 1) Silica particle synthesis 2) Silica particle modification with MPS. 3)Mixing of modified silica particles with polymerization agents, where the broken curves represent surfactant molecules. 4) Poymerization starts both and polymer chains attached onto silica surface. 5) Polymer chains entangle with silica particles nearby. 6) Surfactant, if sufficient, keeps the particles in spherical shape.

Depending on the experimental parameters, composite particles with narrow size distribution or in the form of particle agglomerates are synthesized. TEM and SEM micrographs

show that silica particles are well incorporated into the large PMMA particles. No separated silica uncovered by PMMA was found from SEM observation, indicating high encapsulation efficiency. Compared to pure PMMA synthesized under the same condition, the micron-sized composite particles are several times larger, which is expected because several silica particles are encapsulated into one PMMA particles. Composite particles are also of less regular shape and often have concave/convex surfaces, obviously due to the silica particles encapsulated. Shown in Figure 4.10. are the SEM micrographs of PMMA with 5 wt. % silica particles of 50nm in diameter. Individual or loosely agglomerated composite particles of 2~4 microns in diameter with narrow size distribution were obtained. Correspondingly shown in Figure 4.11. are the TEM micrographs of this sample. Both individual silica particles and silica particle agglomerates were found inside the polymer matrix, probably due to the large number of silica particles added into the system. However, it is not clear whether the coagulated silica particles are just physically close to each other, or chemically bonded with each other.

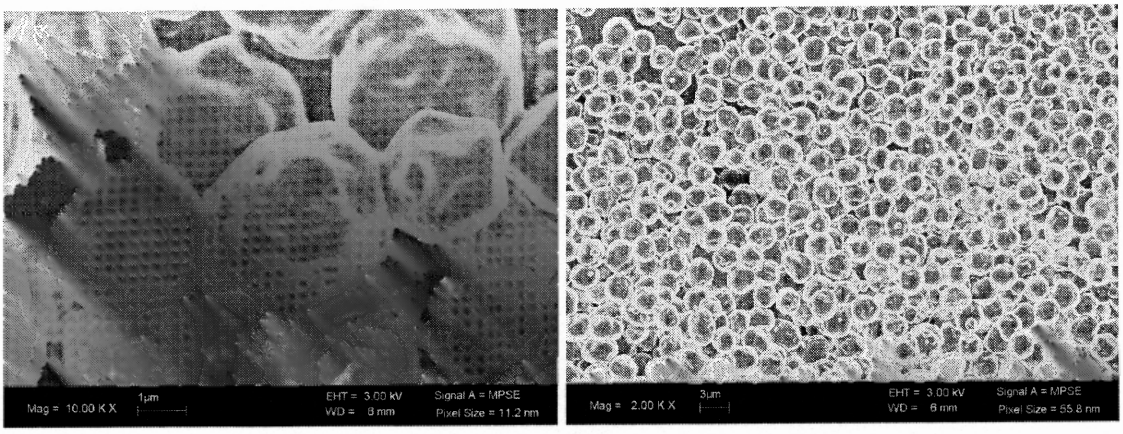

Figure 4.10 Composites prepared with 5 wt.%, 50nm modified Stöber silica particles. A) surface feature. B) narrowly distributed composite particles.

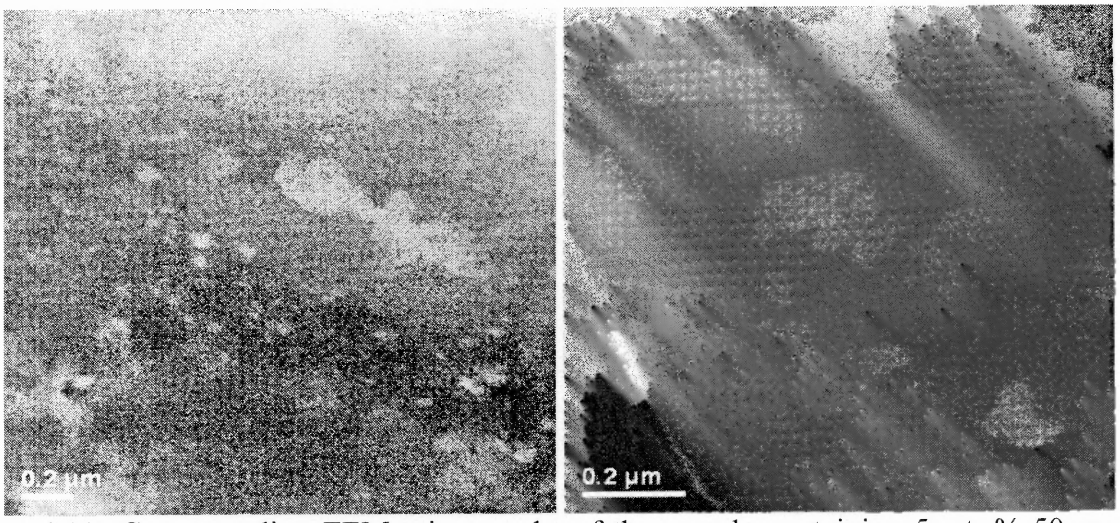

Figure 4.11 Corresponding TEM micrographs of the sample containing 5 wt. % 50nm silica particles. A) Individual silica particles coexist with silica particle agglomerates. B) Loose silica particle agglomerates are dispersed in PMMA.

The final product morphology can be controlled by varying silica particle size, surfactant concentration, and the percentage of silica particles in the composite. Since silica particles are encapsulated into PMMA particles, silica particle size will significantly affect the PMMA particle surface morphology. Shown in Figure 4.12. are SEM micrographs of PMMA with 10 wt. % silica particles of 20nm in diameter. Of notable difference between the composite particles with silica particles of different sizes is the surface roughness. Encapsulation of 20nm particles resulted smaller surface features, as indicated in Figure 4.12. (a).

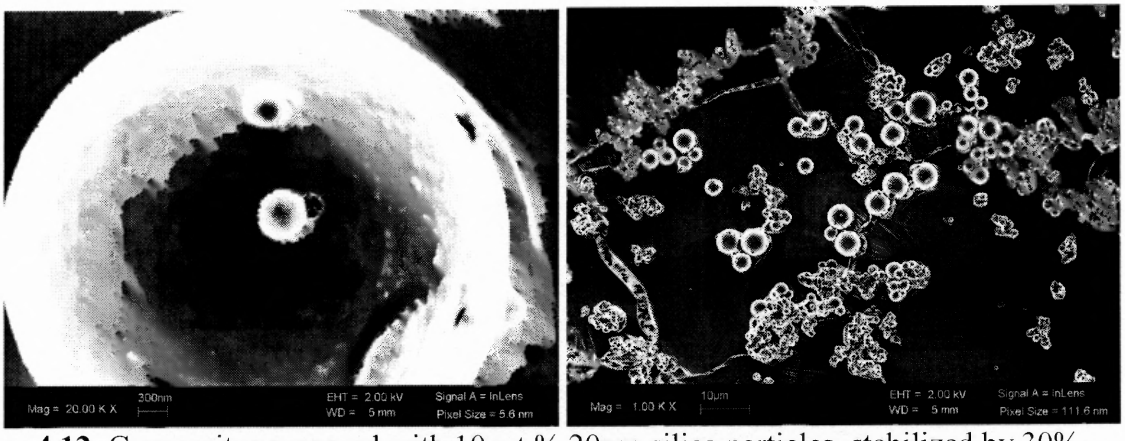

Figure 4.12 Composites prepared with 10 wt.% 20nm silica particles, stabilized by 30% surfactant. (A) Small surface features. (B) Lower magnification shows coexistence of individual particles with particle agglomerates.

The amount of silica particles also strongly affects the product morphology. The more silica particles, the more chances that MPS molecules on different particles will react with each other. As a result, excessive silica particles lead to silica particle agglomeration, which then results in non-uniformity and more chances of composite particle agglomeration in the product. Shown in Figure 4.13. is the micrograph of the composite with 10 wt.% of 50nm silica particles. The composite particles were found to be heavily-agglomerated, and the samples had to be broken for the SEM experiment.

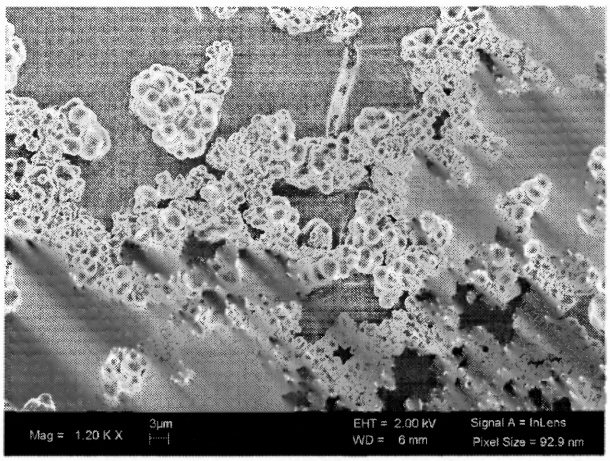

Figure 4.13 Composites prepared with 10 wt.% of 50nm silica particles. Shown here are broken pieces of the heavily-agglomerated particles.

Surfactant plays a key role in stabilizing growing PMMA particles. When insufficient surfactant is present, the PMMA particles are under-stabilized and tend to form agglomerates. To study the stabilization effect, 10 % silica particles of 20nm in diameter were incorporated into the PMMA with 20% surfactant/monomer ratio. Unlike in Figure 4.12., only heavily agglomerated composite particles were found, as shown in Figure 4.14. It should be noticed that composites with 20nm silica particles again have finer surface features, and the agglomeration is more serious than those containing 50nm particles. With the same weight percentage, the number of 20nm particles and total surface area will be much larger than 50nm particles. Since the probability of inter-particle interaction is significantly increased, agglomeration also increases.

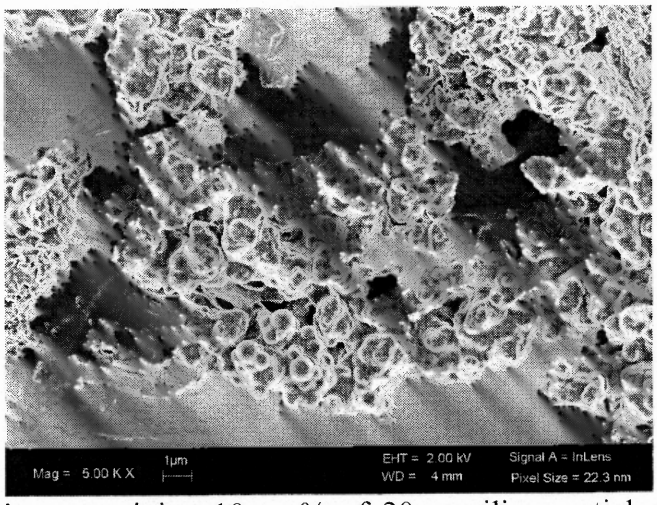

Figure 4.14 Composites containing 10 wt.% of 20nm silica particles with 20% surfactant. Shown here are broken pieces of the heavily-agglomerated particles.

4.3.4 Nanocomposite Thermal Analysis

TGA experiments were carried out to verify the silica weight percentage in two composite samples from modified Stöber particles of 50nm. As shown in Figure 4.15., PMMA sample was found to be not completely decomposed at 500°C. This residue is likely due to the incomplete decomposition of surfactant PDMS-MA, which only starts to decompose at about 350°C. Calculation from the TGA data yielded that the real silica percentage in these two samples are 6.4%, and 10.7% respectively, which is comparable to the added amount of 5% and 10%.

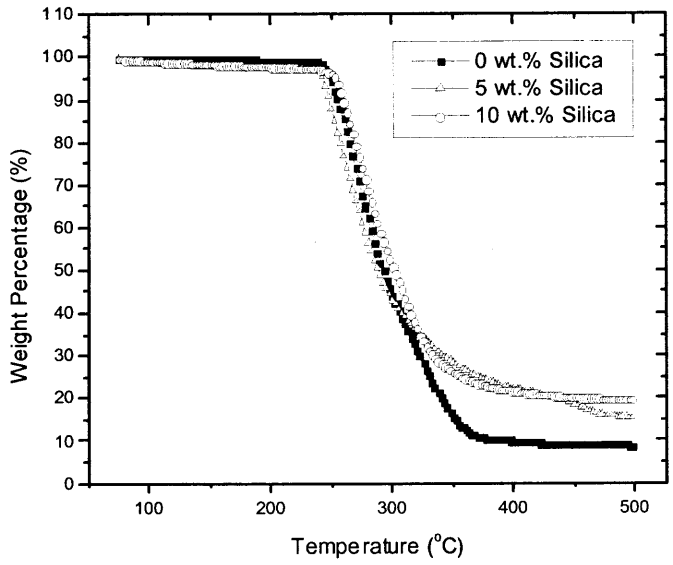

Figure 4.15 TGA results for silica content in two composite samples.

One important feature of nanocomposite is the enhancement of certain physical properties due to the addition of nanofillers, especially the thermal and mechanical properties. In this study, DSC experiement was carried out to test the glass transition temperature change. Since the presence of nanoparticles will hinder the polymer mobility, the glass transiton temperature is usually higher than pure polymer, unless cavities form around the nanoparticles during processing or synthesis[5]. It is found that about 10°C increase in Tg was observed after MPS modified silica particles were incorporated into the PMMA (Figure 4.16.). In contrast, relatively small Tg increase(3-4°C) was observed for the product where commercial and synthesized hydrophilic particles were used. On the other hand, a fairly significant (7°C) increase was observed for the A972 containing PMMA composite.

Several factors may affect the polymer Tg: bond interaction, molecular weight, functionality, branching, all are important. Polymer chains that do not easily undergo bond rotation so as to pass through the glass transition would be expected to melt with difficulty, and result in a high Tg. Besides the hindered chain mobility in nanocomposites, bond rotation may also be limited in the presence of nanoparticles. Low elongation and high tensile strength in materials are aynonymous with high degrees of crosslinking and result in high Tg values.

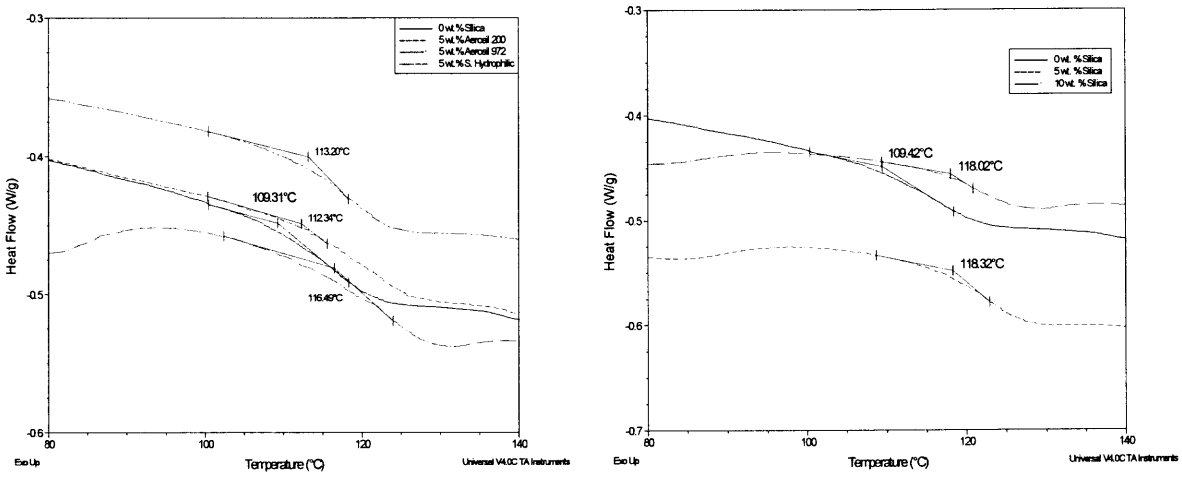

Figure 4.16 DSC results for PMMA and composites. (a) Very small Tg increase was observed when hydrophilic particles were used, hydrophobic particle-containing composites had several degrees increase in Tg. (b) About 10 degree increase in Tg was observed when 50 nm modified particles were used. No Tg difference was observed between 5% and 10% silica particle loading.

In silica polymer composites prepared from conventional physical methods, such as blending and solution casting, silica particles are usually intentionally trapped inside the polymer matrix. As a result, the forced dispersion of silica in polymer usually still results in enhanced physical properties. However, in this in-situ polymerization approach, no external force is applied to incorporate silica into the polymer. Since the composite is formed from spontaneous polymerization, the initial silica particle surface property plays a key role in determining the final success. The significant Tg increase in both composites containing hydrophobic silicas are due to the favorable interaction of PMMA with particle surface. However, it should be noted that the

the polymer matrix. As a result, the forced dispersion of silica in polymer usually still results in enhanced physical properties. However, in this in-situ polymerization approach, no external force is applied to incorporate silica into the polymer. Since the composite is formed from spontaneous polymerization, the initial silica particle surface property plays a key role in determining the final success. The significant Tg increase in both composites containing hydrophobic silicas are due to the favorable interaction of PMMA with particle surface. However, it should be noted that the interactions are likely to be different in these two cases. When A972 are used, polymers may form and grow in the $scCO_2$ media and then precipitate onto silica surface, or may form and attach onto silica followed by polymer growth on silica surface. The first scenario remains to be dispersion polymerization, while the second scenario may resemble precipitation polymerization. When modified Stöber silica particles are used, the resemblance of MPS end group with MMA will enable the silica particles to participate the dispersion co-polymerization. However, when the silica nanoparticles are excessive, combined with a large amount of MPS molecules, the particle interconnection becomes unavoidable. As a result, heavy agglomeration is observed when 10 wt.% silica nanoparticles are added into the initial reaction mixture, as shown in Figures 4.13 and 4.14.

4.4 Conclusions

In this study, a new environmentally friendly method to prepare hybrid silica/PMMA nanocomposite was developed in supercritical CO_2 ($scCO_2$). Four types of silica nanoparticles were used as filler material to be incorporated into the polymer matrix through in-situ polymerization. Results showed that surface property of inorganic

actively involved in the polymerization process and disperse fairly well in polymer matrix. The final composite property and morphology were found to be affected by the silica particle size, silica/PMMA ratio, surfactant concentration.

This method can be expanded to produce nanocomposites with many other inorganic particles , such as Titania and Alumnia, and other polymers. Future work will include detailed studies of the physical properties of the composites and the effect of nanoparticles on polymerization kinetics.

CHAPTER 5

MICROENCAPSULATON OF FUNCTIONALIZED CARBON NANOTUBES IN SUPERCRITICAL CO_2

In order for the research described in this chapter to stand on its own (as a publishable research paper), some of the pertinent prior work that has already been described in Chapter 4 may be repeated here.

5.1 Introduction

There have been growing interests in single wall carbon nanotubes (SWNTs) reinforced polymeric materials, due to the fact that the mechanical properties of SWNTs such as their stiffness, elasticity and high Young's modulus make them ideal candidates for structural reinforcements in the fabrication of high strength, light weight, and high performance composites. Considerable investigations have been conducted on the SWNT based composites by both theoretical and experimental means. These approaches involve dispersion, melt mixing, milling, covalent grafting or in-situ growing SWNTs in different polymers or ceramic matrixes. However, the obtained results are controversial from different studies. Some of them revealed that the introduction of SWNTs in polymer clearly enhances both the physical and mechanical properties (Sen, 2004). On the other side, some of the theoretical and experimental works showed that carbon nanotube contributed no mechanical improvement to the composites (Zhou, 2004).

The ineffective utilization of nanotubes as reinforcement in composites is normally due to two factors, non-uniform dispersion of SWNTs in matrix and poor interfacial bonding between them. Non-uniform dispersion is mainly because of that

SWNTs are normally self-assembled into bundles (van der Waals forces) after production, and the relative strong bungling force makes them difficult to be debundled. Furthermore, SWNTs are chemically inert, not soluble in any solvent. Their smooth surface is the major reason that they have week interfacial bonding with many different materials. This consequently will result in low efficiency of load transfer across the nanotube/matrix interface, and pullout of carbon nanotubes from the matrix can be observed when the composites are under extension.

Recently, several groups reported functionalization of SWNTs with various chemical agents to enhance their interaction with polymer matrix (Mitchell, 2002). Chemically modified SWNTs possess surface properties that allow them to have enhanced interactions with polymer chains, which greatly improve the composite properties. SWNT surface modification with whole polymer chains also has been reported by Lin et al., 2003. However the nature of polymer chains and their usually large molecular weights sometimes make themselves undesirable candidates to penetrate between nanotube bundles. As an alternative, SWNTs have been mixed with monomers, which are then polymerized. The relative high diffusivity of monomers allows them to penetrate into the nanotube bundle matrix and eventually grow into polymers inside the SWNT matrix]. Sonication and heating/refluxing were often used as a method to break down nanotube agglomerates and improve mass transfer during reaction. With the nanotube surface area fixed, the higher diffusivity of the monomers will lead to more polymers in contact with the surface, and better composite is produced as a result.

In this paper, we report on using supercritical carbon dioxide ($scCO_2$) as a media for the synthesis of carbon nanotube/PMMA nanocomoposite. The principle is

functionalization of SWNT surfaces with small molecules containing double bonds followed by in situ dispersion polymerization with vinyl monomers in $scCO_2$. Dispersion polymerization in $scCO_2$ has been well studied in the last decade (Desimone, et al. 1992). It has been applied for particle coating and nanocomposite synthesis]. In this work, the addition of small molecules onto CNT surface not only make the surface reactive, but also enhances the dispersion of CNT due to the high compatibility of the small molecules with $scCO_2$. Taking advantage of the extremely high diffusivity and high salvation strength of $scCO_2$, the reactant (monomer) can reach virtually everywhere in the system, thus the monomer/CNT contact area is maximized.

Recently, these unique properties of $scCO_2$ have attracted interests for the processing of CNT related materials. Thanks to the superb transport property of $scCO_2$, modified "bulky balls" were dissolved in $scCO_2$ and inserted into CNTs. Besides, $scCO_2$ is a "green" solvent, making this method environmental friendly.

5.2 Experimental Section

The SWNTs used in this experiment were obtained from Carbon Nanotechnology Inc. (Hipco process). Carbon dioxide gas was purchased from Matheson with 99>% purity. All other chemicals were purchased form Sigma-Aldrich.Chemicals, including methyl methacrylate (MMA), poly (dimethyl siloxane) methacrylate (PDMS-MA), 2,2'-Azobisisobutyronitrile (AIBN), 2-aminoethyl methacrylate (AEMA), ethanol, acetone and N,N-dimethyl formide (DMF).

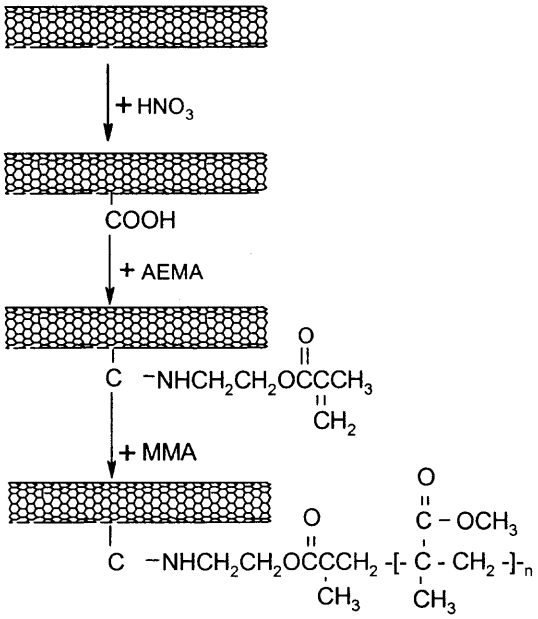

Scheme 5.1 SWNT surface modification followed by in-situ polymerization.

The whole functionalization mechanism is proposed in Scheme 5.1. To generate carboxylic groups (-COOH) and also for removing the catalyst particles remained after production, the received SWNTs were first treated in 70% HNO_3 for 10 minutes using microwave oven (Wang, 2005). Then, 5mg of the acid treated carbon nanotubes (SWNT-COOH) were refluxed with 20 mg AEMA overnight in DMF. The AEMA modified carbon nanotubes (SWNT-AEMA) were obtained after removing the excess AEMA by slow filtration and washing with 100ml distilled water and 100ml ethanol.

For polymerization, the mixture containing 2ml MMA, 40 mg AIBN, 0.2ml PDMS-MA, and 0.2 mg AEMA-modified SWNTs was sonicated for 30 minutes in water bath before transferred into a 25-ml cylindrically shaped Parr® high-pressure reactor vessel. The mixture was then purged with CO_2 at atmospheric pressure for five minutes. Finally, the vessel was pressurized with CO_2 as heating is also supplied. The final pressure was set at 4200±200 psi, while temperature was at 65±2°C. A detailed

description of the experimental setup and temperature/pressure control can be found in reference (Yue, 2005). In control experiment, pristine SWNTs were added into the same polymerization mixture.

During this dispersion polymerization, surfactant poly (dimethyl siloxane) –mono methacrylate (PDMS-MA) prevents PMMA from quickly precipitating out due to agglomeration. The polymerization process was visually monitored through two sapphire windows. SWNTs were found to quickly precipitate out at the bottom of the reactor after the pressurization, due to the extraction of other reactants by $scCO_2$. The polymerization progressed the same way as previous reported by Yue, 2005, e.g. experiencing a transparent-milky-turbid-precipitate transition. After 24 hours of a typical colloid-forming process, a mixture of white (PMMA), black and gray powders (CNTs with PMMA) were collected. To remove PMMA that are physically attached to the SWNTs, the nanocomposite samples were carefully washed three times with acetone, THF, and a combination of both respectively. For a small percentage of the total sample, 20~30ml solvents were used to slowly remove PMMA from the sample on a filter paper during the first two washes. In the third time, the sample was dispersed in 10ml acetone/THF mixture and sonicated for 2 hours at 60°C, followed by a filtration step using 20~30ml solvents.

A sample of the final product was analyzed by Fourier Transform Infrared (FTIR) using a Perkinelmer instrument. The nanocomposite surface morphology was examined with a LEO32® field emission scanning electron microscope (FE-SEM). For comparison, all specimens, including pristine and modified carbon nanotubes, were sputter-coated before characterization. To further verify the coating of PMMA onto CNT surfaces, TEM

tests were performed on a LEO 922 Omega® EF-TEM. 300-mesh copper grids coated with carbon films were used as sample supports.

5.3 Results and Discussions

5.3.1 FTIR Spectra

Samples are mixed with KBr and then pressed for FTIR measurement. Figure 5.1. shows the FTIR spectra of HNO_3 treated SWNT (a), AEMA-modified SWNTs (SWNT-AEMA) (b), and PMMA functionalized SWNT (SWNT-PMMA) (c). In Figure 5.1a, the peak at 1580 cm^{-1} was assigned to stretching mode of C=C bond, which is close to the defect site of the nanotubes. The C=O band at 1730 cm^{-1} indicated successful generation of COOH on the nanotubes. The sharp peak at 1384 cm^{-1} is probably due to the nitration of SWNTs, which occurred during the high pressure HNO_3 treatment in the microwave [24]. After the attachment of AEMA, the C=O band from the formed amide bond is showing at 1650 cm^{-1} in the enlarged inset in Fig 1b. The C-H stretching and bending modes showing at 2911 cm^{-1} and 1434 cm^{-1} provide another prove of the successful reaction between SWNT-COOH and AEMA. The peak at 1730 cm-1 from SWNT-COOH is replaced by the peak at 1710 cm-1, which is the ester C=O stretching band from AEMA. In the spectrum of SWNT-PMMA (Fig. 1c), the peak at 1725 cm-1 is mainly from the C=O band of $-COOCH_3$ groups (scheme 1). Three different C-H stretching bands from the polymer are clearly showing at 2940 cm^{-1}, 2913 cm^{-1} and 2843 cm^{-1}. The peaks at 1259 cm^{-1} from Si-O and at 800 cm^{-1} from Si-C indicate the presence of the surfactant PDMS-MA. It should be noticed that the -MA group of this surfactant allows it to react with MMA and growing PMMA chains.

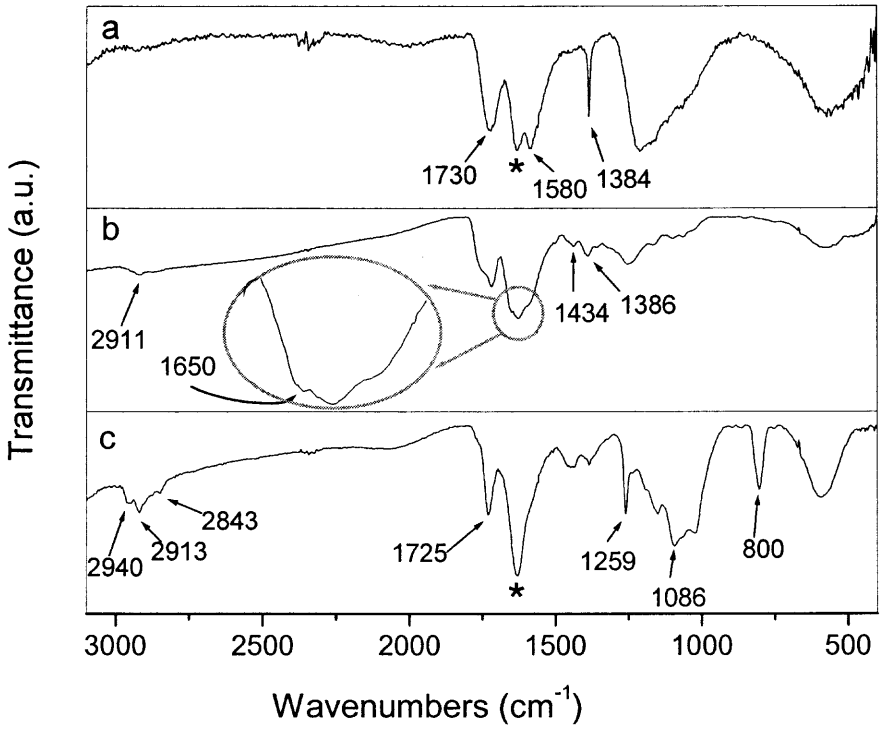

Figure 5.1 FTIR spectra of: (a) SWNT-COOH, (b) SWNT-AEMA and, (c) SWNT-PMMA. (*) denotes the water impurity from KBr.

5.3.2 Microscopic Results

The SEM images of SWNT-COOH and SWNT-AEMA are shown in Fig. 2a and 2b., and the photo insets in the two images are two samples suspension in polymerization mixture. The photo was taken 15 minutes after both suspensions were taken out of a sonication bath, in which they were sonicated for half an hour. As shown by the photo of SWNT-COOH, aggregation and precipitation were observed immediately after the sonication, which the suspension of SWNT-AEMA remained stable. As comparing to the SEM image (Fig. 2a) SWNT-COOH, the SEM image (Fig. 2b) of AEMA modified nanotubes show that lots of area of the nanotube surface and tube ends are covered by some light-color coating, which is an indication of AEMA attachment. The electron conductivity of AEMA is much lower than CNT, so, at the same distance to electron source, the areas covered with AEMA appears brighter on electron micrograph.

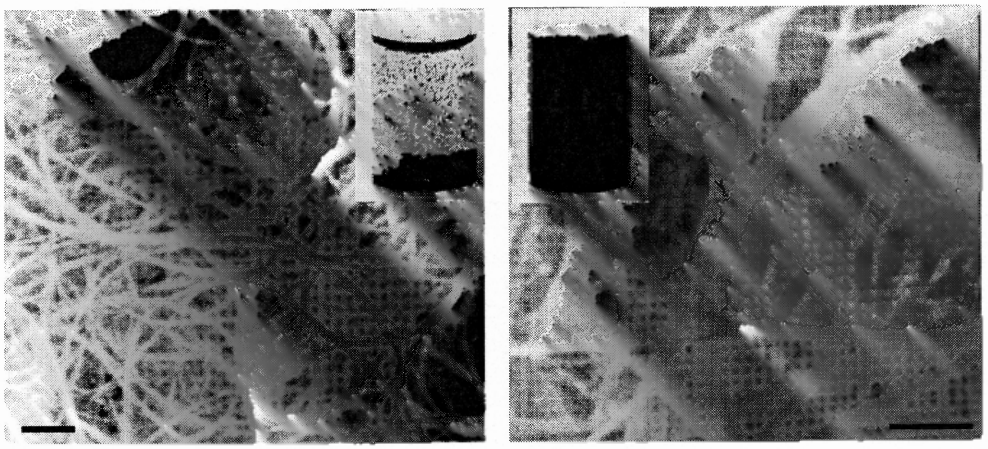

Figure 5.2 SEM images of: Left: (a) SWNT-COOH, scale bar 100 nm. (inset) photo of the nanotube sample in the polymerization mixture. Right: (b) SWNT-AEMA, scale bar, 100 nm. (inset) photo of the nanotube sample in the polymerization mixture.

Typical PMMA particles synthesized with dispersion polymerization in scCO2 are usually in the size range of hundreds to thousands of nanometers[20]. Particle size and degree of agglomeration can be controlled by varying monomer concentration, surfactant ratio, pressure etc. Shown in Figure 5.3.a is a micrograph of pure PMMA sample synthesized under the current polymerization condition. As can be seen, slightly agglomerated particles with primary size of ~300nm were obtained.

5.3.3 Polymerization of MMA with CNT-AEMA in $scCO_2$.

Shown in Figure 5.3.b-f are SEM images of original CNT/PMMA composite samples, in which coexistence of PMMA particles and film coating layer onto CNTs was clearly observed. Unlike loosely agglomerated spherical particles obtained in Figure 5.3.a, the PMMA particles are of less regular shape and broad size distribution, and heavily agglomerate with each other, as shown in Figure 5.3 b&c. The polymer coating thickness onto CNT was found to be non-uniform, probably due to the excessive amount of PMMA produced. Figure 5.3 d-f show the higher magnifications of certain sample points. It was

interesting to find small PMMA particles (<100nm) attached or skewered onto nanotubes.

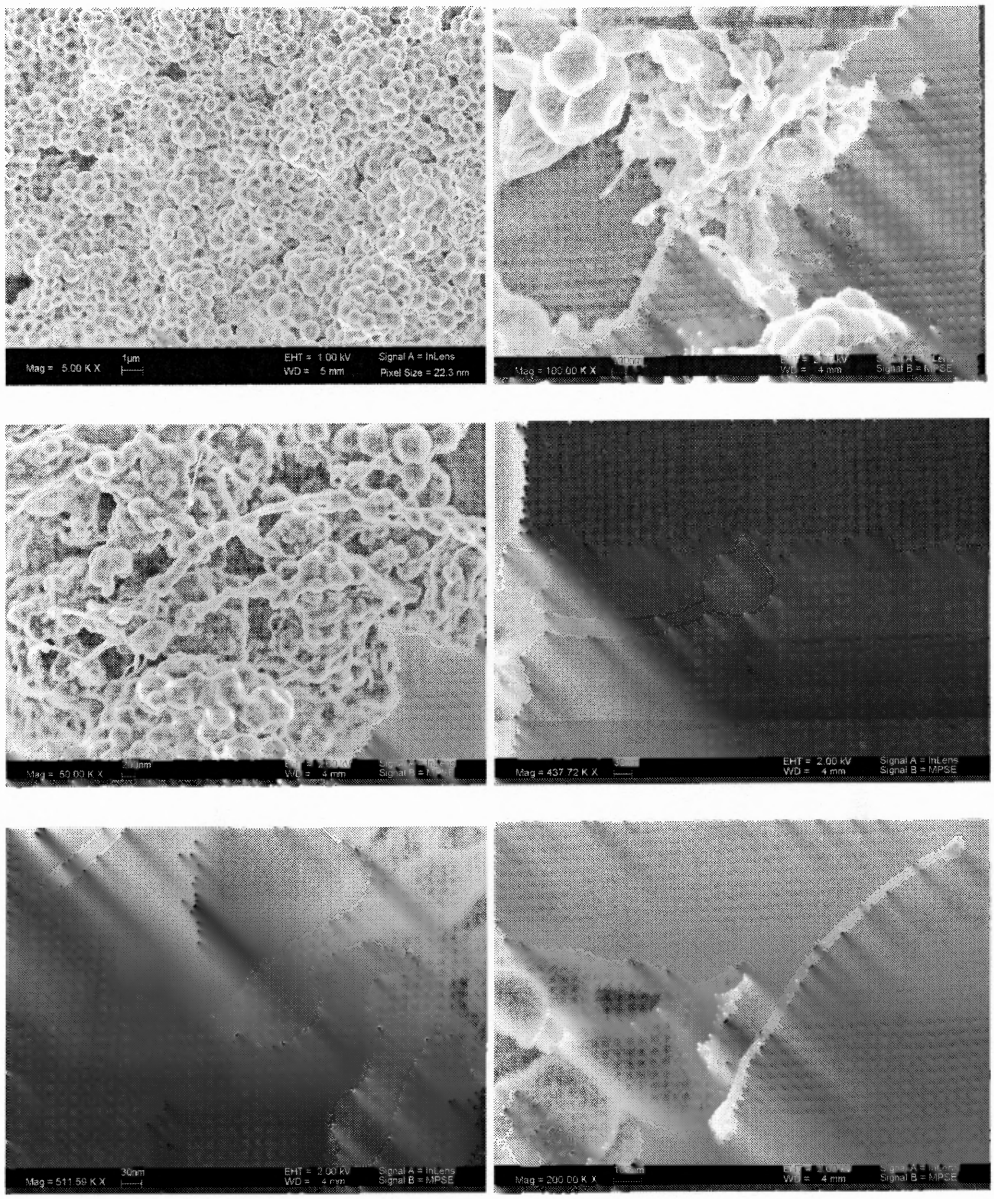

Figure 5.3 SEM image of a) PMMA; b), c) PMMA/CNT composite shown at lower Mag.; d), e), f) PMMA/CNT composite shown at higher Mag.

To verify that some PMMA molecules are covalently bonded onto CNT surfaces, the original samples were intensively washed with acetone or/and DHF to extract the physically attached PMMA molecules. SEM images of the sample after the first and third

washing cycles are shown in Figure 5.4 and 5 respectively. Although TGA quantification experiment was not practical due to the extreme small sample amount, it is clearly found that a large amount of polymers are still attached onto the CNT surface after the washes, indicating the existence of covalent bonds between polymers and CNTs.

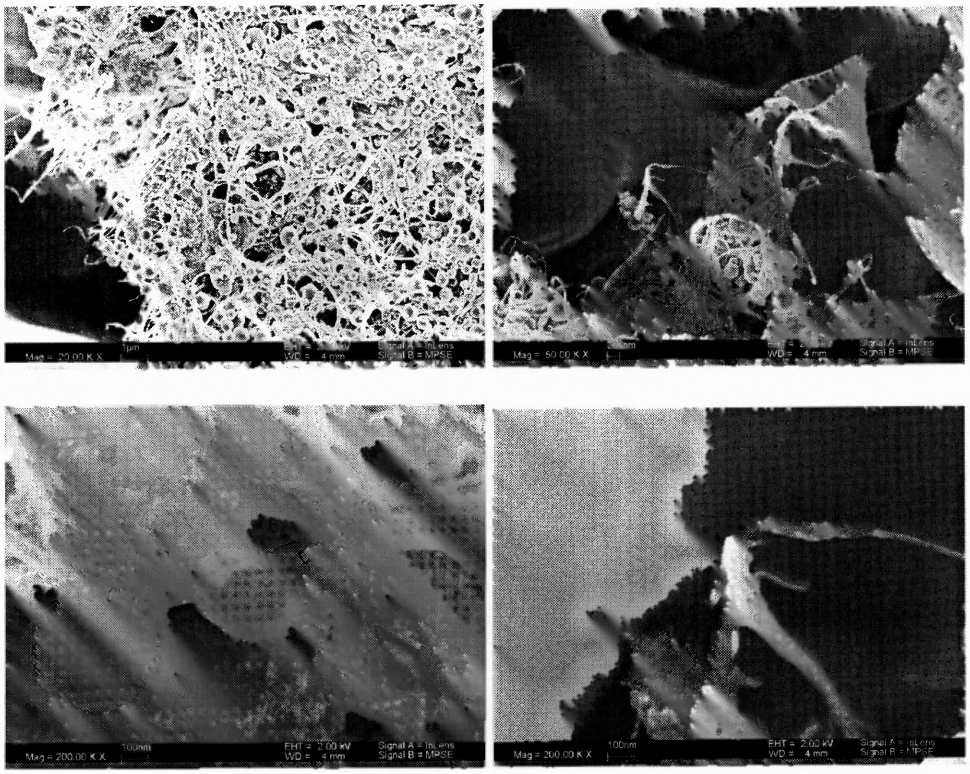

Figure 5.4 Samples after first wash with acetone, a), b) are images at lower Mag, c), d) higher Mag.

After the first wash, the samples become less agglomerated, as indicated in Figure 5.4 a&b. Although the amount of polymer was visually found significantly decreased, a large number of PMMA particles still exist. A detailed examination of the composite surface morphology clearly indicates coating of PMMA onto CNTs, as shown in 4 c&d.

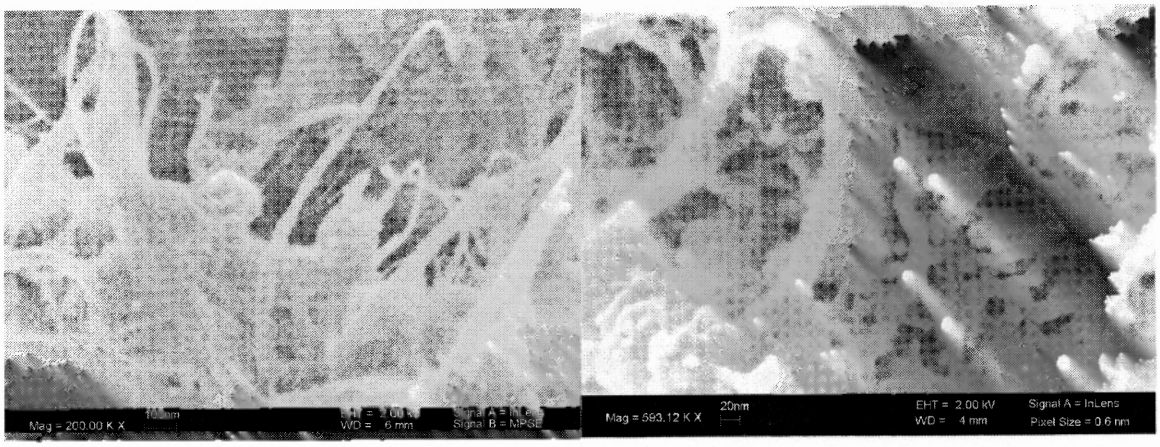

Figure 5.5 PMMA/CNT composite after a) second wash; b) third wash.

With more polymer removed, the composite samples appear more like assembly of PMMA-coated CNTs. Shown in Figure 5.5 a is the sample after second wash, after which individual polymer particles were completely eliminated. More extraction of polymer with heated acetone/THF mixture under sonication led to samples with morphology.. As shown in Figure 5.5b, coated CNTs with diameter of ~20nm were obtained. Such thin coating morphology has rarely been reported in the literature to the best of our acknowledge. The success here is attributed to the extremely high diffusivity and high salvation strength of $scCO_2$, which allow the reactants to easily penetrate the CNT matrix throughout the reaction.

TEM experiment was performed on pristine and reacted CNTs after the final wash to give a more detailed picture of PMMA/CNT interaction. Pristine (as bought) Hipco SWNTs existed in bundles and contained some catalyst particles (Fig a). As shown in Figure 5.6b, the reacted SWNTs were clearly debundled, which might be caused by polymerization in scCO2. The attached polymer is also abservable from the TEM image. Although the coating thicknesses vary, polymers were clearly found to surround the carbon nanotubes. TEM images b), c) indicate that CNT surfaces are not uniformly

covered, which could be due to the incomplete attachment of AEMA functional groups onto the CNT surfaces prior to polymerization.

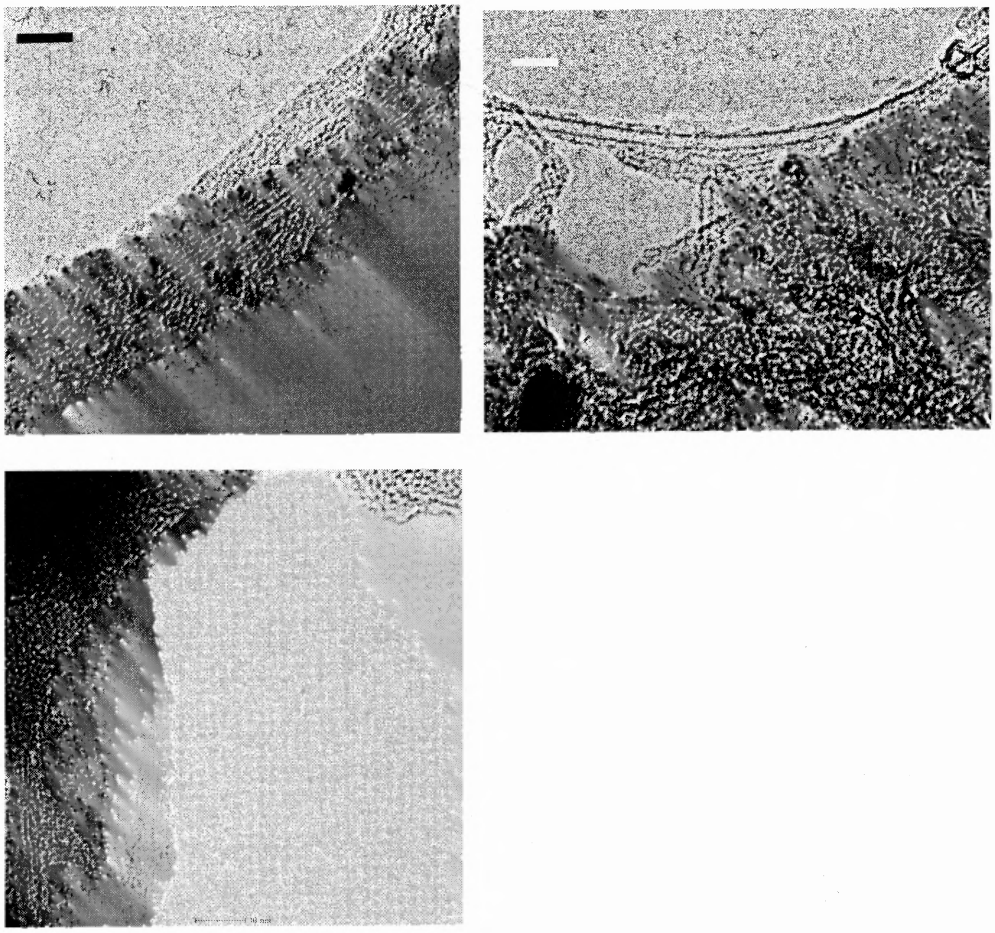

Figure 5.6 TEM images of a) pristine CNTs, b), c) coated CNTs, bar=10nm.

At the early stage of dispersion polymerization, the formation of oligmer/polymer nuclei follows a mechanism of homogeneous nucleation. In contrast, introducing reactive CNTs with high surface area may induce heterogeneous nucleation. It appeared that polymerization occurred simultaneously in the scCO2 and on the surface of CNTs, where grown polymers developed into a coating layer. This latter mechanism of polymer growth is more like a precipitation polymerization compared to dispersion polymerization due to the fact that the reaction sites are constrained on the immobile solid substrates instead of

the dispersed polymer particles growing in the medium. This also explains the heavy agglomeration of PMMA particles, which is typical in precipitation polymerization.

In addition to the heterogeneous nucleation mentioned above, the composite formation mechanism can also be explained using a copolymerization approach, where AEMA-modified CNTs can be regarded as to copolymerize with MMA. It should also be noted that the modified CNTs may function as crosslinkers, thus preventing successful stabilization of individual PMMA particles from happening.

5.3.4 Polymerization of MMA with Unmodified CNTs.

In control experiment, composite material was prepared with unmodified CNTs as filler material. As shown in Figure 5.3 c, bare CNTs do not disperse well in the reactant mixture even with sonication. A through examination of the product with SEM indicated that CNTs are primarily present in the form of large bundles. This is another indication that modification with AEMA helps CNTs to debundle. The bundle surfaces were found to be covered with PMMA, as shown in Figure 5.7. Although it is possible that polymers also formed between individual CNTs inside the large bundles, the CNT/PMMA interaction is not expected to be favorable due to the hydrophilicity difference.

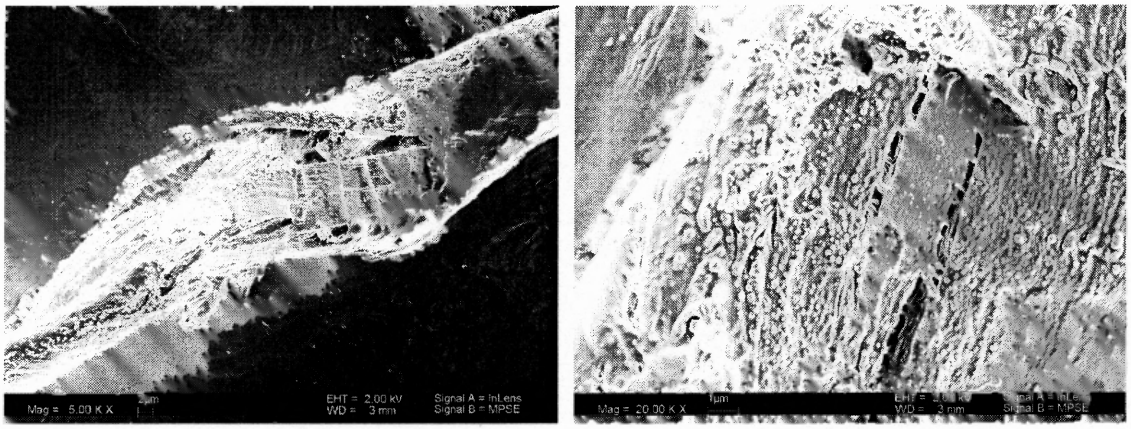

Figure 5.7 a) PMMA coating of unmodified CNT bundles. b) shows higher Mag. of image a).

5.4 Conclusions

Using in situ polymerization based method, CNT/PMMA nanocomposite was successfully prepared in scCO2 in this study. PMMA was found to chemically bonded onto CNT surfaces through copolymerization with AEMA molecules. Excellent surface coverage of CNTs with PMMA throughout all samples was achieved, thanks to the superb diffusivity and solvation strength of scCO2, which allow complete wetting of CNT surfaces with reactants. Surface functionalization with AEMA was found to be critical to the success of nanocomposite synthesis, due to the lack of debundling of CNTs and possibly unfavorable interaction between hydrophilic CNT surfaces and hydrophobic monomers. The success of functionalization of CNT with PMMA using this method can be generalized to various other polymers.

CHAPTER 6

COLLOID DISPERSION AND SYNTHESIS OF MACROPOROUS MONOLITH IN SUPERCRITICAL CO_2

In order for the research described in this chapter to stand on its own (as a publishable research paper), some of the pertinent prior work that has already been described in Chapter 4 may be repeated here

6.1 Introduction

Polymer monolith is known as cross-linked polymer forming interconnected porous structures with the shape and dimension conforms to the closed mold where the polymerization takes place. As a relatively new category of materials, monoliths have attracted great interests in applications such as supports for organic synthesis, separation processes, bioreactors, etc.. One of many examples is to use the single-piece porous material as a stationary phase in chromatography replacing packed columns. Continuous monoliths have the flexibility offer open channels of various sizes allowing the mobile phase to pass through and thus can be used as high performance membrane chromatography or large throughput bioreactors. The flexibility of being prepared to fit the designed shape and size according to the task demands features a great advantage over other materials.

Preparation of monoliths often involves polymerization in a mixture of multifunctional monomers, porogenic diluents, and other solvents to fine tune the systems so that the structures of solid polymers can maintain their homogeneity. Major challenges faced in the preparation in liquid solutions include: high sensitivity of porous

structure to porogneic diluents and solvents, volume shrinkage during polymerization and changes of structures or crack after the removal of solvents, large amount of organic solvents required, etc. During the last decade, researchers found that supercritical CO_2 ($scCO_2$) can replace many organic solvents in polymer synthesis or processing. This greener approach has been studied by several groups for the synthesis of porous polymers to eliminate or reduce the use of organic solvents and the stability and the pore size distribution can be adjusted.

In this work, the synthesis of highly cross-linked macroporous polymeric composite monoliths reinforced by surface-modified inorganic nanoparticles in $scCO_2$ is presented. Under proper conditions, dispersion polymerization of methyl methacrylate (MMA) that encapsulated well-dispersed silica nanoparticles produced a uniform monolith with interconnected pores in size of few microns. The monolith morphology, pore size and specific surface area were found to be tunable by varying conditions such as the size of inorganic particles and loads. Surface-modified silica nanoparticles were first to form encapsulated microspheres through in-situ polymerization and dispersed uniformly in the reactor (mold), followed by a sol-gel transition in a later stage that formed cross-linked interconnected porous monoliths. Poly (dimethyl siloxane) methacrylate (PDMS-MA) was used as the surfactant stabilizer to prevent dispersed PMMA colloids and nanocomposites from premature agglomeration. It was reported by O'Neill, et al, 1998 that the cloud point pressure of PMDS decreases with the concentration of MMA in $scCO_2$. The origin of sol-gel transition is likely induced by the consumption of monomer which lowers the solvency power of the medium to pull out and swell the PDMS chains. After the one-step process, CO_2 was vented from the reactor

and no sign of shrinkage or crack been observed; monoliths of low bulk density (about 0.1g/cm^3) were collected.

6.2 Experimental Section

6.2.1 Materials and Equipment

Polymerization chemicals, including monomer methyl methacrylate (MMA), surfactant poly (dimethyl siloxane) methacrylate (PDMS-MA, Mw=10K) and initiator 2,2'-Azobisisobutyronitrile (AIBN), were obtained from Sigma-Aldrich (Milwaukee) and were used as received. Chemicals for silica particle synthesis: tetraethyl orthosilicate (TEOS), ammonium hydroxide (NH_4OH) and ethanol were purchased from Sigma-Aldrich and used without further purification. Silica particle surface grafting agent 3-(trimethoxysilyl) propyl methacrylate(MPS) was obtained from Fisher Scientific. Carbon dioxide gas was purchased from Matheson with 99>% purity. The experiment apparatus consists of a 25-ml cylinder Parr® high-pressure reactor vessel with two sapphire windows at both ends of the long axis.

6.2.2 Silica Nanoparticle Synthesis and Modifiction

Silica nanoparticles were synthesized according to a process introduced by Stöber et al.[10a] through which TEOS was hydrolyzed to form silica particles in ethanol with NH_4OH catalyst. Monodisperse spherical particles can be fabricated for sizes from tens to thousands of nanometers. In each batch, TEOS, ethanol, NH_4OH, and deionized water were mixed according to certain molar ratios and stirred for two days at room temperature. Silica particles synthesized with this method are hydrophilic, with –OH groups on the surface. A well-established coupling method was followed[10b] for surface

modification by which MPS was added in the silica particle dispersion and stirred for two more days. MPS not only attaches to the silica surface and changes it into hydrophobic, but also introduces methacrylate terminal groups providing grafting sites for polymer tethering to increase the affinity between the particles and polymer. The end-functional groups also form a corona protection layer preventing the condensation reaction between silica particles during the drying process. Particles were then dried and made ready for polymerization as shown in Figure 6.1.

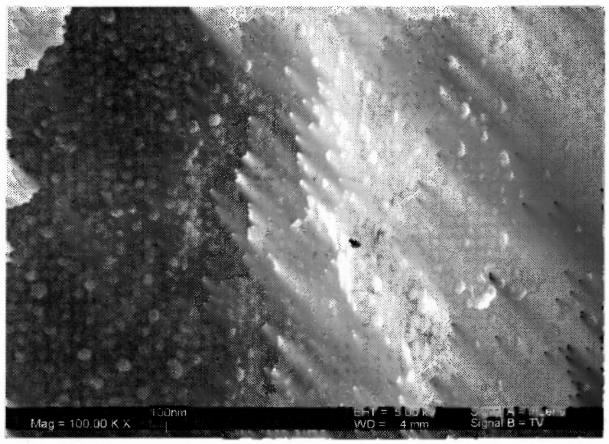

Figure 6. 1 SEM image of modified silica nanoparticles with average diameter of~60nm, bar=100nm.

6.2.3 Monolith Preparation

Monolith synthesis with in situ dispersion polymerization was conducted inside the high-pressure reaction vessel. In each run, 2 ml of monomer MMA, 0.04g of initiator AIBN, and 0.4ml of macromonomer PDMS-MA were premixed, followed by the dispersion of various amount of silica particles into the mixture. After purging with low-pressure CO_2 gas for five minutes, liquefied CO_2 was pumped into the reactor at room temperature until an appropriate pressure was reached[9]. Before the reaction started, the monomer,

stabilizer and initiator were all dissolved in CO_2, while the silica particles are uniformly suspended in the reactor vessel with magnetic stirring. The vessel was then heated to 65°C to initiate the free-radical polymerization when the pressure also reached its desired final value. The reactor remained closed during the experiment and a pressure decrease of 100~200 psia due to volume shrinkage from the polymerization was observed. The experiments ran for 24 hours, after when CO_2 was released and the reactor was cooled down to room temperature for sample collection.

6.2.4 Characterization

The surface morphology of the monoliths was examined with a LEO32® field emission scanning electron microscope (FE-SEM). Specimens were sputter-coated with thin carbon film before characterization. To investigate the silica distribution inside the PMMA particles, a LEO 922 Omega® EF-TEM was used. Samples were embedded in epoxy resin and then microtomed before examination. Surface area was measured with a five-point BET analysis on a Quantachrome® Nova300 analyzer. Glass transition temperature (Tg) was measured with differential scanning calorimetry (DSC) on a TA-Q100® calorimeter.

6.3 Results and Discussion

6.3.1 Dispersion Polymerization of PMMA

For comparison, we have synthesized pure PMMA in $scCO_2$. The initial transparent reaction medium was found to exhibit an increasing turbidity in the first 4 hours after initiation of the polymerization; no white precipitation was observed until a few more

hours later. Upon the completion of the polymerization, PMMA in the form white powders were collected at the bottom of the reactor. The white powders consist of loosely agglomerated spherical particles in the range of a few hundred nanometers. Figure 6.2a depicts the SEM micrograph of PMMA agglomerate with individual particle size of ~300nm. Our result is similar to those reported from literature(O'Neill, 1998).

6.3.2 Monolith

The premise of fabricating monoliths of homogeneous structures is to have good dispersion of silica nanoparticles in the reactor (mold). Unlike unmodified hydrophilic silica particles that quickly precipitated out in $scCO_2$, the MPS-modified silica nanoparticles were observed to disperse well in $scCO_2$ even without stirring due to the favorable interactions between MPS molecules and CO_2. Previously, Johnston et al., 1998, found that silica particles can be stabilized by PDMS or PFOMA in $scCO_2$. In a different study, Vistin et al., 2004, have proved that silica nanoparticles modified with fluorinated chlorosilanes can also be well dispersed in $scCO_2$. Here we have demonstrated successful dispersions of silica nanoparticles in $scCO_2$ with MPS modification.

After polymerization, the monolith filled up the reactor mold with no volume shrinkage observed after the release of CO_2. Depending on the experimental parameters, product morphology varied. Figure 6.2b depicts SEM micrograph of the monolith prepared from PMMA with 20wt.-% 50nm silica particles. The micron-sized polymer composites formed an interconnected macroporous structure which extended uniformly

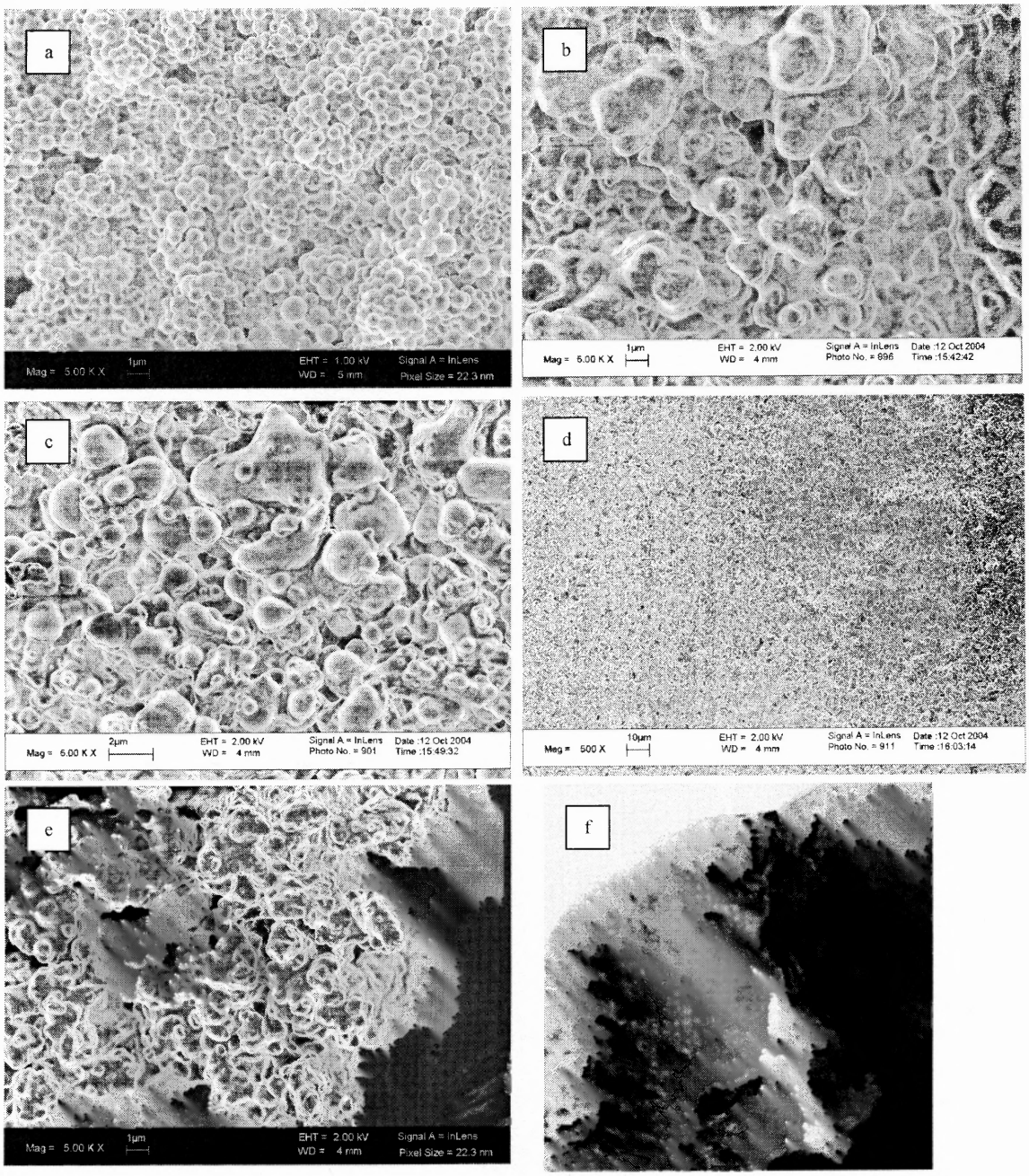

Figure 6.2 SEM images of a) PMMA particles synthesized from dispersion polymerization in $scCO_2$; b) monolith containing 20 wt.-% 50nm silica nanoparticles; c) monolith containing 10 wt.-% 50nm silica; d) lower magnification of sample c); e) monolith containing 10 wt.-% 20nm silica; f) TEM image of sample e), bar=20nm, embedded silica particles are seen clearly.

into the entire space of the mold. The size of the primary composite particles was several times larger than pure PMMA synthesized without silica (Figure 6.2a) and the shapes of

the composite particles appeared less regular. Small encapsulated silica particles can be seen from the surface morphology of the nanocomposites; no naked silica particle was found excluded from the PMMA matrix. The pore size distribution was broad but in a range of few micrometers. Reducing the amount of silica to 10wt% results in many small coagulated particles attached to the network structures as shown in Figure 6.2c, however, the macroscopic morphology remained uniform (Figure 6.2d).

Further reduction of the particle load to 5 wt.-% resulted in formations of loosely agglomerated spherical composites of size around 1 μm (data not shown). Reducing the size of silica particle to 20 nm while keeping the same load of 10 wt-% led to a network structure consisting of very irregularly coagulated nanocomposite, as shown in Figure 6.2e. The roughness of the surface increased drastically compared to Figure 6.2b and 2c. Figure 6.2f depicts the TEM micrograph of silica nanoparticles embedded in the PMMA matrix.

Ideally, PMMA, PDMS, and PMMA-co-PDMS can tether to the silica surface through reaction with the surface vinyl groups. Tethered PMMA chains can greatly improve the dispersion of silica nanoparticles in PMMA matrix. With the co-solvent MMA, PDMS tails can provide adequate steric repulsions to prevent premature flocculation of the particles. The critical flocculation density (CFD) of $scCO_2$ for the given PDMS can be regarded as a function of the MMA concentration under the given reaction conditions[8]. At the early stage of the reaction, the medium CO_2 density ρ_{CO_2} is above CFD and PDMS stabilizes the particles effectively, however, as the conversion of MMA increases, CFD increases and eventually exceeds the medium density. The onset of gelation occurs when CFD is equal to ρ_{CO_2} and the dispersed colloids start to

experience failure of stabilization and flocculate to form macroporous "gel". The rate of flocculation "reaction" against the diffusion of dispersed nanocomposites affects the porous structures of the monolith. Note that our reactor pressure is slightly below the reported upper critical solution pressure (UCSP, 4060 psia, 65°C) of the PDMS under study(Yates 2000). The chain length of PDMS and CO_2 pressure could be used to adjust the onset of gelation. Recent neutron reflectivity study showed that bare silica surface has strong short-range attractive interactions with the siloxane groups of PDMS, which form a dense layer on the solid substrate even under high scCO2 density (Sirard 2003). It is sure that in our case, MPS and grafted PMMA have effectively screened such interactions. Upon gelation, the monoliths are strengthened by the interfusion of polymers and by the polymer-grafted silica particles, which are the "cross-linkers" throughout the polymer micro-domains.

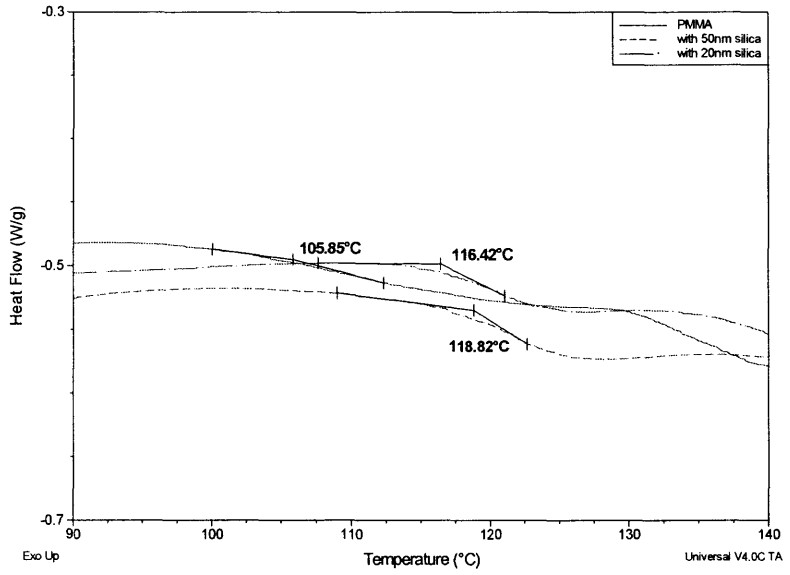

Figure 6.3 DSC results of PMMA and composite monolith containing 10 wt.-% silica nanoparticles.

Following the discussion above, PMMA-grafted silica nanoparticles can serve as nuclei allowing live PMMA chains growing on the surface to continue propagation/ termination reactions simultaneously with other PMMA particles formed in the bulk. Nanoparticles with coronas of polymer brushes embedded in the composites should affect the mobility of PMMA even under CO_2 plasticization and retain the conformations after coagulations. In addition, grafted PMMA can react and form both bridge and loop configurations. The former literally transforms the nanoparticles into multifunctional crosslinkers; the latter enhances polymer entanglements and leads to low mobility. Less mobility of polymer implicates an increase of the characteristic "reaction time" for flocculation during the sol-gel process and also facilitates the stabilization of the monoliths from further structural changes. Comparing Figure 6.2c and 2e, under the same load, the smaller the nanoparticles the more nucleation sites and crosslinkers observed from the rougher surface. The effect of other process variables, such as pressure, monomer and surfactant concentrations, etc. will be addressed elsewhere. An important feature of nanocomposites is the enhancement of thermal and mechanical properties by the nanofillers. Attractive interaction between nanoparticles and polymer can result in an increase of the glass transition temperature Tg. DSC results showed that an increase about ~10°C of Tg was observed after MPS-modified silica particles were incorporated in the PMMA composites (as shown in Fig. 6.3). With the same load (10 wt.-%), monolith containing smaller silica (20 nm) was found to have a higher Tg (ΔTg=2.4 °C) compare to the samples with 50nm silica. On the other hand, no obvious change in PMMA

morphology nor Tg was observed when unmodified hydrophilic silica particles were added into the reaction mixture (data not shown).

Since the pore sizes of the monoliths are of micron scale, the specific surface area measured by BET was relatively low, varying from ~1m^2/g to 7m^2/g in the investigated cases. Specimens containing smaller silica particles show rougher surfaces and larger surface area. The relatively small specific surface area may find potential applications in separation of large molecules such as proteins after further development. Endeavors are underway for the detailed characterization of physical properties of these monolith materials, including mechanical properties, pore size control, etc.

6.4 Conclusions

Polymer monoliths containing silica nanoparticles were synthesized via a one-step sol-gel process in $scCO_2$. This new environmentally benign process offers advantages of easy operation and resolves problems related to monolith shrinkage and solvent removal. It was suggested that mechanism of controlled steric stabilization of poly(dimethyl siloxane) (PDMS) in the early stage of reaction followed by subsequent failure due to the depletion of MMA monomer could explain the observed macroporous structures. The morphology and property of the monoliths can be adjusted by varying reaction conditions, such as particle load ratio, size, etc. which could also enhance the thermal and mechanical properties of monoliths. Similar procedures can be extended to other polymer/ inorganic nanoparticle systems.

CHAPTER 7

SELF ASSEMBLY OF HIGHLY STABLE BI-MIMETIC LIPID VESICLES FOR MICROENCAPSULATION

In order for the research described in this chapter to stand on its own (as a publishable research paper), some of the pertinent prior work that has already been described in Chapter 1 may be repeated here.

7.1 Introduction

Unilamellar vesicles (ULV), consisting of a single closed bilayer are considered to be one of the better drug encapsulation and delivery devices. Although liposomal ULV often form spontaneously in *vivo*, they are seldom found in simple aqueous solutions. Over the last decade, several groups have investigated spontaneously forming ULV occurring in certain cationic-anionic surfactant and cationic surfactant systems (Kaler 1992, Hoffmann 1992). However, because of biocompatibility issues, surfactants systems are normally considered less suitable for biological applications.

Conventional methods for the preparation of lipid ULV are tedious and involve procedures such as, repeated freezing and thawing, multiple extrusions and sonications. Normally, high pressure is required to produce small, extruded ULV (pore size ~ 50nm or smaller) and the production rate is very low. Another concern of extruded vesicles is that the samples are almost always contaminated with larger multi-lamellar vesicles (MLV). In contrast, spontaneous forming ULV have many advantages including ease of preparation, good size reproducibility, high stability over time, and less contamination from MLV. Since these ULV are formed "spontaneously", they can either be

energetically stable or kinetically trapped. For the purposes of drug delivery, of great interest are their low polydispersity and size (50 – 150 nm). Here, we report on the characteristics of spontaneously forming, stable phospholipid ULV. Their size, polydispersity and the insensitivity of these two characteristics to changes in lipid concentration and salinity make them likely candidates as drug delivery vehicles.

Spontaneously forming ULV were previously observed in solutions consisting of long- and short-chain lipid mixtures (Gabriel, 1984; Ollivan, 2000). Typically, they were obtained from micelle-to-vesicle transitions induced by detergent elimination (Egelhaaf, 1999) or a temperature jump (Nieh, 2002). In those studies, the average vesicle radius, $<R_o>$, was always found to change with lipid concentration, C_{lp}, indicating that the ULV were sensitive to the chemical potential of the lipids. A recent study (Nieh, 2003) has shown that the structure and size of spontaneous forming DMPG or Ca^{2+} doped ULV were practically independent over a wide range of C_{lp}. However, when the systems were doped with both DMPG and Ca^{2+}, vesicle radius again became sensitive to changes in C_{lp}. It is known that adding Ca^{2+} to lipid mixtures alters the ionic strength of the solution and the bilayer's charge density due to the strong chemical binding of Ca^{2+} ions with PC headgroups (Seelig, 1987). In the present study we attempt to minimize these complications by using NaCl, instead of $CaCl_2$, as Na^+ does not bind with the lipid as strongly as Ca^{2+}, but instead forms a "loose" counterion layer surrounding the headgroups, as revealed by NMR (Kirland, 1979).

Most theoretical studies of spontaneous vesiculation and ULV stability were applied to equilibrium systems. Using Helfrich's model (Helfrich, 1973) and fluid lipid bilayers, the microscopic energy *per* spherical vesicle has a simple scale-free relationship

of $4\pi(2k_b + k_G)$, where k_b and k_G are the bending modulus and Gaussian modulus. These moduli depend on factors such as surfactant distribution, co-surfactants, surface charge, molecule packing, etc. Winterhalter and Helfrich, 1988, and other groups have examined the effect of electrostatic double layers on the bending elasticity of fluid membranes using a Poisson-Boltzmann (P-B) theory. One of the most prominent findings is that the Gaussian modulus, depending on the charge density and the Debye length, must be negative for the spontaneous formation of ULV. Safran et al., 1990 and 1991, calculated the free energy of ULV formed in surfactant mixtures and suggested that, compared to extended lamellae, surfactant mixtures with a high bending modulus may yield a lower elastic energy if there is a strong attraction between the two surfactants. Bergstrom and Eriksson, 1996 and 1998, derived an effective k_b for surfactant mixtures by considering a variety of contributions such as, geometric packing, coulombic and head group interactions, chain conformation, and mixing. Oberdisse et al. (1996, 1997, 1998) applied the so-called "vesicle cell model" (VCM) and P-B theory to investigate the effect of charge density (ρ), dilution, salinity, and the bending modulus on ULV size. On the other hand, Israelachvili et al. developed mean-field theories in 1976 by considering molecular geometric packing, self-assembly, and interactions among surfactant molecules and lipids. More sophisticated molecular models, which consider the energy change related to molecular translation and rotation, head group interaction, chain conformation and electrostatic interactions, have also been employed to predict the size of small ULV (Yuet, 1996).

It has recently been reported that spontaneously forming ULV may be kinetically trapped. These findings led to the kinetic model proposed by Leng et al., 2003, which

suggests a growth mechanism for bicelles upon dilution and the closure of large bicelles to form vesicles once the perimeter line tension dominates the bending elastic energy. The size of the kinetically trapped vesicles can thus be determined by controlling C_{lp} and C_s.

The present work investigates the self-assembled structures of DMPC/DMPG/DHPC mixtures doped with Na^+, using SANS and DLS. Surface charge is introduced by doping with the negative-charged lipid, DMPG. Compared to Ca^{2+}, Na^+ does not tenaciously bind to lipid headgroups, thus the surface charge density of Na^+-doped mixtures can simply be controlled by the DMPG/DMPC molar ratio. Nevertheless, it is noticed that the Zeta-potential of the vesicles may be affected by the electro-chemical double layer, and thus the concentration of NaCl. The vesicle size was monitored as a function of lipid concentration (C_{lp}), solution salinity (C_s), temperature (T) and time (t). Throughout the experiment, the molar ratio of long- (DMPC) to short-chain (DHPC) lipids remained constant at 4.0, while the DMPG/DMPC ratio, for all samples, was 60. These molar ratios were selected based on our previous experimental results (data not shown), which indicate that stable ULV only exist for DMPC/DHPC molar ratios between 2 and 5. Beyond this range, DMPG/DMPC mixtures form discoidal bicelles and MLV (Nieh, 2002, 2003). A structural phase diagram of lipid mixtures in the dilute regime ($C_{lp} < 1.00$ wt%) is presented. It is found that under numerous experimental conditions the ULV size is insensitive to both C_{lp} and C_s. The structural phase diagram is consistent with Winterhalter and Helfrich's prediction, namely that at the surface charge densities and Debye lengths studied, the calculated Gaussian modulus and total elastic energy are negative, predicting the spontaneous formation of ULV. As salinity increases,

the total elastic energy increases, eventually leading to a ULV-MLV transition. The origin of nearly constant-size vesicles as a function of lipid concentration and salinity is presently not clear: at low C_{lp} it may be the result from the dominant role of enthalpic interactions, or due to the kinetics of the system. Despite this lack of detailed physical understanding, the DLS results are highly reproducible and most samples remained unchanged for weeks, and even months, at low C_{lp}. Strong mechanical energy input, such as vortexing, centrifugation and even bath sonication, were applied to the ULV, but no size change was observed once they were formed.

7.2 Experimental Section

7.2.1 Materials

DMPC, DHPC and DMPG were purchased from Avanti Polar Lipids* (Alabaster AL); sodium chloride (NaCl) was obtained from Sigma-Aldrich (St. Louis, MO). All chemicals were used as received. Prior to use, deuterium oxide (99.8 %, Fisher Scientific) was filtered through a 0.1 μm Millipore Millex-VV sterile syringe driven PVDF filter.

7.2.2 Sample Preparation

Stock solutions of DMPC/DHPC (molar ratio = 4/1) and DMPC/DMPG/DHPC (molar ratio = 60/2/15) were prepared to a C_{lp} of 5.00 wt% in D_2O. Vortexing and temperature cycling from 4 °C to 50 °C was used to dissolve the lipids. The two 5.00 wt% solutions were then mixed accordingly to a final DMPC/DMPG/DHPC molar ratio of 60/1/15.

* The identification of any commercial product or trade name does not imply endorsement or recommendation by the National Institute of Standards and Technology (NIST).

After equilibrating for 24 hours at T = 4°C, the solutions were diluted to C_{lp} = 1.00 wt% using filtered D_2O. Sodium chloride was then added to yield a C_s in the range of 0.10 % to 1.00 %. The solutions were then frozen at –10 °C followed by a single thawing step to room temperature for homogenization. Finally, solutions were diluted with appropriate amounts of D_2O to the final C_{lp} values. After preparation, samples were stored at 4 °C for four months while selected samples were further incubated at 30 °C for a period of one month. Most samples were occasionally tested using DLS over the five-month period, while all SANS experiments were conducted one month after the sample preparation.

7.2.3 Small Angle Neutron Scattering

7.2.3.1 Theory. The scattered intensity, I (Q), from a solution composed of particles can be expressed in terms of a form factor, F(Q), and a structure factor, S(Q), where Q is the scattering vector ($Q = (4\pi/\lambda)\sin(\theta/2)$). The form factor reveals the geometric characteristics of the single aggregate in solution, while the structure factor accounts for correlations due to interparticle interactions. The form factor and the structure factor are assumed to be independent and the scattering intensity can be expressed as

$$I(Q) \propto n_p \left| \langle F(Q) \rangle^2 \right| S(Q) \qquad (1)$$

where n_p is the number density of the scattering particles.

In our case, the F(Q) of a ULV can be simulated using a spherical shell model with three parameters: vesicle size, bilayer (shell) thickness, and polydispersity. For the structure factor, S(Q), an analytical form can be obtained through solving the Ornstein-Zernike equation using a mean spherical approximation (MSA).[48] The derived S(Q), which accounts for the repulsive electrostatic interactions between particles, was used in

fitting the ULV system. The parameters pertaining to ULV charge density and salt concentration can be estimated from C_{lp} and C_s; a 20% variation is allowed in the fitting procedure.

The ULV form factor was based on a core shell sphere (CSS) model, where the bilayer is approximated as a single layer of constant scattering length density ($\rho_{lipid} = 3.2 \times 10^{-7}$ Å^{-2}). In reality, the scattering length density across the bilayer is not uniform due to the differences in the composition of the headgroup and chain regions. However, the above model with a constant value of ρ_{lipid} (the single-well profile), which reduces the number of fitting parameters as well as simplifies the calculation, is found to be sufficient to describe the experimental data. The total radius of the vesicle was taken to be the inner radius of the sphere plus the bilayer thickness. As in the case of bicelles, the radius was not constrained, whereas the thickness was restricted to lie between 25 and 45 Å. Detailed mathematical expressions for ULV model can be found in reference (Nieh, 2004).

7.2.3.2 Experiment. SANS experiments were conducted using the 30m NG7 SANS (Glinka, et al., 1998) located at the NIST Center for Neutron Research (Gaithersburg, MD). Neutron wavelength was 0.81 nm with a FWHM spread of 0.11. Two sample-to-detector distances (1.50 m and 15.30 m) were selected, covering an effective Q range between 0.002 and 0.3 A^{-1}. A detector offset of 20cm was employed to provide adequate overlap for combining data sets. The ambient background and empty cell scattering were subtracted from the 2-D raw data. The corrected data were then circularly averaged to yield a 1-D intensity distribution, I(Q), which was put on an absolute scale (cross section per unit volume) using the incident neutron flux. The incoherent scattering was obtained

from the intensity plateau at high Q of the reduced data, and was subtracted from the raw data. All the SANS experiments were carried out at 30 °C.

7.2.4 Dynamic Light Scattering

7.2.4.1 Theory. For a dilute solution of spherical noninteracting particles, where each particle, i, of radius Ri undergoes Brownian motion, the Stokes-Einstein equation describes the relationship between Ri and the diffusion coefficient, Di,

$$D_i = \frac{kT}{6\pi\eta_w R_i}, \tag{2}$$

where k, T, and ηw are the Boltzmann constant, absolute temperature, and the viscosity, in our case, of D_2O, respectively. For nonspherical particles (e.g., disks, cylinders, etc.), an equivalent hydrodynamic radius, RHi is used to replace Ri in Eq. 1. In the DLS measurement, the time-dependant intensity autocorrelation function, G(τ), is obtained, and is given by

$$G(\tau) = \int_0^\infty I(t)I(t+\tau)dt, \tag{3}$$

where τis the time delay. From the Siegert relation, G(τ) can be expressed in terms of the field autocorrelation function, g(τ) as

$$G(\tau) = 1 + \gamma g(\tau)^2, \tag{4}$$

where γis the instrumental coherence factor. g(τ) represents the time decay of the position autocorrelation function of the particles and in a polydisperse system can be written as:

$$g(\tau)=\sum_{i} A_i e^{-D_i Q^2 \tau}. \tag{5}$$

with the decay rate being:

$$\Gamma_i = D_i Q^2 \tag{6}$$

In this expression, Q is the scattering vector and Ai represents the light-scattering amplitude of the particle i with diffusion coefficient Di.

Cumulant analysis methods and regularization methods such as CONTIN are usually employed in analyzing the experimental data to obtain the diffusion coefficient (Santos and Castanho, 1996). Cumulant analysis is usually applied to systems having a monomodal and sometimes bimodal size distribution so that the characteristic function $g(\tau)$ of the size probability distribution is expanded as a series of cumulants. At small τ, the first cumulant can be expressed in the form of DeffQ2, where Deff is the effective diffusion coefficient.

For analysis methods such as CONTIN, the aim is to solve Eq. 4 through eigenvalue decomposition combined with regularization, a smoothing technique. The size distribution function can then be resolved in terms of the eigenvalues, Di (or RHi), and the average hydrodynamic radius, RH, is obtained by normalizing it to the scattered intensity of the particles (z-average), but not by their volume (Pencer et al., 2001). We mostly used cumulant analysis to interpret our data from monodisperse samples, whereas CONTIN sometimes was used for samples with bimodal size distributions to understand possible structures in the system. In some cases, the size distribution function obtained from the CONTIN analysis has three or more maxima. Currently, we do not know

whether these distributions are reliable or if they are artifacts due to strong interparticle interactions.

7.2.4.2 Experiment. DLS experiments were performed on a Beckman N4 Plus Photon Correlation Spectrometer at a scattering angle of 90°. The instrument is equipped with a laser source of wavelength 632.8 nm and an 80-channel correlator with multi-channel spacing. Before experimentation, the instrument was calibrated using a standard latex solution. All samples were tested at three different temperatures, 10 oC, 30 °C and 50 °C. The viscosities at these temperatures are 1.679, 0.9759 and 0.6519 respectively. At comparable temperatures, solutions with D_2O, compared to those with H_2O, exhibit a higher viscosity due to increased hydrogen bonding. Both intensity and number weighted results were obtained. For quantitative comparisons of DLS results with SANS data, only number-weighted average histograms are shown in the paper. However, intensity-weighted histograms are better suited in distinguishing large particles such as, MLV.

7.3 Results

7.3.1 Visual Observations

All ULV solutions were transparent with some "bluish" appearance, commonly seen in mixtures of vesicles with diameters in the range of tens of nanometers. The non-DMPG stock solution of $C_{lp} = 5.0$ wt% became opaque as the temperature increased from 4 °C to 25 °C and *vice versa*, presumably due to a transition from bicelles to MLV. At high concentrations and low T (≈ 10 °C), the non-doped lipid mixtures formed bicelles. Due to the small size of this structure, bicellar solutions are also transparent. On the other hand, MLV solutions usually appear opaque, and over a period of time MLV colloids can

separate macroscopically from solution. The DMPC/DMPG/DHPC = 60/2/15 stock solution (also 5 wt%) remained transparent and became highly viscous when T was increased from 4 to 25 °C.

After mixing the two stock solutions to yield the desired DMPC/DMPG ratios, the mixture was stored at 4 °C for one day, and was then diluted to 1.00 wt%. After a single freeze/thaw cycle, all 1.00 wt% solutions became totally transparent around 10 °C. When these samples (1 wt%) were heated to room temperature, their appearance turned from transparent, to bluish, and finally, to opaque, indicative of a bicelle-ULV-MLV-phase transition. These low NaCl solutions (< 2%) were stable only at low temperature for days, while mixtures with very high amounts of NaCl (10%) remained clear for at least six months at 4 °C. Addition of NaCl can induce phase separation resulting in an opaque appearance at room temperature - a similar change has also been observed in surfactant systems. Though the appearance of the solution was used as a subjective determinant of MLV formation, DLS intensity weighted histograms have indicated the presence of a multi-modal distribution with large particles (> 100 nm).

All ULV samples were prepared by directly diluting the 1.00 wt% transparent solutions (bicelle phase) with D_2O at room temperature, exception being the 0.033 wt % sample which was diluted from a 0.10 wt % sample at room temperature. Samples at 4 °C were subjected to a T-jump and underwent a bicelle-to-vesicle transition with an accompanying change of appearance, from clear to bluish, that remained unchanged for months at 4 °C. No phase separation was observed in samples with C_{lp} lower than 0.5 wt % and C_s lower than 0.33 wt% for four months. Phase separation occurred after only days or weeks with C_{lp} > 0.5 wt % or C_s > 0.33 wt % samples. Slight cloudiness was

observed in samples with C_{lp} higher than 0.33 wt% after a four-month storage period in a refrigerator but was easily eliminated by shaking or heating the samples to room temperature. A similar observation was previously reported in CTAB/SOS surfactant systems. A 2-D schematic phase diagram is presented in Figure 7.1 summarizing the various observations described.

7.3.2 Effects of C_{lp} and C_s on Vesicle Stability and Size

To study the effect of C_{lp} on the resultant self-assembled structures present in the various mixtures, we measured ULV size at a series of C_{lp} concentrations: 0.033, 0.10, 0.33, 0.50 and 0.75 wt% with a C_s = 0.1 wt%. As mentioned previously, SANS experiments were conducted at 30 °C after the samples were incubated at 4 °C for a period of one month. DLS experiments were conducted at 10 °C, 30 °C and 50 °C immediately after sample preparation and at intervals during the four months of storage. The only exception being the 0.75 wt% sample which turned opaque at T > 30 °C. The 0.75 wt% sample was only tested at 10 °C immediately after preparation.

SANS data and the corresponding best-fit curves using the three-parameter spherical shell model are presented in Fig. 7. 2. A detailed mathematical expression of the model has been described elsewhere. For better comparison, the SANS data for the 0.50 and 0.75 wt % samples were offset by scaling factors of 100 and 200, respectively. The best-fit results from the spherical shell model are found to be in good agreement with the experimental data for $C_{lp} \leq 0.5$ wt% samples. The results also indicate that, as a function of C_{lp}, bilayer thickness (~ 3.2 nm) remains unaltered, and in agreement with previously reported values.

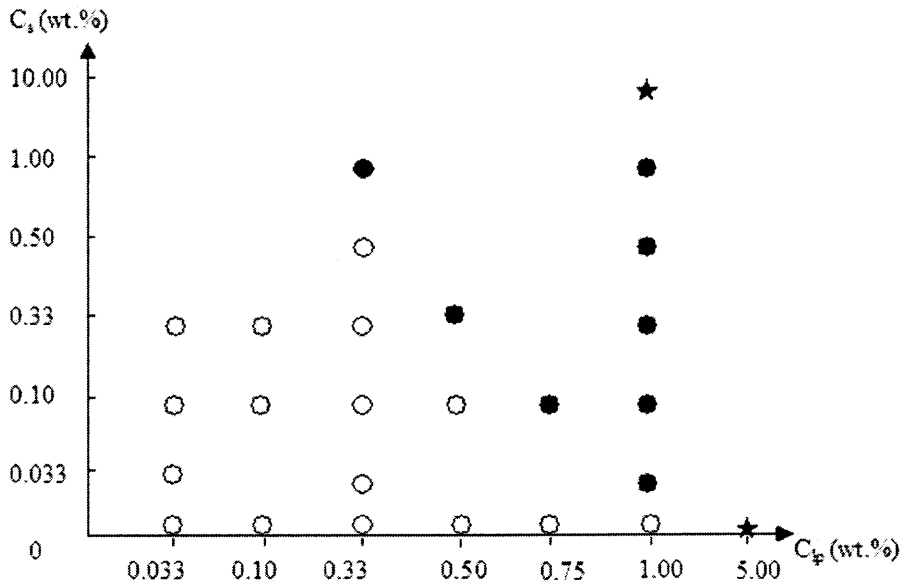

Figure 7.1 Schematic diagram of sample appearance as a function of C_{lp} and C_s. Empty circles: transparently bluish at both high and low temperatures for a long period of time; filled circles: transparent only at low T for a short period of time; filled stars: transparent and stable only at low T, but for an extended period of time.

SANS data and the corresponding best-fit curves using the three-parameter spherical shell model are presented in Fig. 7. 2. A detailed mathematical expression of the model has been described elsewhere. For better comparison, the SANS data for the 0.50 and 0.75 wt % samples were offset by scaling factors of 100 and 200, respectively. The best-fit results from the spherical shell model are found to be in good agreement with the experimental data for $C_{lp} \leq 0.5$ wt% samples. The results also indicate that, as a function of C_{lp}, bilayer thickness (~ 3.2 nm) remains unaltered, and in agreement with previously reported values. Moreover, vesicle radii remain virtually constant (24 ± 1 nm), and are independent of lipid concentration for $C_{lp} \leq 0.33$ wt% samples. Larger monodisperse ULV (~31 nm) are observed for the $C_{lp} = 0.5$ wt% sample. For $C_{lp} = 0.75$ wt%, SANS data show a monotonic decay in intensity with a slope of -2, implying the existence of large, polydisperse aggregates, possibly large ULV. DLS measurements

(Fig. 3) for $C_{lp} \leq 0.33$ wt% samples depict a unimodal size distribution of low polydispersity and a number-weighted average hydrodynamic radius, R_H, of about 25 ± 2 nm. Of note is that the best-fit vesicle radius from SANS experiments is usually slightly smaller than the hydrodynamic radius (R_H) measured by DLS. This is possibly due to the fact that R_H includes the contribution from associated water molecules, while the radius obtained from SANS studies, does not. Both SANS and DLS results demonstrate that the size of ULV remains practically unchanged over a range of C_{lp} (≤ 0.33 wt%). As C_{lp} is increased to 0.5 wt%, ULV size was found to increase. A clear bimodal distribution has

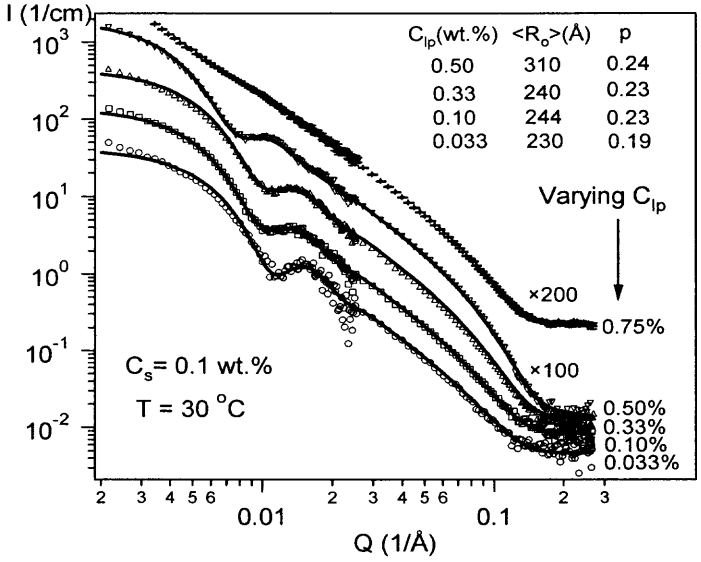

Figure 7.2 SANS data and fitting results for various C_{lp}s and a C_s of 0.10 wt%; C_{lp}= 0.033, 0.10, 0.33, 0.50 and 0.75 wt %, respectively. To better compare, scaling factors of 100 and 200 were applied to the 0.50 and 0.75 wt % data. An obvious size increase was observed when the C_{lp} reached 0.50 wt%. The data of the C_{lp} = 0.75 wt% sample were not fitted because of the large object size and high polydispersity.

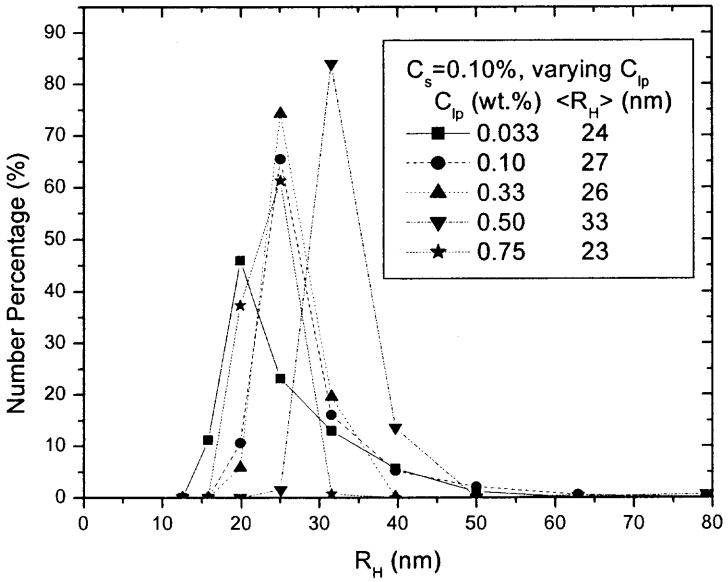

Figure 7.3 DLS size distribution functions for various C_{lp} (0.033, 0.10, 0.33, 0.50 and 0.75 wt %) at a fixed C_s=0.10 wt%. <R_H>s remained close at the three low concentrations (0.033%, 0.10% and 0.33%) but shifted, to larger size, for the 0.50 wt% sample. Note that all the data shown above are taken after one month of storage time except for the 0.75% sample, which was tested at 10°C immediately after preparation to avoid phase separation.

been observed in the intensity weighted histogram (not shown) for a C_{lp} = 0.75 wt.% sample, indicating the presence of large aggregates. Although highly stable ULV were found when doped either with a charged lipid (i.e., DMPG) or a salt (i.e., $CaCl_2$), this is the first observation of a highly stable ULV system doped simultaneously with a charged lipid (DMPG) and a salt (NaCl).

To study the effect of ionic strength, NaCl was added to liposomal solutions. Unlike Ca^{2+}, which strongly binds to lipid bilayers and, in some cases, induces vesicle fusion(Koynova, 1998), sodium salts such as NaCl and NaBr do not bind tenaciously with the lipid's headgroup. They can thus be used to efficiently control the ionic strength in surfactant and liposomal systems. The effect of ionic strength on vesicles was tested by using samples prepared at three C_{lp}: 0.033, 0.1 and 0.33 wt%. For the C_{lp} = 0.33 wt%

sample, five salt concentrations (C_s = 0, 0.10, 0.33, 0.50 and 1.00 wt%) were examined, whereas only two C_s samples (0.10 and 0.33 wt%) were studied for the other C_{lp}.

(a)

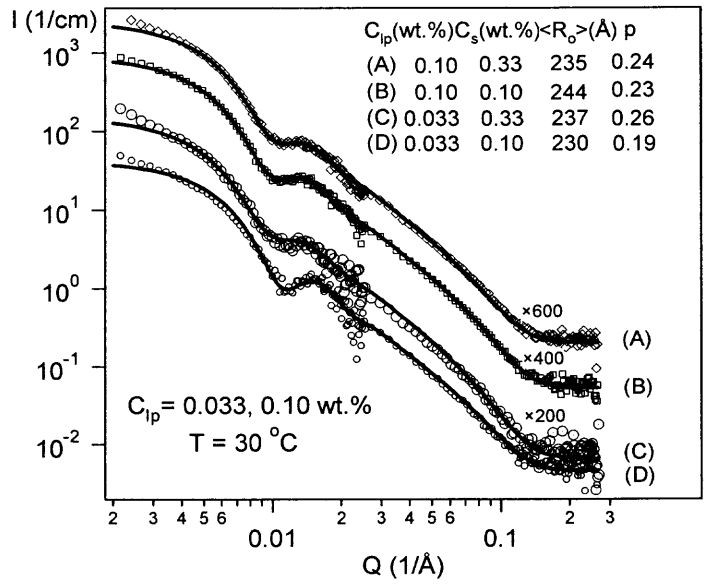

(b)

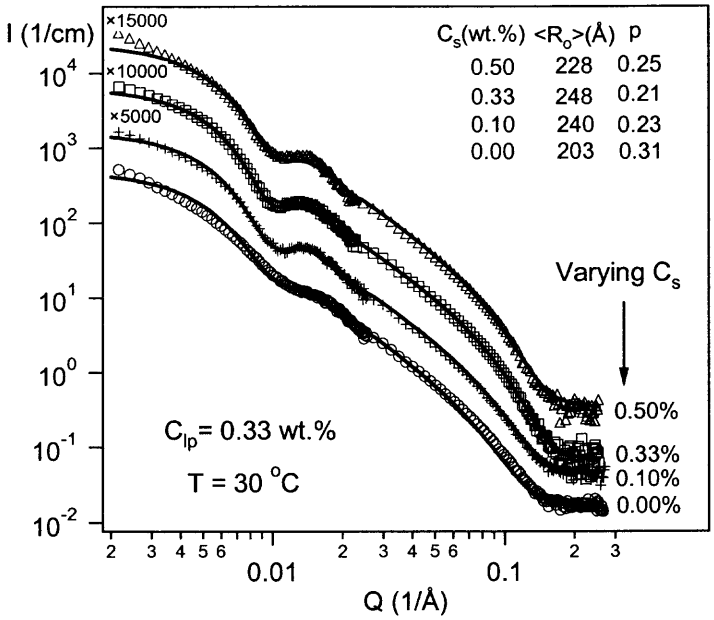

Figure 7.4 SANS data and best fit results for samples with various C_s at (a) C_{lp}=0.033, 0.10 wt% and (b) 0.33 wt%. Two salt concentrations (C_s = 0.1 and 0.33 wt%) were investigated for samples with C_{lp}= 0.033 and 0.10 wt %, whereas four C_s's (0, 0.1, 0.33 and 0.5 wt%) were examined. Data were rescaled to better compare. The vesicle radii were found to be nearly constant except for the sample without NaCl (C_s = 0 wt%) where the radius was smaller.

Figures 4 (a) and 4(b) depict SANS data for the above-mentioned samples. With the exception of the lowest (0 wt.%) and highest (1 wt.%) C_s, the best fits from SANS data yield a radius of 24 ± 1 nm and a polydispersity of ~ 20%. The sample with $C_s = 0$ wt% (non-NaCl doped) had a slightly smaller radius (~ 20 nm) and also, a slightly higher polydispersity (~30%); the sample with the highest C_s (1.00 wt%) turned opaque one day after preparation, presumably forming MLV.

The finding of forming nearly constant-size ULV was also examined by DLS. Figures 5(a) and 5(b) show the size distributions obtained from DLS which exhibited similar histograms for all samples. Though the polydispersity in the samples varied with salt and lipid concentrations, it is shown that all number weighted $\langle R_H \rangle$ were around 25 ± 3 nm, except for the $C_s = 0\%$ sample, whose $\langle R_H \rangle$ is 16nm. From intensity weighted size distribution analysis, another small peak with a much larger R_H (>100nm) was found in few samples. Their negligible number percentages were not seen in the number weighted histograms. The existence of the few large particles is a realistic scenario in explaining the discrepancy between the SANS data and the fit to the data at very low Q values (< 0.04 nm^{-1}).

7.3.3 Time Evolution

The stability of ULV size *versus* time for four different C_{lp} (0.033, 0.1, 0.33, 0.5 wt%) samples was monitored using DLS. All samples were kept at 4 °C for the first four months before experimentation. DLS measurements were taken immediately after the temperature was increased to 30 °C. Table 1 depicts the evolution of the number average $\langle R_H \rangle$ of four samples over a four-month period. For $C_{lp} \leq 0.1$ wt%, $\langle R_H \rangle$ of ULV were

(a)

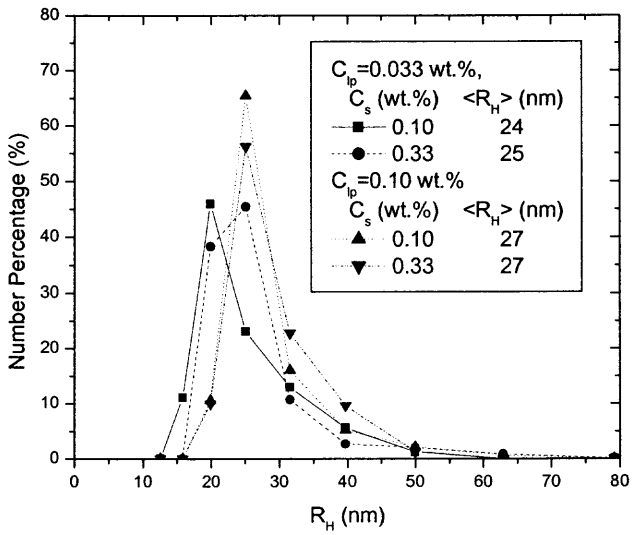

(b)

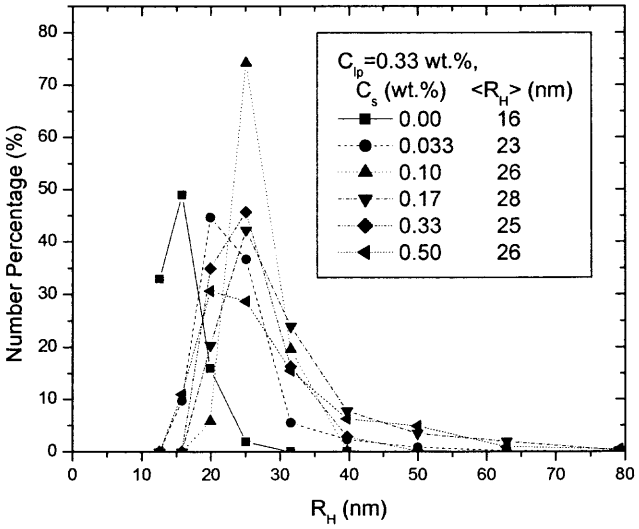

Figure 7.5 Size distribution functions under different salt concentrations and lipid concentrations: (a) C_{lp} = 0.033 and 0.10 wt%, and (b) C_{lp} = 0.33 wt %. Monodisperse vesicles with nearly constant size were observed for all samples except for the one with C_s = 0 in (b), where vesicle size is smaller.

found to be practically invariant over the four-month period stored at 4 °C, in addition to one-month storage at 30°C. For the most part, ULV size remains practically unchanged. The C_{lp}/C_s = 0.50/0.1% sample became unstable after two months of storage and had phase separated. Figure 7.6 shows the size evolution of a C_{lp}/C_s=0.33/0.33% mixture, exhibiting a narrow unimodal distribution immediately after sample preparation. The

appearance of the sample remained unchanged during the first four months, but became cloudy after one-month storage at 30 °C. In this case, another peak (>100nm) is observed in the intensity histogram (not shown), indicative of formation of large aggregates, possibly MLV.

Table 7.1 Number-Weighted Average Hydrodynamic Radius $<R_H>$ (Nm) Obtained From 4 Selected Samples Versus Time After When the DLS Measurements Were Taken. In General, the ULV Size Increases Very Slightly Over the Period of Testing

C_{lp},C_S (wt.%)	0 month	1 month	2 months	4 months	5 months
0.033, 0.33	26	25	26	27	25
0.10, 0.10	25	27	X	X	28
0.33, 0.33	24	25	24	27	28
0.50, 0.10	34	33	X	X	X

7.3.4 Effect of Temperature

The structural phase transition of DMPC/DHPC mixtures is often observed when the temperature is increased beyond the chain melting transition of DMPC, around 23 °C (Nieh 2002). Within the range of C_{lp} investigated (< 1 wt%), most of the structures formed above T_M were structures with a higher curvature (e.g. ULV), and in contrast to bicelles, which are found at temperatures below T_M. An exception to this, are certain DMPC/DHPC mixtures which form ULV both above and below T_M. This may imply changes to DMPC's hydrocarbon chain conformation may not directly affect the self-assembled structure.

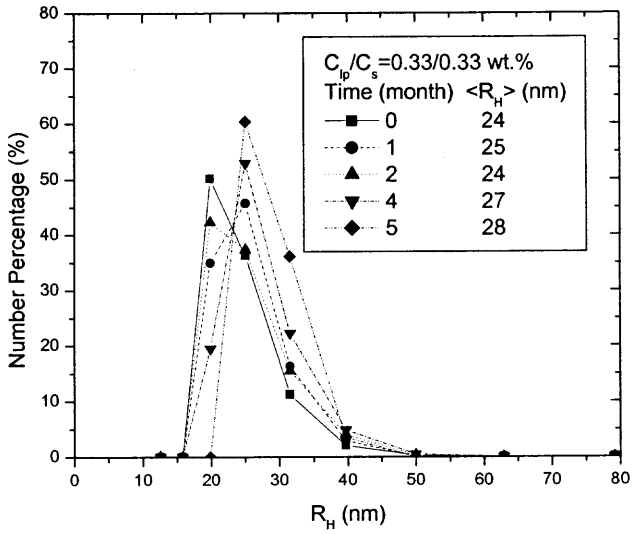

Figure 7.6 Size evolution as a function of time for the 0.33/0.33 wt% sample. A slight increase was observed after five months.

In the present study, ULV stability as a function of temperature was examined *via* DLS for samples prepared at three lipid concentrations. Figure 7.7 shows the size distribution for a C_{lp}/C_s = 0.1/0.33 wt% sample at 10, 30 and 50 °C. Size distributions are practically indistinguishable, and appear to narrow at higher temperatures. A similar behavior has been observed in the C_{lp}=0.33 wt% sample, however, the C_{lp} = 0.75 wt% sample became opaque at T > 25 °C indicating the presence of MLV.

7.4 Discussion

7.4.1 Effect of Lipid Concentration, C_{lp}

The size of spontaneously forming ULV, in general, varies with C_{lp}. Our observations of samples with C_{lp} > 0.33 wt% are consistent with those previously reported. For cases of $C_{lp} \leq$ 0.33 wt%, the vesicle size becomes C_{lp}-independent, similar to the systems doped with either DMPG or Ca^{2+} ions, but not with both. A previous study of non-doped ([DMPC]/[DMPG] = ∞) and strongly DMPG-doped ([DMPC]/[DMPG] =15) systems, at

the same temperature and lipid concentration, has confirmed the presence of MLV and bicelles, respectively. MLV are vesicles composed

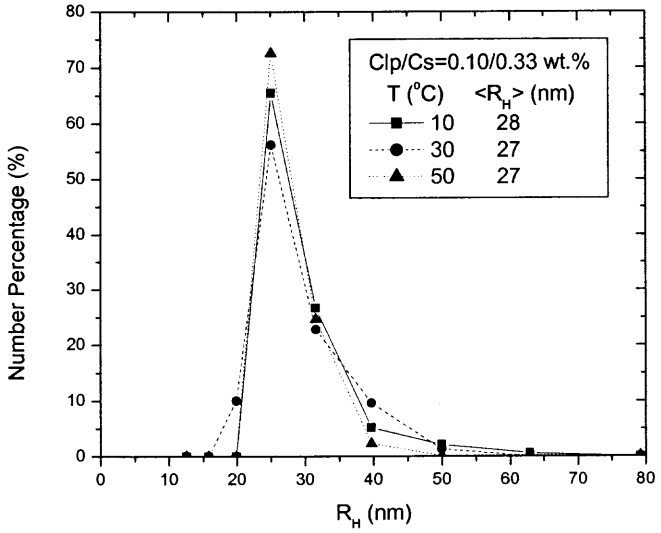

Figure 7.7 Size distribution for a $C_{lp} = 0.10$ and $C_s = 0.33$ wt% sample at 10 °C, 30 °C and 50 °C. The data show that as a function of temperature ULV size remains practically unaltered.

of a wide range of radii and conformations, which are entropically stabilized and incur only a small penalty for deviating from the spontaneous curvature. The formation of bicelles systems with elevated DMPG levels implies that strong coulombic interactions between charged lipids may stiffen the membrane and drive the short chain DHPC lipids towards the rim of the disk-like bicellar structure. When introduced with an appropriate amount of charge, DMPC/DHPC mixtures form a vesicular structure with a specific radius (possibly related to the spontaneous curvature of the system). This implies that an appropriate surface charge may induce a reasonably deep local free energy minimum resulting in the observed size insensitivity. Note that the ratio between charged (DMPG) and non-charged lipids was held constant during the entire study, with the assumption that the ULV membrane composition remains unaltered as a function of temperature and concentration. The size insensitivity to lipid concentration also contradicts the predictions

by Oberdisse et al., 1997, 1998, whose results, for a given surface charge density, indicate a size increase with increasing lipid concentration. In our experiments, the range of total lipid concentration, whereby ULV radii remained unaltered, was small (< 0.5 wt%), and even smaller for the case of charge density. The insensitivity of ULV to a changing chemical potential may be the result of a deep local free energy in forming the self-assembled structures.

Recently, Leng, Egelhaaf and Cates, 2002 proposed a kinetic model to explain the formation of vesicles in a lecithin/bile salt system. The model stated that ULV could be kinetically trapped as the detergent (charged short-chain lipid) molecules are removed from the rim of disk-like micelles (bicelles) upon dilution. In the Leng et al. study, bicelles coalesce into a larger planar structure to compensate for the loss of short-chain lipids. As the radius of the newly formed bicelles reaches a critical radius, r*, the rate of vesicle formation exceeds the rate of forming larger bicelles, and most of the short-chain lipids (bile salt) are released from the bicelle's rim into the bulk solution. The vesicle size is, therefore, approximately equal to r*/2, depending on the interaction between aggregates, packing constraints and salt concentrations. Once vesicles are formed, the size may be insensitive to certain changes in salt or lipid concentration since only a small amount of bile salt remained in the membranes. The formation of ULV in our study is different from the scenario just described. Although bicelles were found at C_{lp} = 1 wt% and low temperature, the short chain DHPC lipid does not carry any charge, and most likely, localizes itself at the rim of the bicelle. Most of the charged DMPG molecules are expected to stay in the bilayers with DMPC, for both compounds have the same chain length. This, of course, does not preclude the formation of ULV from another kinetically

controlled mechanism. However, more studies on the stability and the size of ULV formed *via* various pathways are needed.

7.4.2 Effect of Ionic Strength

The screening effect of coulombic interactions on the self-assembled charged structures can be studied by changing the ionic strength (e.g. salt concentrations) of the solution and thus the Debye length, χ_D. Our experimental results show a slightly smaller vesicle radius for the NaCl-free mixtures (~ 20 nm, SANS), compared to those mixtures with NaCl (~ 24 nm, SANS). Assuming complete dissociation of DMPG in a NaCl-free mixture with C_{lp} = 0.33 wt%, the calculated χ_D is about 38.5 nm, larger than the radius of curvature. The surface charge density of a DMPC/DMPG bilayer (neglecting the charge difference between the inner and outer layers and taking R_o = 24 nm and R_i = 21 nm) is about 3.5×10^{-3} C/m^2. Compared to calculations by Winterhalter and Helfrich,[30,31] the above experimental charge density and Debye length fall result in a small positive bending modulus and a negative Gaussian modulus, leading to a negative total elastic energy favoring spontaneous vesiculation. Reducing the screening length (by increasing salt concentration) reduces the bending modulus, however, under the present charge density conditions, the negative Gaussian modulus *increases* with ionic strength, eventually leading to a positive total energy at certain threshold $C_{s,MLV}$, where the transition from ULV to MLV takes place.

Figure 7.1 depicts such a trend as a function of salt concentration. An increase of vesicular size (from 20 to 24 nm according to SANS data) upon the addition of NaCl agrees with the above explanation. For samples doped with NaCl, the Debye length χ_D varies from 4 nm (C_s =0.033 wt%, 5.6mM) to 1.3 nm (C_s = 0.33 wt%, 56mM), with ULV

size remaining unaltered. Again, our observations of ULV size insensitivity is in contradiction to what has been predicted by Oberdisse et al., 1997, 1998. In their case, the size monotonically increased with salinity at higher charge densities. Though there is no direct comparison between our data and calculations from a more detailed treatment, such as P-B theory with translational entropy, asymmetric charge density, etc., the insensitivity of vesicular size may be attributed to a low entropic contribution, due to low lipid concentration and a dominant enthalpic contribution. As the lipid concentration increases, other degrees of freedom should be considered and the entropic contribution should increase with the total lipid concentration, eventually destabilizing the ULV structure at a threshold salinity $C_{s,MLV}$, which decreases with total lipid concentration (as shown in Fig. 1). A more extensive study is presently in progress to better understand the various structures and their stabilities at present lipid and salt concentrations.

7.4.3 Aging and Temperature Effect

The size evolution of ULV systems depends on the rate of exchange between the surfactant/lipid from aggregates to solution, and the flip-flop rate of surfactant/lipid molecules between the inner and outer leaflets. Although it is found that the size of certain surfactant vesicles remained unaffected over a period of months, Marques, 2000, sometimes vesicle size was observed to increase rapidly over a short period of time and then slowly stabilized over a period of months. Non sterically stabilized lipid vesicles are rarely stable for extended periods.

Despite an invariant ULV size (Figure 7.6), the issue of whether these ULV are kinetically trapped or thermodynamically stable is not yet understood. After four months,

a slight increase in size and polydispersity is observed in the C_{lp} = 0.33 wt% sample, implying either a slow structural evolution or lipid degradation. Note, that samples were stored at 4 °C, lower than the T_M of DMPC, except during measurements. For the most part, DMPC was in the gel phase, a more rigid molecular structure than the L_α phase, hence, the exchange rate of DMPC from ULV to solution or *vice versa* was slow. The invariant ULV size at low temperature (4 °C) may suggest that ULV are kinetically trapped. After four months of storage at 4 °C, the C_{lp} = 0.33 wt% sample was heated to 30 °C and incubated for a period of one month. After incubation, the sample was studied with DLS indicating the possible presence of MLV.

7.5 Conclusions

Low polydispersity, spontaneously forming ULV were found in DMPC/DMPG/DHPC phospholipid mixtures by diluting a high concentration lipid solution at low temperature (4 °C). SANS and DLS results show that the ULV are reasonably stable over extended periods of time and are unaffected by certain changes in lipid concentration, ionic strength of the solution, and temperature. Under the imposed constant surface charge density, the structural phase diagram could be explained by the theoretical predictions of Winterhalter and Helfrich, 1973. However, the nearly constant ULV size as a function of lipid concentration (C_{lp} < 0.33%), salinity (C_s < 0.5 wt%), and temperature is different from theoretical predictions and experimental reports. A possible explanation may be the enthalpic contribution from the negative Gaussian modulus that dominates at low lipid concentrations. Another possibility may be the energetically favorable packing of DMPC

and DMPG that renders a slow response to changes in chemical potential and structural transformation at low concentrations.

Further work on stable structures obtained *via* various pathways in systems with the same chemical composition is needed to understand the formation mechanism of these ULV. Such an understanding may then facilitate the design of ULV for prolonged stability and encapsulation needed for pharmaceutical and biomedical applications.

CHAPTER 8

CONCLUSIONS AND RECOMMENDATIONS FOR FUTURE WORK

8.1 Conclusions

The research presented in this dissertation has focused on the development of environmentally friendly microencapsulation methods, for a variety of application in chemical, agricultural and pharmaceutical industries. An important potential commercial application of microencapsulation is for controlled drug release system design in pharmaceutical formulation. Two main processes have been investigated: in situ polymerization based approach in supercritical CO_2, and liposome based approach in aqueous solution. Compared to many other microencapsulation methods, these two methodologies feature reduction/prevention of using organic solvents, making them particularly attractive green technologies.

For polymer-based microencapsulation, a novel in situ polymerization based process to encapsulate various types of fine particles, include drugs, fire retardant, inorganic nanoparticles, and carbon nanotubes, was developed. In the process, host particles, monomers and other components are first mixed together followed by polymerization and phase transition-induced encapsulation. Coating morphology was controlled by varying experimental parameters. Under certain conditions, thin-film coating was achieved for particle size above 1μm. Nanoparticles were encapsulated with polymers to form nanoparticles. Surface functionalization was employed for increasing interfacial interactions and dispersion. Under appropriate conditions, nano-silica particles

were found undergoing sol-gel transition to form porous monoliths. Dispersion, debundling, and polymer encapsulation of single-walled carbon nanotubes (SWNTs) were also reported.

Despite the great potential posed by bio-mimetic phospholipids in drug delivery, commercial products are quite limited. To address the structure stability of liposome-based microencapsulationm in a more fundamental level, the mechanism of spontaneous formation of monodispersed unilamellar vesicles with scattering technique using neutron and light sources was studied. Vesicle phase was studied systematically as a function of lipid concentration, salinity, temperature and time duration, etc. The results contribute to the understanding and selection of appropriate lipid system and process for microencapsulation of drugs.

8.2 Recommendations for Future Work in Particle Coating

Based on the research results presented above, the following are recommended for our future research.

8.2.1 Coating of Carbon Nanotube in $scCO_2$

The success in uniformly encapsulating individual carbon nanotubes laid the foundation for further study of carbon nanotube/polymer in supercritical carbon dioxide. In current study, we used randomly oriented carbon nanotubes, which may have limited enhancement in mechanical properties. Aligned carbon nanotubes provide more desirable mechanical properties. Naturally, the next research on this area should focus on encapsulating aligned carbon nanotubes, followed by mechanical property test.

Other interesting research could involve encapsulating carbon nanotubes with other polymers for other properties. For example, we are currently investigating coating CNT with PVP, a water-soluble polymer and surfactant. Modification with hydrophilic functional groups could lead to dispersion of CNT in water. Also of strong interest is the use of electronic conducting polymers for encapsulation to achieve unique electronic properties.

8.2.2 Mechanical Property of Synthesized Nanocomposite

In this research, we have successfully synthesized PMMA/silica nanocomposites and monoliths with different compositions. Although we have done detailed characterization in terms of morphology and thermal properties. It would be interesting to test their mechanical properties, especially for monolith material. The results could then serve as a guide for further optimization of preparation conditions. Mechanical property is also crucial for potential application of monolith in chromatography.

8.3 Recommendation for Future Work in Spontaneous Liposome

It was found that the spontaneous unilamellar vesicles prepared in this study are highly stable under studied conditions. But it remains interesting to test their stability under wider storage conditions, such as introduction of more cations, PH change, and sudden concentration change. Currently, we are investigating the effect of multiple dialysis on vesicle stability change.

The successful preparation of spontaneous unilamellar lipid vesicles serves as a platform for application of these vesicles. The ultimate goal of liposome research is to use it as a drug delivery device. Of particular interest are biopharmaceuticals, such as

peptides, DNA and proteins. So next study should involve the preparation of lipid/drug conjugate and stability study.

REFERENCES

Aboubakar, M., Puisieux, F., Couvreur, P., Vauthier, C. "Physico-chemical characterization of insulin-loaded poly(isobutylcyanoacrylate) nanocapsules obtained by interfacial polymerization." *International Journal of Pharmaceutics*, 183,1999, 63.

Agkerman, A. and Yeo, S. "Supercritical extraction of organic components from aqueous slurries", *Supercritical Fluid Engineering Science*, eds, E. Kiran and J. F. Brennecke, *ACS Symp, Ser. 514*, American Chemical Society: Washington, D. C., 1989.

Andelman, D., M. M. Kozlov, and W. Helfrich. 1994. "Phase-transitions between vesicles and micelles driven by competing curvatures". *Europhys. Lett.* 25, 1994, 231.

Andrews, A. T., Ahlert, R. C., Kosson, D. S., "Supercritical extraction of aromatic contaminants from a sandy loam soil", *Env. Prog.*, 17, 1991, 1.

Ash, B. J., Schadler, L. S., Siegel, R. W. "Thermal and Mechanical Properties of Alumina/Polymethylmethacrylate (PMMA) Nanocomposites". *Polym. Prepr.* 42, 2001, 52.

Barenholz, Y., Crommelin, D. "Liposomes as pharmaceutical dosage forms." In: Swarbrick, J., Boylan, J., eds. "Liposomes as pharmaceutical dosage forms to microencapsulation." New York: Marcel Dekker, 1994, 1-39.

Baxter, G., "Microencapsulation technology and modern business forms", *Tappi*, 60, 1977, 84.

Benita, S., Zouai, D., Benoit, J. P., "5-Fluorouracil: Carnauba wax microspheres for chemoembolization, an in vitro evaluation", *J. Pharmac. Sci.*, 75, 1986, 847.

Bergna, H. E., *US Patent 4 677 084*, 1987.

Bergstrom, M. 1996. "Thermodynamics of vesicle formation from a mixture of anionic and cationic surfactants" *Langmuir*. 12, 2454-2463.

Bergstrom, M. "Thermodynamics of unilamellar vesicles: influence of mixing on the curvature free energy of a vesicle bilayer". *J. Colloid Interface Sci.* 240, 2001, 294-306.

Bergstrom, M., and J. C. Eriksson. "The energetics of forming equilibrated bilayer vesicles". *Langmuir*. 12, 1996, 624-635.

Bergstrom, M., and J. C. Eriksson. "Size distribution of reversibly formed bilayer vesicles". *Langmuir*. 14, 1998, 288-299.

Bergstrom, M., and J. S. Pedersen. "A small-angle neutron scattering study of surfactant aggregates formed in aqueous mixtures of sodium dodecyl sulfate and didodecyldimethylammonium bromide". *J. Phys. Chem. B.* 104, 2000, 4155-4163.

Bergstrom, M., J. S. Pedersen, P. Schurtenberg, and S. U. Egelhaaf. "Small-angle neutron scattering (SANS) study of vesicles and lamellar sheets formed from mixtures of an anionic and a cationic surfactant." *J. Phys. Chem. B.* 103, 1999, 9888-9897.

Berends, E. M., Bruinsma, O. S. L., Graauw, J. D., Rosmalen, G. M., "Crystallization of phenanthrene from toluene with carbon dioxide by the GAS process", *AIChE J.*, 42, 1996, 431-439.

Bertie, J. E., and Z. Lan. "The refractive index of colorless liquids in the visible and infrared: contributions from the absorption of infrared and ultraviolet radiation and electronic molar polarizability below 20500 cm-1". *J. Chem. Phys.* 103, 1995, 10152-10161.

Bertucco, A. and Vaccaro, F., "Drugs encapsulation using a compressed gas antisolvent technique", *The Forth Italian Conference on Supercritical Fluids and their Application*, E. Reverchon (Ed.), September 7-10, Capri, 1997, 327-334.

Blanco-Príeto, M. J., Fattal, E., Gulik, A., Dedieu, J. C., Roques, B. P., Couvreur, P., "Characterization and morphological analysis of a cholecystokinin derivative peptide-loaded poly(lactide-co-glycolide) microspheres prepared by a water-in-oil-in-water emulsion solvent evaporation method", *J. Control. Rel.*, 43, 1997, 81-87.

Blasig, A., Shi, C., Enick, R. M., Thies, M. C., "Effect of concentration and degree of saturation on RESS of a CO_2-soluble fluoropolymer", *Ind. Eng. Chem. Res.*, 41, 2002, 4976-4983.

Bourgeat-Lami, E., Lang, J. "Encapsulation of Inorganic Particles by Dispersion Polymerization in Polar Media: 1. Silica Nanoparticles Encapsulated by Polystyrene." *J. Colloid Interface Sci.* 197, 1998, 293.

Breitenbach, A., Mohr, D., Kissel, T., "Biodegradable semi-crystalline comb polyesters influence the microsphere production by means of a supercritical fluid extraction technique (ASES)", *J. Control. Rel.*, 63, 2000, 53-68.

Brennecke, J., "New applications of supercritical fluids", *Chemistry & Industry*, 4, 1996, 831-834.

Bristow, S., Shekunov, T., Shekunov, Yu. B., York, P., "Analysis of the supersaturation and precipitation process with supercritical CO_2", *J. Supercrit. Fluids*, 21, 2001, 257-271.

Brannon-Peppas, L., "Recent advances on the use of biodegradable microparticles and nanoparticles in controlled drug delivery", *Intl. J. Pharm.*, 116, 1995, 1-9.

Cai, J. G., Liao, X. C., Zhou, Z. Y., "Microparticle formation and crystallization rate of HMX using supercritical dioxide anti-solvent recrystallization", *The 4th International Symposium on Supercritical Fluids*, May 11-14, Sendai, Japan, 1997, 23-26.

Canelas, D. A., Betts, D. E., DeSimone, J. M., "Poly (vinyl acetate) and poly (vinyl acetate-*co*-ethylene) latexes via dispersion polymerizations in carbon dioxide", *Macromolecules,* 31, 1998, 6794-6805.

Capan, Y., Woo, B. H., Gebrekidan, S., Ahmed, S., DeLuca, P. P., "Influence of formulation parameters on the characteristics of poly (D, L-lactide-co-glycolide) microspheres containing poly (L-lysine) complexed plasmid DNA", *J. Control. Rel.*, 60, 1999, 279-286.

Chang, C. J. and Randolph, A. D., "Precipitation of microsize organic particles from supercritical fluids", *AIChE J.*, 35, 1989, 1876.

Chang, C. J. and Randolph, A. D., "Solvent expansion and solute solubility predictions in gas-expanded liquids", *AIChE J.*, 36, 1990, 939.

Chang, S.-Y., Liu, L., Asher, A. A., "Preparation and properties of tailored morphology, monodisperse colloidal silica-cadmium sulfide nanocomposites", *J. Am. Chem. Soc.*, 116, 1994, 6739-6744.

Charoenchaitrakool, M, Dehghani, F, Foster, N. R., "Micronization by rapid expansion of supercritical solution to enhance the dissolution rate of poorly water-soluble pharmaceuticals", *Ind. Eng. Chem. Res.*, 39, 2000, 4794-4802.

Chattopadhyay, P. and Gupta, R. B., "Supercritical CO_2 based production of fullerence nanoparticles", *Ind. Eng. Chem. Res.*, 39, 2000, 2281-2289.

Chattopadhyay P. and Gupta, R. B., "Protein nanoparticles formation by supercritical antisolvent with enhanced mass transfer", *AIChE J.,* 48, 2002, 235-244.

Chattopadhyay, P. and Gupta, R. B., "Production of antibiotic nanoparticles using supercritical CO_2 as antisolvent with enhanced mass transfer", *Ind. & Eng. Chem. Res.*, 40, 2001, 3530-3539.

Chiannikulchi, N., Driouich, Z., Benoit, J. P., Couvreur, P., "Doxorubicin-loaded nanoparticles: Increased efficiency in murine hepatic metastase", *Select. Cancer. Therap.*, 5, 1989, 1.

Chiou, J. S., Barlow, J. W., Paul, D. R., "Plasticization of glassy polymers by CO_2", *J. Appl. Polym. Sci.*, 30, 1985, 493.

Cho, C. H., J. Urquidi, S. Singh, and G. W. Robinson. "Thermal offset viscosities of liquid H_2O, D_2O and T_2O". *J. Phys. Chem.* 103, 1999, 1991-1994.

Chou, Y. H. and Tomasko, D. L., "GAS Crystallization of Polymer-Pharmaceutical Composite Particles" *The 4th International Symposium on Supercritical Fluids*, May 11-14, Sendai, Japan, 1997, 55-57.

Chung, J., and J. H. Prestegard. "Characterization of field-oriented aqueous liquid crystals by NMR diffusion measurements." *J. Phys. Chem.* 97, 1993, 9837-9843.

Cocero, M. J. and Ferrero, S., "Crystallization of β-carotene by a GAS process in a batch effect of operating conditions", *J. Supercrit. Fluids*, 22, 2002, 237-245.

Condo, P. D., Paul, D. R., Johnston, K. P., "Glass transition of polymers with compressed fluid diluents: Type II and III behavior", *Macromolecules*, 27, 1994, 365-371.

Cohen, H., Levy, R. J., Gao, J., Kousaev, V., Sosnowski, S., Slomkowski, S., Golomb, G., "Sustained delivery and expression of DNA encapsulated in polymeric nanoparticles", *Gene Therapy*, 7, 2000, 1896.

Cooper, A. I. "Polymer synthesis and processing using supercritical carbon dioxide," J. Mater. Chem., 2000, 10, 207-234.

Davies, R., Schur, G. A., Meenan, P., Nelson, R. D., Bergna, H. E., Brevett, C. A. S., Goldbaum, R. H., "Engineered Particle Surfaces", *Advanced Materials,* 10, 1998, 1264-1270.

Debenedetti, P.G. and Kumar, S. K., "Infinite dilution fugacity coefficients and general behavior of dilute binary systems", *AIChE J.*, 32, 1986, 1253.

DeSimone, J. M., Guan, Z., Elsbernd, C. S., "Synthesis of fluoropolymers in supercritical carbon dioxide", *Science*, 257, 1992, 945.

Carson, T., Lizotte, J., Desimone, J. M. "Dispersion polymerization of 1-vinyl-2-pyrrolidone in supercritical carbon dioxide", Macromolecules 33 (2000) 1917-1920.

Dixon, D. J., Johnston, K. P., Bodmeier, R. A., "Polymeric materials formed by precipitation with a compressed fluid antisolvent", *AJChE J.*, 39, 1993, 127-139.

Dillow, A. K., Dehghani, F., Foster, N., Hrkach, J., Langer, R. S., "Production of polymeric support materials using supercritical fluid anti-solvent process", *The 4th International Symposium on Supercritical Fluids*, May 11-14, Sendai, Japan, 1997, 247-250.

Domingo, C., Berends, E. M., Van Rosmalen, G. M., "Precipitation of ultrafine benzoic acid by expansion of a supercritical carbon dioxide solution through a porous plate nozzle", *J. Crystal Growth*, 166, 1996, 989-995.

Dorski, C. K., Doyle, F. J., Pappas, N. A., "Preparation and characterization of glucose-sensitive P(MAA-g-EG) hydrogels", *Polym. Mater. Sci. Eng. Proceed.*, 76, 1997, 281-282.

Egelhaaf, S. U., and P. Schurtenberger. "Micelle-to-vesicle transition: a time-resolved structural study." *Phys. Rev. Lett.* 82, 1999, 2804-2807.

Elvassore, N., Bertucco, A., Caliceti, P., "Production of protein-loaded polymeric microcapsules by compressed CO_2 in a mixed solvent", *Ind. Eng. Chem. Res.*, 40, 2001, 795-800.

Falk, R., Randolph, T. W., Meyer, J. D., Kelly, R. M., Manning, M. C., "Controlled release of ionic compounds from poly (L-lactide) microspheres produced by precipitation with a compressed antisolvent", *J. Control. Rel.*, 44, 1997, 77-85.

Falk, R. F. and Randolph, T. W., "Process variable implications for residual solvent removal and polymer morphology in the formation of gentamycin-loaded poly (L-lactide) microparticles", *Pharm. Res.*, 15, 1998, 1233-1237.

Falk, R., Randolph, T. W., Meyer, J. D., Kelly, R. M., Manning, M. C., "Controlled release of ionic compounds from poly (L-lactide) microspheres produced by precipitation with a compressed antisolvent", *J. Control. Rel.*, 44, 1997, 77-85.

Fattal, E., Youssef, P., Couvreur, P., Andremont, A., " Treatment of experimental salmonellosis in mice with ampicillin-bound nanoparticles", *Antimicrob. Agent Chimother.*, 33, 1989, 1540.

Fitzgerald, J. F. and Corrigan, O. I., "Investion of the mechanisms governing the release of levamisole from poly-lactide-co-glycolide delivery systems", *J. Control. Rel.*, 42, 1996, 125-132.

Fu, K., Griebenow, K., Hseih, L., Klibanov, V. M., Langer, R., "FTIR characterization of the secondary structure of proteins encapsulated within PLGA microspheres", *J. Control. Rel.*, 58, 1999, 357.

Gabriel, N. E., and M. F. Roberts. "Spontaneous formation of stable unilamellar vesicles". *Biochemistry.* 23, 1984, 4011-4015.

Gallagher, P. M., Coffey, M. P., Krukonis, V. J., "Gas anti-solvent recrystallization of RDX: Formation of ultrafine particles of a difficult-to-comminute explosive", *J. Supercrit. Fluids*, 5, 1992, 130-142.

Gallagher, K. M. and Corrigan, O. I., "Mechanistic aspects of the release of levamisole hydrochloride from biodegradable polymers", *J. Control. Rel.*, 69, 2000, 261-272.

Gennis, R. B. 1989. Biomembranes: Molecular Structure and Function. Springer-Verlag New York Inc., New York.

Ghaderi, R., Artursson, P., Carlfors, J., "A new method for preparing biodegradable microparticles and entrapment of hydrocortisone in D,L-PLG microparticles using supercritical fluids", *European J. of Pharm. Sci.*, 10, 2000, 1-9.

Glinka, C. J., J. G. Barker, B. Hammouda, S. Krueger, J. J. Moyer, and W. J. Orts. "The 30-m small-angle neutron scattering instruments at the National Institute of Standards and Technology". *J. Appl. Crystallogr.* 31, 1998, 430-445.

Gradzielski, M., M. Müller, M. Bergmeier, H. Hoffmann, and E. Hoinkis. "Structural and macroscopic characterization of a gel phase of densely packed monodisperse, unilamellar vesicles". *J. Phys. Chem. B.* 103, 1999, 1416-1424.

Gregoriadis, G. "Engineering liposomes for drug delivery." *Trends Biotechnol.* 13, 1995, 527-537.

Gu, S., Kondo, T., Konno M. "Preparation of silica-polystyrene core-shell particles up to micron sizes", J. Coll. Inter. Sci. 272, 2004, 314.

Hannay, J. and Hoghart, "On the solubility of solids in gases", *J. Proc. Roy. Soc.* (London), 29, 1879, 324.

Hayter, J. B. "Determination of structure and dynamics of micellar solutions by neutron small angle scattering". In Physics of Amphiphiles—Micelles, Vesicles, and Microemulsions. V. Degiorgio and M. Corti, editors. Elsevier, Amsterdam, The Netherlands. 1985, 60-93.

Hayter, J. B., and J. Penfold. "An analytic structure factor for macroion solutions". Mol. Phys. 42, 1981, 109-118.

Helfgen, B., Hils, P., Holzknecht, Ch., Türk, M., Schaber K., "Simulation of particle formation during the rapid expansion of supercritical solutions", *J. Areosol Sci.*, 32, 2001, 295-319.

Helfrich, W. "Elastic properties of lipid bilayers: theory and possible experiments". *Z. Naturforsch.* 28, 1973, 693-703.

Hoefling, T. A., Beitle, R. R., Enick, R. M., Beckman, E. J., "Design and synthesis of highly CO_2-soluble surfactants and chelating agents, *Fluid Phase Equilibria*, 83, 1993, 203-212.

Hrkach, J. S., Peracchia, M. T., Domb, A., Lotan, N., Langer, R., "Nanotechnology for biomaterials engineering: Structural characterization of amphiphilic polymeric nanoparticles by ^{1}H NMR spectroscopy", *Biomaterials*, 18, 1997, 27.

Hung, W. C., and F. Y. Chen. "Osmotic threshold and water association for phospholipid gel phase bilayers." *Chinese J. Phys.* 38, 2000, 882-892.

Ike, O., Shimizu, Y., Wada, R., Hyon, S. -H., Ikada, Y., "Controlled cisplatin delivery system using poly (D, L-Lactic acid)," *Biomaterials,* 13, 1992, 230-234.

Israelachvili, J. 1992. Intermolecular and Surface Forces. Academic Press, San Diego.

Ivanova, E., Teunou, E., Poncelet, D. "Encapsulation of water sensitive products: effectiveness and assessment of fluid bed dry coating" *Journal of Food Engineering*, 71, 2005, 223-230.

Ivy, E. E. and Pencap, M., "Improved methylparathion formulation", *J. of Economic Entomology*, 65, 1972, 473.

Jaracz, S., Chen, J., Kuznetsova L. V., Ojima, I., "Recent advances in tumor-targeting anticancer drug conjugates " Bioorganic & Medicinal Chemistry, 2006, In press.

Jennings, D. W., Deutsch, H. M., Zalkow, L. H., Teja, A. S., "Supercritical extraction of taxol from the bark of Taxus brevifolia", *J. Supercrit. Fluids*, 5, 1992, 1-6.

Jessop, P. G., Ikariya, T., Noyori, R., "Homogeneous catalysis in supercritical fluids", *Chem. Rev.*, 99, 1999, 475.

Jong, Y. S., Jacob, J. S., Yip, K. -P., Gardner, G., Seitelman, E., Whitney, M., Montgomery, S., Mathiowitz, E., "Controlled release of olasmid DNA", *J. Control. Rel.*, 47, 1997, 123.

Jung, H. T., B. Coldren, J. A. Zasadzinski, D. J. Iampietro, and E. W. Kaler. "The origins of stability of spontaneous vesicles". Proc. Natl. Acad. Sci. USA. 98, 2001, 1353-1357.

Kage, H., Takahashi, T., Yoshida, T., Ogura, H., Matsuno, Y., "Coating efficiency of seed particles in a fluidized bed by atomization of a powder suspension", *Powder Technol.*, 86, 1996, 243-250.

Kaler, E. W., K. L. Herrington, A. K. Murthy, and J. A. N. Zasadzinski. "Phase behavior and structures of mixtures of anionic and cationic surfactants." J. Phys. Chem. 96, 1992, 6698-6707.

Kaler, E. W., A. K. Murthy, B. E. Rodriguez, and J. A. N. Zasadzinski. "Spontaneous vesicle formation in aqueous mixtures of single-tailed surfactant." *Science.* 245, 1989, 1371-1374.

Katsaras, J., R. L. Donaberger, I. P. Swainson, D. C. Tennant, Z. Tun, R. R. Vold, and R. S. Prosser. "Rarely observed phase transitions in a novel lyotropic liquid crystal system." *Phys. Rev. Lett.* 78, 1997, 899-902.

Katayama, T., Ohgaki, K., Maekawa, G., Goto, M., Nagano, T., "Isothermal vapor-liquid equilibria of acetone-carbon dioxide and methanol carbon dioxide systems at high pressures", *J. Chem. Engr. of Japan*, 8, 1975, 89-92.

Kendall, J. L., Canelas, D. A., Young, J. L., DeSimone, J.M., "Polymerizations in supercritical carbon dioxide", *Chem. Rev.,* 99, 1999, 543.

Kim, J. H., Paxton, T. E., Tomasko, D. L., "Microencapsulation of naproxen using rapid expansion of supercritical solutions", *Biotechnol. Prog.*, 12, 1996, 650-661.

Kiran, E. and Pöhler, H., "Alternative solvents for cellulose derivatives: miscibility and density of cellulosic polymers in carbon dioxide + acetone and carbon dioxide + ethanol binary fluid mixtures", *J. Supercrit. Fluids*, 13, 1998, 135-147.

Kiran, E., Debenedetti, P. G., Peters, C. J., *Supercritical fluids: Fundamentals and applications*, *NATO Science Series*, E 366, Kluwer Academic Publishers, 2000.

Ko, J. A., Park, H. J., Hwang, S. J., Park, J. B., Lee, J. S., "Preparation and characterization of chitosan microparticles intended for controlled drug delivery", *Intl. J. of Pharm.*, 249, 2002, 165-174.

Kordikowski, A, Schenk, A. P., Van Nielen, R. M., Peters, C. J., "Volume expansions and vapor-liquid equilibria of binary mixtures of a variety of polar solvents and certain near-critical solvents", *J. Supercrit. Fluids,* 8, 1995, 205-216.

Krukonis, V, "Supercritical fluid nucleation of difficult-to-comminute solids", paper 140f, *AIChE meeting*, San Francisco, Number, 1984.

Lasic, D. D. "Liposomes, from physics to applications". Amsterdam: Elsevier, 1993.

Lasic, D. D. "Liposomes in Gene Delivery", Boca Raton, FL: CRC Press, 1997

Lee, H. J. 2002. Protein drug oral delivery: the recent progress. Arch. Pharm. Res. 25:572-584.

Lele, A and Shine, A. D., "Effect of RESS dynamics on polymer morphology", *Ind. Eng. Chem. Res.*, 33, 1994, 1476-1485.

Leng, J., S. U. Egelhaaf, and M. E. Cates. "Kinetics of micelle-to-vesicle transition: aqueous lecithin-bile salt mixtures." *Biophys. J.* 85, 2003, 1624-1646.

Lengsfeld, C. S., Delplangue, J. P., Barocas, V. H., Randolph, T. W., "Mechanism Governing Microparticle Morphology during Precipitation by a Compressed Antisolvent: Atomization vs. Nucleation and Growth. *J. Phys .Chem. B*, 104, 2000, 2725-2735.

Leong, K. W., Mao, H. -Q., Truong-Le, V. L., Roy, K., Walsh, S. M., August, J. T., "DNA-polycation nanospheres as non-viral gene delivery vehicles", *J. Control. Rel.*, 53, 1998, 183.

Leroux, J. C., Allémann, E., Jaeghere, F. D., Doelker, E., Gurny, R., "Biodegradable nanoparticles-from sustained release formulations to improved site specific drug delivery", *J. Control. Rel.*, 39, 1996, 339.

Lesieur, P., M. A. Kiselev, L. I. Barsukov, and D. Lombardo. "Temperature-induced micelle to vesicle transition: kinetic effects in DMPC/NaC system." *J. Appl. Crystallogr.* 33, 2000, 623-627.

Li, G., Yates, M. Z., Johnston, K. P. "In-situ investigation on the mechanism of dispersion polymerization in supercritical carbon dioxide", Macromolecules 33 (2000) 4008-4014.

Lim, G. B., Lee, S. Y., Koo , K. K., Park, B. S., Kim, H. S., "Gas anti-solvent recrystallization of molecular explosives under sub-critical to supercritical conditions", *Proceedings of the 5th Meeting on Supercritical Fluids*, Tomel, ISBN 2-905-267-28-3, March 23-25, Nice, France, 1998, 271.

Lin, R. Ng, L. Wang, C. "In vitro study of anticancer drug doxorubicin in PLGA-based microparticles" *Biomaterials,* 26, 2005 4476-4485.

Liu, H. and Yates, M. Z., "Development of a carbon dioxide-based microencapsulation technique for aqueous and ethanol-based latexes", *Langmuir,* 18, 2002, 6066 - 6070.

Lin, Y., Zhou, B., Fernando, K. A. Shiral, Liu, P., Allard, L. F., Sun, Y-P. "Polymeric Carbon Nanocomposites from Carbon Nanotubes Functionalized with Matrix Polymer." *Macromolecules* 36(19), 2003, 7199-7204.

Lora, M., Bertucco, A., Kikic, I., "Simulation of the semicontinuous supercritical antisolvent recrystallization process", *Ind. Eng. Chem. Res.,* 39, 2000, 1487 - 1496.

Losonczi, J. A., and J. H. Prestegard. "Improved dilute bicelle solutions for high resolution NMR of biological macromolecules." *J. Biomol. NMR.* 12, 1998, 447-451.

Lück, M., Pistel, K.-F., Li, Y.-X., Blunk, T., Müller, R. H., Kissel, T., "Plasma protein adsorption on biodegradable microspheres consisting of poly(D, L-lactide-co-glycolide), poly(L-lactide) or ABA triblock copolymers containing poly(oxyethylene): Influence of production method and polymer composition", *J. Control. Rel.*, 55, 1998, 107-120.

Luna-Xavier, J.-L., Guyot, A., Bourgeat-Lami, E., "Synthesis and characterization of silica/poly (methyl methacrylate) nanocomposite latex particles through emulsion polymerization using a cationic azo initiator", *J. Colloid and Interface Science*, 250, 2002, 82-92.

Marques, E. F. " Size and stability of cationic vesicles: effects of formation path, sonication and aging." *Langmuir.* 16, 2000, 4798-4807.

Marques, E. F., O. Regev, A. Khan, M. da Graça Miguel, and B. Lindman. "Vesicle formation and general phase behavior in the catanionic mixture SDS-DDAB-water. the anionic-rich side". *J. Phys. Chem. B.* 102, 1998, 6746-6758.

Matson, D. W., Fulton, J. L., Petersen, R. C., Smith, R. D., "Rapid expansion of supercritical fluid solutions: solute formation of powders, thin film, and fibers", *Ind. Eng. Chem. Res.*, 26, 1987, 2298-2309.

Matson, D. W., Peterson, R. C., Smith, R. D., "Production of fine powders by the rapid expansion of supercritical fluid solutions", *Adv. Ceram.*, 21, 1987, 109-120.

Maurer, N., A. Mori, L. Palmer, M. A. Monck, K. W. C. Mok, B. Mui, Q. F. Akhong, and P. R. Cullis. "Lipid-based systems for intracellular delivery of genetic drugs." *Mol. Membr. Biol.* 16, 1999, 129-140.

Mawson, S., Johnston, K. P., Combes, J. R., DeSimone, J. M., "Formation of poly (1,1,2,2,-tetrahydroperfluorodecyl acrylate) submicron fibers and particles from supercritical carbon dioxide solutions", *Macromolecules*, 28, 1995, 3182-3191.

Mawson, S., Kanakia, S., Johnston, K. P., "Coaxial nozzle for control of particle morphology in precipitation with a compressed fluid antisolvent", *J. Appl. Polym. Sci.*, 64, 1997, 2105-2118.

Mawson, S., Yates, M. Z., O'Neill, M. L., Johnston, K. P., "Stabilized polymer microparticles by precipitation with a compressed fluid antisolvent. 2. Poly (propylene oxide)- and poly (butylene oxide)-based copolymers", *Langmuir*, 13, 1997, 1519 -1528.

McHugh, M. and Krukonis, V. J., *Supercritical Fluid Extraction: Principles and Practice*, Butterworths, Boston, 1986.

McHugh, M. and Krukonis, V. J., *Encyclopedia of Polymer Science and Engineering*, 2 nd., N. M. Bikales, C. G. Overberger, and G Menges, eds., Wiley, New York, 1988.

McHugh, M. and V. J. Krukonis, *Supercritical Fluid Extraction: Principles and Practice*, 2nd edition, Stoneham, MA: Butterworths-Heinemann, 1994.

Mishima, K., Matsuyama, K., Tanabe, D., Yamauchi, S., Young, T. J., Johnston, K. P., "Microencapsulation of proteins by rapid expansion of supercritical solution with a nonsolvent", *AIChE J.*, 46, 2000, 857-865.

Mohamed, R. S., Debenedetti, P. G., Prud'homme, R. K., "Effects of process conditions on crystal obtained from sypercritical mixtures", *AIChE J.*, 35, 1989, 325.

Moneghini, M., Kikic, I., Voinovich, D., Perissutti B., Filipović-Grčić, J., "Processing of carbamazepine-PEG 4000 solid dispersions with supercritical carbon dioxide: preparation, characterisation, and in vitro dissolution", *Intl. J. Pharm.*, 222, 2001, 129-138.

Moshashaée, S., Bisrat, M., Forbes, R. T., Nyqvist, H., York, P., "Supercritical fluid processing of proteins. I: Lysozyme precipitation from organic solution", *European J. Pharm. Sci.*, 11, 2000, 239-245.

Moyler, D. A., *Extraction of natural products using near-critical solvents*, eds, M. B. King and T. R. Bott, Chapman & Hall, Glasgow, 1993.

Muhrer, G., Mazzotti, M., Müller, M., "Gas antisolvent recrystallization of an organic compound. Tailoring product PSD and scaling-up", *J. Supercrit. Fluids*, 27, 2003, 195-203.

Muhrer, G., Lin, Cheng, Mazzotti, M, "Medelling the GAS antisolvent recrystallization process", *Ind. Eng. Chem. Res.*, 41, 2002, 3566-3579.

Murthy, A. K., E. W. Kaler, and J. A. N. Zasadzinski. "Spontaneous vesicles from aqueous solutions of aerosol OT and choline chloride compounds." *J. Colloid Interface Sci.* 145, 1991, 598-600.

Mutz, M., and W. Helfrich. "Unbinding transition of a biological model membrane." *Phys. Rev. Lett.* 62, 1989, 2881-2884.

Nägele, G., and P. Baur. "Long-time dynamics of charged colloidal suspensions: hydrodynamic interaction effects." *Physica A.* 245, 1997, 297-336.

Nieh, M.-P., C. J. Glinka, S. Krueger, R. S. Prosser, and J. Katsaras. "SANS study of structural phases of magnetically alignable lanthanide-doped phospholipid mixtures." *Langmuir.* 17, 2001, 2629-2638.

Nieh, M.-P., C. J. Glinka, S. Krueger, R. S. Prosser, and J. Katsaras. "SANS study on the effect of lanthanide ions and charged lipids on the morphology of phospholipid mixtures". *Biophys. J.* 82, 2002, 2487-2498.

Nieh, M.-P., T. A. Harroun, V. A. Raghunathan, C. J. Glinka, and J. Katsaras. "Concentration-independent spontaneously forming biomimetic vesicles." *Phys. Rev. Lett.* 91, 2003, 1581.

Oberdisse, J. "Transition from small to big charged unilamellar vesicles". *Eur. Phys. J. B.* 3, 1998, 463-469.

Oberdisse, J., C. Couve, J. Appell, J. F. Berret, C. Ligoure, and G. Porte. "Vesicles and onions from charged surfactant bilayers: a neutron scattering study". *Langmuir.* 12, 1996, 1212-1218.

Oberdisse, J., and G. Porte. "Size of microvesicles from charged surfactant bilayers: neutron scattering data compared to an electrostatic model." *Phys. Rev. E.* 56, 1997, 1965-1975.

Ogawa, Y., Yamamoto, M., Takada, S., Okada, H., Shimamoto, T., "A new technique to efficiently entrap Leuprolide acetate into microcapsules of poly (lactic acid) or copoly (lactic/glycolic acid) and Controlled release of Leuprolide acetate from poly (lactic acid) or copoly (lactic/glycolic acid) microcapsules: Influence of molecular weight and copolymer ratio of polymer", *Chem. Pharm. Bull.*, 36, 1988, 1095 and 1502.

Ollivon, M., S. Lesieur, C. Grabrielle-Madelmont, and M. Paternotre. "Vesicle reconstitution from lipid-detergent mixed micelles." *Biochim. Biophys. Acta.* 1508, 2000, 34-50.

O'Neill, M. L., Cao, Q., Fang, M., Johnston, K. P., Wilkinson, S. P., Smith, C., Kerschner, J. L., Jureller, S. H., "Solubility of homopolymers and copolymers in carbon dioxide", *Ind. Eng. Chem. Res.*, 37, 1998, 3067-3079.

Özyazici, M., Sevgi, F., Ertan, G., "Micromeritic studies on nicardipine hydrochloride microcapsules", *Intl. J. Pharm.*, 138, 1996, 25-35.

Pencer, J., G. F. White, and F. R. Hallett. "Osmotically induced shape changes of large unilamellar vesicles measured by dynamic light scattering." *Biophys. J.* 81, 2001, 2716-2728.

Peng, D.-Y. and Robinson, D. B., "A New Two-Constant Equation of State", *Ind. Eng. Chem. Fundam.*, 15, 1976, 59-64.

Pessey, V., Garriga, R., Weill F., Chevalier, B., Etourneau, J., Cansell, F., "Core-shell materials elaboration in supercritical mixture CO2/ethanol, Ind. Eng. Chem. Res., 39, 2000, 4714.

Pessey, V., Mateos, D., Weill, F., Cansell, F., Etourneau, J., Chevalier, B., "$SmCo_5$/Cu particles elaboration using a supercritical fluid process", *J. Alloys and Compounds,* 323, 2001, 412.

Pessey, V., Garriga, R., Weill F., Chevalier, B., Etourneau, J., Cansell, F., "Core-shell materials elaboration in supercritical mixture CO_2/ethanol, *Ind. Eng. Chem. Res.,* 39, 2000, 4714.

Pfeffer, R., Dave, R. N., Wei, D., Ramlakhan, M., "synthesis of engineered particulates with tailored properties using dry particle coating", *Powder Technol.*, 117, 2001, 40-67.

Philipse, A. P., and A. Vrij. "Determination of static and dynamic interactions between monodisperse, charged silica spheres in optically matching, organic solvent." *J. Chem. Phys.* 88, 1988, 6459-6470.

Platzer, B. and Maurer, G., "A generalized equation of state for polar and nonpolar fluids", *Fluid Phase Equilibria*, 51, 1989, 223-236.

Prosser, R. S., S. A. Hunt, J. A. DiNatale, and R. R. Vold. "Magnetically aligned membrane model systems with positive order parameter: switching the sign of Szz with paramagnetic ions." *J. Am. Chem. Soc.* 118, 1996, 269-270.

Prosser, R. S., J. S. Hwang, and R. R. Vold. "Magnetically aligned phospholipid bilayers with positive ordering: a new model membrane system." *Biophys. J.* 74, 1998, 2405-2418.

Randolph, T. W., Randolph, A. D., Mebes, M., Yeung, S., "Sub-micrometer-sized biodegradable particles of poly (L-lactic acid) via the gas antisolvent spray precipitation process", *Biotechnol. Prog.*, 9, 1993, 429-435.

Reverchon, E. and Porta, G. Della, "Production of antibiotic micro- and nano-particles by supercritical antisolvent precipitation", *Powder Technol.*, 106, 1999, 23-29.

Reverchon, E., Porta, G. Della, Pallado, P., "Supercritical antisolvent precipitation of salbutamol microparticles", *Powder Technol.*, 106, 1999, 17-22.

Reverchon, E., Porta, G. Della, Rosa, I. D., Subra, P., Letourneur, D., "Supercritical antisolvent micronization of some biopolymers", *J. Supercrit. Fluids*, 18, 2000, 239-245.

Reverchon, E., Porta, G. Della., Trolio, A. Di., Pace, P., "Supercritical antisolvent precipitation of nanoparticles of superconductor precursors", *Ind. Eng. Chem. Res.*, 37, 1998, 952-958.

Reverchon, E., Porta, G. Della, Sannino, D., Ciambelli P., "Supercritical antisolvent precipitation of nanoparticles of a zinc oxide precursor", *Powder Technol.*, 102, 1999, 127-134.

Reverchon, E., "Supercritical antisolvent precipitation of micro- and nano-particles", *J. Supercrit. Fluids*, 15, 1999, 1.

Riberio Dos Santos, I., Richard, J., Pech, B., Thies, C., Benoit, J. P., "Microencapsulation of protein particles within lipids using a novel supercritical fluid process", *Intl. J. Pharm.*, 242, 2002, 69-78.

Riese, D. O., G. H. Wegdam, W. L. Vos, and R. Sprik. "Effective screening of hydrodynamic interactions in charged colloidal suspension." *Phys. Rev. Lett.* 85, 2000, 5460-5463.

Ruys, A. J. and Mai, Y. W., "The nanoparticle-coating process: A potential sol-gel route to homogeneous nanocomposites", *Materials Sci. and Eng., A*, 265, 1999, 202-207.

Safran, S. A., P. Pincus, and D. Andelman. "Theory of spontaneous vesicle formation in surfactant mixtures." *Science.* 248, 1990, 354-356.

Safran, S. A., P. Pincus, D. Andelman, and F. C. Mackintosh. "Stability and phase behavior of mixed surfactant vesicle." *Phys. Rev. A.* 43, 1991, 1071-1078.

Sanders 2nd, C. R., and G. C. Landis. " Reconstitution of membrane-proteins into lipid-rich bilayered mixed micelles for NMR-studies". *Biochemistry.* 34, 1995, 4030-4040.

Sanders 2nd, C. R., and J. H. Prestegard. "Magnetically orientable phospholipid bilayers containing small amounts of bile salt analogue, CHAPSO". *Biophys. J.* 58, 1995, 447-460.

Schreiber, R., Vogt, C., Werther, J., Brunner G., "Fluidized bed coating at supercritical fluid conditions", *J. Supercrit. Fluids*, 24, 2002, 137-151.

Schurtenberger, P., N. Mazer, and W. Kanzig. "Preparation of monodisperse vesicles with variable size by dilution of mixed micellar solutions of bile salt and lecithin." *J. Phys. Chem.* 89, 1985, 1042-1049.

Schurtenberger, P., N. Mazer, S. Waldvogel, and W. Kanzig. "Micelle-to-vesicle transition in aqueous solutions of bile salt and phosphatidylcholine." *Biochim. Biophys. Acta.* 775, 1984, 111-114.

Sglavo, V. M., Dal Maschio, R., Soraru, G. D., Bellosi, A., "Fabrication and characterization of polymer-derived silicon nitride oxide zirconia (Si_2N_2O-ZrO_2) nanocomposite ceramics", *J. Mater. Sci.,* 28, 1993, 6437-6441.

Shaffer, K. A., Jones, T. A., Canelas, D. A., DeSimone, J. M., "Dispersion polymerizations in carbon dioxide using siloxane-Based stabilizers", *Macromolecules*, 29, 1996, 2704 -2706.

Shi, D., Wang, S. X., Ooij, W. J., Wang, L. M., Zhao, J. G., Yu, Z., "Uniform deposition of ultrathin polymer films on the surfaces of Al_2O_3 nanoparticles by a plasma treatment", *Appl. Phys. Lett.*, 78, 2001, 1243-1245.

Shiho, H. and DeSimone, J. M., "Dispersion polymerization of acrylonitrile in supercritical carbon dioxide", *Macromolecules,* 33, 2000, 1565 -1569.

Shim, J.-W., Kim, J.-W., Han, S.-H., Chang, I.-S., Kim, H.-K., Kang, H.-H., Lee, O.-S., Suh, K.-D., "Zinc oxide/polymethylmethacrylate composite microspheres by in situ suspension polymerization and their morphological study", *Colloids and Surfaces A: Physicochemical and Engineering Aspects*, 207, 2002, 105-111.

Sievers, R. E., Sellers, S. P., Kusek, K. D., Clark, G. S., Korte, B. J., "CO_2-activated nebulization and `bubble' spray drying to form fine (1-5 μm) particles of proteins and small molecules for inhalation drug therapy", *Conference on Drug Delivery*, Breckenbridge, July, 1999.

Soppimath, K. S., Kulkarni, A. R., Aminabhavi, T. M., "Encapsulation of antihypertensive drugs in cellulose-based matrix microspheres: Characterization and release kinetics of microspheres and tableted microspheres", *J. Microencapsulation* 18, 2001, 397-409.

Steckel, H., Thies, J., Müller, B. W., "Micronizing of steroids for pulmonary delivery by supercritical carbon dioxide", Intl. J. Pharm., 152, 1997, 99-110.

Stöber, W, Fink, A. "Controlled Growth of Monodisperse Silica Spheres in the Micron Size Range." *J. Colloid Interface Sci.* 26, 1968, 62.

Struppe, J., and R. R. Vold. " Dilute bicellar solutions for structural NMR work." *J. Magn. Reson.* 135, 1998, 541-546.

Sudsakorn, K. and Turton, R., "Nonuniformity of particle coating on a size distribution of particles in a fluidized bed coater", *Powder Technol.*, 110, 2000, 37-43.

Sumita, M., Tsukihi, H., Miyasaka, K. and Ishikawa K. "Dynamic Mechanical Properties of Polypropylene Composites Filled with Ultrafine Particles." *J. Appl. Polym. Sci.*, *29*, 1994, 1523.

Takeo, O., Koichi, N., Katsuaki, S., "Formation of carbon nanocapsules with SiC nanoparticles prepared by polymer pyrolysis", *J. Mater. Chem.*, 8, 1998, 1323-1325.

Thies, J. and Müller, B. W., "Size controlled production of biodegradable microparticles with supercritical gases", *European J. Pharm. Biopharm.*, 45, 1998, 67-74.

Tom, J. W. and Debenedetti, P. G., "Formation of bioerodible polymeric microspheres and microparticles by rapid expansion of supercritical solutions", *Biotechnol. Prog.*, 7, 1991, 403-411.

Tom, J. W., Debenedetti, P. G., Jerome, R., "Precipitation of poly (L-lactic acid) and composite poly (L-lactic acid)-pyrene particles by rapid expansion of supercritical solutions", *J. Supercrit. Fluids*, 7, 1994, 9-29.

Tsutsumi, A.., Nakamoto, S., Mineo, T., Yoshida, K., "A novel fluidized-bed coating of fine particles by rapid expansion of supercritical fluid solutions", *Powder Technol.*, 85, 1995, 275-278.

Tu, L. S., Dehghani, F., Foster, N. R., "Micronisation and microencapsulation of pharmaceuticals using a carbon dioxide antisolvent", *Powder Technol.*, 126, 2002, 134-149.

Türk, M., "Influence of thermodynamic behaviour and solute properties on homogeneous nucleation in supercritical solutions", *J. Supercrit. Fluids*, 18, 2000, 169-184.

Villeneuve, M., S. Kaneshina, T. Imae, and M. Aratono. "Vesicle-micelle equilibrium of anionic and cationic surfactant mixture studied by surface tension." *Langmuir.* 15, 1999, 2029-2036.

Visintin, P. M., Denison, G. M., Bessel, C. A., Schauer, C. K., DeSimone, J. M. 227th ACS National Meeting, 2004 Anaheim.

Von Werne, T., Suehiro, I. M., Farmer, S., Patten, T. E. "Composite Films of Polymer-inorganic Hybrid Nanoparticles Prepared Using Controlled "Living" Radical Polymerization." *Polym. Mater. Sci. Eng. 82*, 2000, 294.

Viseu, M. I., K. Edwards, C. S. Campos, and S. M. B. Costa. "Spontaneous vesicle formed in aqueous mixtures of two cationic amphiphiles". *Langmuir.* 16, 2000, 2105-2114.

Vollath D. and Szabó, D. V., "Coated nanoparticles: A new way to improved nanocomposites", *J. Nanoparticle Res.,* 1, 1999, 235-242.

Walas, S. M., *Phase Equlibria in Chemical Engineering*, Butterworth, Boston, ch. 2 1985.

Walter, E., Moelling, K., Pavlovic, J., Merkle, H. P., "Microencapsulation of DNA using poly (DL-lactide-co-glycolide): stability issues and release characteristics", *J. Control. Rel.*, 61, 1999, 361-374.

Wan, S. C. and Lai, W. F., "Multilayer drug-coated cores: A system for controlling drug release", *Intl. J. Pharm.*, 81, 1992, 75-88.

Wang, D., Robinson, D. R., Kwon, G. S., Samuel, J., "Encapsulation of plasmid DNA in biodegradable poly(D, L-lactic-co-glycolic acid) microspheres as a novel approach for immunogene delivery", *J. Control. Rel.*, 57, 1999, 9-18.

Wang F. -J. and Wang, C. -H., "Sustained release of etanidazole from spray dried microspheres prepared by non-halogenated solvents", *J. Control. Rel.*, 81, 2002, 263-280.

Wang, T. J., Tsutsumi, A., Hasegawa, H., Mineo, T., "Mechanism of particle coating granulation with RESS process in a fluidized bed", *Powder Technol.*, 118, 2001, 229-235.

Wang, Y., Wei, D., Dave, R., Pfeffer, R., Sauceau, M., Letourneau, J.-J., Fages, J., "Extraction and precipitation particle coating using supercritical CO_2", *Powder Technol.*, 127, 2002, 32-44.

Wang, Y., Dave, R., Pfeffer, R., "Nanoparticle encapsulation with heterogeneous nucleation in a supercritical antisolvent process", *J. Supercrit. Fluids*, 28, 2004, 85-99.

Wang, Y., Iqbal, Z. and Mitra, S. "Microwave-induced rapid chemical functionalization of single-walled carbon nanotubes" *Carbon* 43, 2005, 1015-1020.

Watkins, J. J., McCarthy, T. J. Polymer/Metal Nanocomposite Synthesis in Supercritical CO_2. *Chem. Mater. 7*, 1995, 1991.

Werling, J. O. and Debenedetti, P. G., "Numerical modeling of mass transfer in the supercritical antisolvent process", *J. Supercrit. Fluids*, 16, 1999, 167-181.

Werling, J. O. and Debenedetti, P. G., "Numerical modeling of mass transfer in the supercritical antisolvent process: miscible conditions", *J. Supercrit. Fluids*, 18, 2000, 11-24.

Wieland-Berghausen, S., Schote, U., Frey, M., Schmidt, F., "Comparison of microencapsulation techniques for the water-soluble drugs nitenpyram and clomipramine HCl", *J. Control. Rel.*, 85, 2002, 35-43.

Winter, M. A., Frankel, D. Z., Debenedetti, P. G., Carey, J., Devaney, M., Przybycien, T. M., "Protein purification with vapor-phase carbon dioxide", *Biotechnol. Bioeng.*, 62, 1999, 247-258.

Winter, M. A., Knutson, B. L., Debenedetti, P. G., Sparks, H. G., Przybycien, T. M., Stevenson, C. L., Prestrelski, S. J., "Precipitation of proteins in supercritical carbon dioxide", *J. Pharm. Sci.*, 85, 1996, 586-594.

Winterhalter, M., and W. Helfrich. "Bending elasticity of electrically charged bilayers: coupled monolayers, neutral surfaces and balancing stresses." *J. Phys. Chem.* 96, 1992, 327-330.

Wissinger, R. G. and Paulaitis, M. E., "Glass transitions in polymer-CO_2 mixtures at elevated pressures", *J. Polym. Sci., Part B*, 29, 1991a, 631.

Wissinger, R. G. and Paulaitis, M. E., "Molecular thermodynamic model for sorption and swelling in glassy polymer-CO_2 systems at elevated pressures", *Ind. Eng. Chem. Res.*, 30, 1991b, 842.

Yatcilla, M. T., K. L. Herrington, L. L. Brasher, E. W. Kaler, S. Chiruvolu, and J. A. N. Zasadzinski. "Phase behavior of aqueous mixtures of cetyltrimethylammonium bromide (CTAB) and sodium octyl sulfate (SOS)". *J. Phys. Chem.* 100, 1996, 5874-5879.

Yamaguchi, Y., Takenaga, M., Kitagawa, A., Ogawa, Y., Mizushima Y., Igarashi, R., "Insulin-loaded biodegradable PLGA microcapsules: initial burst release controlled by hydrophilic additives", *J. Control. Rel.*, 81, 2002, 235-249.

Yang, T. H., Dong, A., Mayer, J., Johnson, O. L., Cleland, J. L., Carpenter, J. F., "Use of infrared spectroscopy to access secondary structure of human growth hormone within biodegradable microsphere", *J. Pharm. Sci.*, 88, 1999, 161.

Yates, M. Z., Li, G., Shim, J. J., Maniar, S., Johnston, K. P., Lim, K. T., Webber, S., "Ambidextrous surfactants for water-dispersible polymer powders from dispersion polymerization in supercritical CO_2", *Macromolecules*, 32, 1999, 1018 -1026.

Yen, S.-Y., Sung, K. C., Wang, J.-J., Hu, Y.-P., "Controlled release of nalbuphine propionate from biodegradable microspheres: in vitro and in vivo studies", *Intl. J. Pharm.*, 220, 2001, 91-99.

Yeo, S-D., Choi, J.-H, Lee T-J., "Crystal formation of $BaCl_2$ and NH_4Cl using a supercritical fluid antisolvent", *J. Supercrit. Fluids*, 16, 2000, 235-246.

Yeo, S.-D., Lim, G.-B., Debenedetti, P. G., Bernstein, H., "Formation of microparticulate protein powders using a supercritical fluid antisolvent", *Biotech. Bioeng.*, 41, 1993, 341.

Yeo, S. -D., Debenedetti, P. G., Patro, S. Y., Przybycien, T. M., "Secondary structure characterization of microparticulate insulin powders", *J. Pharm. Sci.*, 83, 1994, 1651-1656.

Young, T. J., Johnston, K. P., Mishima, K., Tanaka, H., "Encapsulation of lysozyme in a biodegradable polymer by precipitation with a vapor-over-liquid antisolvent", *J. Pharm. Sci.,* 88, 1999, 640-650.

Yuet, P. K., and D. Blankschtein. "Molecular-thermodynamic modeling of mixed cationic/anionic vesicles." *Langmuir.* 12, 1996, 3802-3818.

Yuet, P. K., and D. Blankschtein. "Effect of surfactant tail-length asymmetry on the formation of mixed surfactant vesicles." *Langmuir.* 12, 1996, 3819-3827.

Xu, C.Y., Sievers, R.E., Karst, U., Watkins, B. A., Karbiwnyk, C. M., Andersen, W. C. , Schaefer, J. D., Stoldt, C. R., "Supercritical carbon dioxide assisted aerosolization for thin films deposition, fine powder generation, and drug delivery", *Chapter 18 in Green Chemistry: Frontiers in Benign Chemical Synthesis and Processes*, P.T. Anastas and T.C. Williamson (Eds.), Oxford University Press, Oxford, 1998, 313-335.

Xu, C. Y., Watkins, B., Sievers, R. E., Jing, X., Trowga, P., Gibbons, C. S., Vecht, A., "Submicron-sized spherical yttrium oxide based phosphors prepared by supercritical CO_2-assisted aerosolization and pyrolysis", *Appl. Phys. Lett.,* 71, 1997, 1643-1645.

Xu, J., Wlaschin, A., Enick, R. M., "Thickening carbon dioxide with the fluoroacrylate-styrene copolymer", *SPE J.,* 8, 2003, 85-91.

Zhang, J. X. and Gao, L. Q., "Nanocomposite powders from coating with heterogeneous nucleation processing", *Ceramics International*, 27, 2001, 143-147.

Zhang, Y., Zhang, Q., Li, Y., Wang, N., Zhu, J., "Coating of carbon nanotubes with tungsten by physical vapor deposition", *Solid State Communications*, 115, 2000, 51-55.

Zhou, X., Shin, Eungsoo, Wang, K. W., Bakis, C. E. "Interfacial damping characteristics of carbon nanotube-based composites." *Composites Science and Technolog,* 64(15), 2004, 2425-2437.